GA 1485(REV. 11/80) (PED-81-2200)REV/1

DOE/ET/35300--T3

ISSUE SUMMARY

TITLE: FISSION-PRODUCT SiC REACTION IN HTGR FUEL

☒ R & D ☐ DV & S ☐ DESIGN

APPROVAL LEVEL 3

DISCIPLINE	SYSTEM	DOC. TYPE	PROJECT	DOCUMENT NO.	ISSUE NO./LTR.
N	18	RGE	6400	905837	1

QUALITY ASSURANCE LEVEL	SAFETY CLASSIFICATION	SEISMIC CATEGORY	ELECTRICAL CLASSIFICATION
I	1	CAT I	N/A

ISSUE	DATE	PREPARED BY	APPROVAL			ISSUE DESCRIPTION
			ENGINEERING	QA	PROJECT	
1	JUL 13 1981	F.Montgomery O.Stansfield 7/6/81 W.Kovacs 7/6/81 W.A. Simon 7/8/81			MASTER	Initial Issue. 6422020103.

INFO ONLY

NOTICE

PORTIONS OF THIS REPORT ARE ILLEGIBLE. It has been reproduced from the best available copy to permit the broadest possible availability.

DOE/ET/35300--T3

DE82 007189

CONTINUE ISSUE SUMMARY ON GA FORM 1485-1.

NEXT INDENTURED DOCUMENTS

905545

NON-CONTROLLED COPY
VERIFY ISSUE STATUS
WITH DOCUMENT CONTROL
PRIOR TO USE

DISTRIBUTION OF THIS DOCUMENT IS UNLIMITED

REV																										
SH																										
REV																										
SH	29	30	31	32	33	34	35	36	37	38	39	40	41	42	43	44	45	46	47	48	49	50	51	52	53	54	55	56
REV																										
SH	1	2	3	4	5	6	7	8	9	10	11	12	13	14	15	16	17	18	19	20	21	22	23	24	25	26	27	28

DISCLAIMER

DOE/ET/34300--T3

905837/1

TABLE OF CONTENTS

LIST OF TABLES

LIST OF TABLES (continued)

LIST OF FIGURES

LIST OF FIGURES (continued)

LIST OF FIGURES (continued)

LIST OF FIGURES (continued)

1. INTRODUCTION

Fuel for the High-Temperature Gas-Cooled Reactor (HTGR) consists of coated fuel particles bonded into fuel rods. The active core of the HTGR is comprised of these fuel rods contained in graphite fuel elements. TRISO fissile and fertile particles currently under development consist of a fuel kernel surrounded by successive coatings of a pyrolytic carbon buffer, an isotropic pyrolytic carbon (IPyC), silicon carbide (SiC), and a second isotropic pyrolytic carbon (OPyC).

Prior to 1977, the reference fuel cycle for the HTGR was the highly enriched uranium (HEU)[a] cycle using uranium dicarbide (UC_2) fissile particles and thorium dioxide (ThO_2) fertile particles. However, concerns about nuclear proliferation with the HEU cycle led to an evaluation of the performance of low enriched uranium (LEU)[b] fissile fuel. Associated with this change in fuel enrichment was an evaluation of the performance of uranium dioxide (UO_2), uranium oxycarbide (UC_xO_y) and UC_2 as the fissile kernel material. In addition, a new fuel type, TRISO UO_2*, was tested in which a UO_2 kernel was first coated with a 5-10 μm ZrC layer and then TRISO coated.

The primary barrier to release of fission product from any of the fuel types into the primary circuit of the HTGR are the coatings on the fuel particles. Both pyrolytic carbon (Ref. 1) and silicon carbide coatings are very effective in retaining fission gases under normal operating conditions. Silicon carbide is also effective in retaining most fission metals (Ref. 2). Thus, release of fission products from fuel particles under normal operating conditions depends on failure of these coatings. Coating failures can be caused during manufacturing, as well as during irradiation. One of the possible performance limitations which has been observed in irradiation tests of TRISO fuel is chemical interaction of the SiC layer with fission products (Ref. 3). This reaction reduces the thickness of the SiC layer in TRISO particles and can lead to release of fission products

---

[a] Defined as fuel with 93% U-235
[b] Defined as fuel with ∿20% U-235

from the particles if the SiC layer is completely penetrated.

The experimental section of this report describes the results of work at General Atomic concerning the reaction of fission products with silicon carbide. The discussion section describes data obtained by various laboratories and includes (1) a description of the fission products which have been found to react with SiC; (2) a description of the kinetics of silicon carbide thinning caused by fission product reaction during out-of-pile thermal gradient heating and the application of these kinetics to in-pile irradiation; and (3) a comparison of silicon carbide thinning in LEU and HEU fuels.

2. EXPERIMENTAL PROCEDURES

The rate at which fission products react with SiC in irradiated, TRISO HTGR fuel was studied during out-of-pile thermal gradient heating. The samples tested and the techniques used in these tests are described in this section.

2.1 Sample Descriptions

The TRISO particles used in these experiments had been irradiated prior to the out-of-pile tests. The kernels and coatings were prepared using standard fuel fabrication procedures and then irradiated as loose particles in accelerated tests under conditions similar to those expected in HTGR operation. Description of the kernel and coating characteristics of the particles is given in Table 2.1. Table 2.2 gives the conditions of the accelerated irradiation tests. Characteristics of the kernels and coatings for particles which exhibited fission product-SiC reactions during irradiation are given in Table 2.3. Table 2.4 gives the conditions of the irradiation tests.

2.2 Pre-test Fuel Particle Characterization

The fuel particles used in the out-of-pile heating are characterized before testing using gamma-ray spectroscopy to measure fission product inventories and x-ray radiography to determine fission product distribution within the fuel particles. Measurement of the gamma-ray spectrum from irradiated fuel particles is useful in determining the performance and fission product retention characteristics of fuel particles during irradiation (Refs. 4, 5). This is accomplished by comparing the ratio of volatile-to-nonvolatile fission products in the particles to the calculated ratio. In particular, the activity ratios of Cs-137, Ru-106, Zr-95 and Ce-144

Table 2.1

COATING AND KERNEL CHARACTERISTICS OF PARTICLES TESTED AT GENERAL ATOMIC IN OUT-OF-PILE THERMAL GRADIENT TESTS

Particle Parameters	HEU UC_2[a] 6151-17-016	HEU UC_2[a] 6151-17-025	HEU UC_2 4413-5E	HEU UC_2 4161-01-030	HEU UC_2 4161-01-032	HEU UC_2 4161-01-034	LEU UC_2 6151-21-0111-5	LEU UC $_{36}O_{1.64}$ 6157-09-0120-1	LEU UO_2 6152-01-0111-3	LEU UO_2* (18 µm, ZrC) 6152-03-0111-6
KERNEL										
Density, Mg/m^3	11.27	10.62	--	10.90	10.90[a]	10.90[a]	11.04	10.22	10.55	10.78
Diameter, µm	204.0	204.0	106	203	240	179.9	343.6	365.9	299.6	310.4
Std. Dev., µm	25.4	24.0	--	25.40	12.5	8.6	12.5	11.8	8.2	9.4
BUFFER										
Density, Mg/m^3	1.08	1.20	1.30	1.26	1.26[a]	1.26[a]	0.94	0.93	1.15	0.91
Thickness, µm	94.06	99.90	53	87.00	74.5	74.9	89.1	125.5	101.9	84.1
Std. Dev., µm	13.99	12.15	--	9.57	10.6	10.9	8.3	16.2	8.2	9.3
IPyC										
Density, Mg/m^3	1.87	1.87	1.83	1.91	1.91[a]	1.91[a]	1.86	1.92	1.91	1.92
Std. Dev.	1.4×10^{-2}	8.4×10^{-3}	--	9.0×10^{-3}	9.0×10^{-3}[a]	9.0×10^{-3}[a]	1.96×10^{-3}	7.44×10^{-3}	4.66×10^{-3}	7.02×10^{-3}
Thickness, µm	35.85	35.0	24	28.00	28.00	28.00	36.9	42.9	40.7	35.3
Std. Dev., µm	4.21	4.95	--	3.98	3.98	3.98	4.8	3.5	3.1	3.2
SiC										
Density, Mg/m^3	3.21	3.20	3.20	3.20	3.20	3.20[a]	3.16	3.16	3.21	3.2
Std. Dev.	4.4×10^{-3}	2.3×10^{-2}	--	7.0×10^{-3}	7.0×10^{-3}[a]	7.0×10^{-3}[a]	5.0×10^{-3}	1.37×10^{-2}	8.0×10^{-3}	8.19×10^{-3}
Thickness, µm	36.88	29.57	20	29.00	27.6	29.0	44.4	41.4	36.7	39.1
Std. Dev.	3.15	3.39	--	3.95	2.1	3.6	2.3	3.4	2.2	3.5
OPyC										
Density Mg/m^3	1.81	1.84	1.80	1.81	1.80[a]	1.80[a]	1.82	1.85	1.87	1.87
Std. Dev.	1.3×10^{-2}	4.5×10^{-3}	--	1.0×10^{-2}	1.0×10^{-2}[a]	1.0×10^{-2}[a]	1.01×10^{-2}	4.99×10^{-3}	5.1×10^{-3}	7.02×10^{-3}
Thickness, µm	37.80	33.18	23	32.0	35.8	35.7	49.8	43	40.8	40.8
Std. Dev. µm	3.85	5.19	--	5.0	3.2	3.7	3.9	3.2	3.6	4.3

[a] Data from parent batch

Table 2.2

IRRADIATION PARAMETERS FOR PARTICLES USED IN OUT-OF-PILE THERMAL GRADIENT HEATING TESTS

Out-of-Pile Experiment Number	Data Retrieval Number	Irradiation Test		Reactor	Sample Configuration	Fast Flux > 29 fJ n/m^2-s x 10^{17}	Fast Fluence > 29 fJ n/m^2 x 10^{25}	Kernel Burnup (% FIMA)	Irradiation Length hr	Irradiation Temperature °C
		Vehicle	Position							
78TG	6151-17-016	HB-5	T210	GETR	Unbonded	(c)	5.5	∿60	2300	<600
78TG	6151-17-025	HB-5	T250	GETR		(c)	5.5	∿60	2300	<600
80TG	6151-21-0111-5	HRB-15B	T172	HFIR-RB		(c)	3.6 HTGR	21.8	4055	915 (d)
80TG	6157-09-0120-1	HRB-15B	T22	HFIR-RB		(c)	4.5 HTGR	21.7	4055	860 (d)
80TG	6152-01-0111-3	HRB-15B	T174	HFIR-RB		(c)	3.5 HTGR	21.5	4055	915 (d)
80TG	6152-03-0111-6	HRB-15B	T176	HFIR-RB		(c)	3.4 HTGR	21.2	4055	915 (d)
5217-5	4413-5E	P13L	C3T3	ETR		(c)	7.8	∿74	6552	1250 (b)
7013	4161-01-030	FTE-14	TS56	Peach Bottom		4.6	1.44 (a)	23.00	8712	∿1400 (e)
6804	4161-01-030	FTE-14	TS36	Peach Bottom		4.5	1.40 (a)	24.16	8712	∿1100 (e)
6804	4161-01-032-002	P13P	CIP4	ETR		6.8	6.0	60.6	4752	1350 (b)
7013	4161-01-034-002	P13P	CIP2	ETR		6.7	5.9	60.2	4752	1420 (b)

(a) Calculated by GAUGE/Fever

(b) Not known if particle surface or kernel temperature

(c) Not reported

(d) Maximum particle surface temperature

(e) Linear time weighted maximum temperature

Table 2.3

COATING AND KERNEL CHARACTERISTICS OF TRISO PARTICLES WHICH EXHIBITED FISSION PRODUCT REACTION WITH SiC DURING IRRADIATION

Particle Parameters	ThO_2 6252-17-010	LEU $(Th/U)O_2$ 6155-05-020	LEU UO_2 6152-01-010	LEU $UC_{0.7}O_{0.5}$ 6157-08-010	LEU $UC_{0.7}O_{0.5}$ 6157-08-020	ThO_2 6252-14-0161	ThO_2 6252-15-0161	ThO_2 6252-16-0161	HEU UC_2 4161-01-031 4161-01-030
KERNEL									
Density, Mg/m^3	9.78	10.40	10.55	11.91	12.03	9.9[a]	9.90[a]	9.90[a]	10.90
Diameter, μm	455	360	299	354	353	448	450	451	203
Std. Dev.	8.9	10.1	8.11	15.0	15.6	7.6	7.2	6.8	25.40
BUFFER									
Density, Mg/m^3	0.93	1.09	1.15	1.20	1.15	1.1	1.07	1.07	1.26
Thickness, μm	90	110	122	108	90	63	56	57	87.00
Std. Dev.	22.32	12.98	20.0	15.15	15.41	7.0	6.9	6.5	9.57
IPyC									
Density, Mg/m^3	1.79	1.89	1.91	1.88	1.87	1.84	1.85	1.85	1.91
Std. Dev.	1.37×10^{-2}	1.63×10^{-2}	4.66×10^{-3}	9.27×10^{-3}	1.0×10^{-2}	2.8×10^{-2}[a]	1.99×10^{-2}[a]	1.99×10^{-2}[a]	9.0×10^{-3}
Thickness, μm	40	32	41	37	35	32	36	36	28.00
Std. Dev.	5.1	3.89	3.07	4.35	4.61	4.4	4.4	4.4	3.98
SiC									
Density, Mg/m^3	3.22	3.22	3.21	3.21	3.21	3.22	3.22	3.21	3.20
Std. Dev.	4.82×10^{-3}	8.5×10^{-6}	8.0×10^{-6}	4.64×10^{-3}	4.0×10^{-3}	3.1×10^{-3}[a]	3.10×10^{-3}[a]	4.6×10^{-3}	7.0×10^{-3}
Thickness, μm	36	36	32	36	30	37	38	39	29.00
Std. Dev.	3.36	3.69	5.55	4.24	5.55	2.6	2.1	2.0	3.95
OPyC									
Density, Mg/m^3	1.95	1.86	1.87	1.90	1.91	1.97	1.81	1.96	1.81
Std. Dev.	4.26×10^{-3}	3.0×10^{-3}	5.08×10^{-3}	1.96×10^{-3}	2.0×10^{-3}	4.5×10^{-3}[a]	1.1×10^{-2}[a]	2.72×10^{-3}[a]	1.0×10^{-2}
Thickness, μm	49	48	40	48	49	44	45	48	32.00
Std. Dev.	7.1	6.63	5.53	4.92	5.77	4.8	5.1	5.8	5.0

[a] Data from parent batch

Table 2.3 (continued)

COATING AND KERNEL CHARACTERISTICS OF TRISO PARTICLES WHICH EXHIBITED FISSION PRODUCT REACTION WITH SiC DURING IRRADIATION

Particle Parameters	TRISO[c] WAR-A $UC_{4.12}O_{0.47}$ A615	TRISO WAR-D $UC_{4.83}O_{1.09}$ OR-2458-H	TRISO WAR-D $UC_{4.80}O_{1.06}$ OR-2460-H	TRISO WAR-D $UC_{4.48}O_{0.62}$ OR-2471-H	TRISO WAR-A $UC_{4.58}O_{1.13}$ OR-2486-H	TRISO WAR-A $UC_{4.60}O_{1.10}$ OR-2494-H
KERNEL						
Density, Mg/m^3	3.076	2.47	2.45	2.53	3.186	3.203
Diameter, μm	354.1	413.4	396.1	391.4	361.4	363.3
Std. Dev.	15.7	21.7	20.7	20.0	22.2	23.1
BUFFER						
Density, Mg/m^3	1.33[d]	1.25	(f)	1.25	1.27	1.304
Thickness, μm	51.0	45.9	(f)	47.6	48.2	43.3
Std. Dev.	12.3	4.9	-	5.6	6.5	6.6
IPyC						
Density, Mg/m^3	1.857[e]	1.962	1.95	1.956	2.004	2.010
Std. Dev.	0.009	0.008	(f)	0.009	0.008	0.007
Thickness, μm	30.7	34.3	36.3	34.7	40.2	36.6
Std. Dev.	3.3	2.4	3.4	2.6	3.37	3.9
SiC						
Density, Mg/m^3	3.200	3.203	3.159	3.194	3.190	3.197
Std. Dev.	0.008	0.007	0.004	0.008	0.004	0.004
Thickness, μm	29.5	36.0	35.3	34.4	30.7	32.2
Std. Dev.	1.5	2.0	2.4	1.3	1.5	1.3
OPyC						
Density, Mg/m^3	1.910[e]	2.005	2.008	1.992	2.020	2.027
Std. Dev.	0.004	0.005	0.010	0.007	0.006	0.006
Thickness, μm	32.4	38.4	33.8	33.9	40.4	36.4
Std. Dev.	4.2	2.8	2.5	3.8	2.9	3.0

(c) WAR-A is amberlite weak-acid resin; WAR-D is duolite weak-acid resin

(d) After depositing

(e) Corrected gradient density

(f) Not reported

Table 2.3 (continued)

COATING AND KERNEL CHARACTERISTICS OF TRISO PARTICLES WHICH EXHIBITED FISSION PRODUCT REACTION WITH SiC DURING IRRADIATION

Particle Parameters	HEU TRISO UC_2 4000-302	HEU TRISO UC_2 4000-325	HEU TRISO UC_2 6151-12-015	HEU[b] TRISO UC_2 6151-00-010	LEU WAR[b] TRISO UC_2 OR 52A	HEU[b] TRISO UC_2 6151-00-035	HEU[b] TRISO UC_2 6151-08-015
KERNEL							
Density, Mg/m^3	10.43	10.43	10.46	10.99	6.2	10.99	10.99
Diameter, μm	100.0	93.00	191.1	199	367	201	202
Std. Dev.	(f)	15.56	16.4	14.4	53	13.8	12.58
BUFFER							
Density, Mg/m^3	1.31	1.29	1.11	1.18	0.95	1.07	1.07
Thickness, μm	50.0	50.0	96.75	97	44.6	87	95
Std. Dev.	(f)	(f)	13.64	11.5	6	12.4	13.58
IPyC							
Density, Mg/m^3	1.84	1.82	1.93	1.94	1.95	1.92	1.92
Std. Dev.	(f)	(f)	1.5×10^{-2}	0	(f)	9×10^{-3}	9×10^{-3}
Thickness, μm	18.00	22.00	23.20	35	31	33	33
Std. Dev.	(f)	(f)	3.44	4.95	4	3.5	3.5
SiC							
Density, Mg/m^3	3.19	3.19	3.21	3.20	(f)	3.20	3.21
Std. Dev.	(f)	1.00×10^{-2}	4.74×10^{-3}	0	(f)	4.6×10^{-3}	4.74×10^{-3}
Thickness, μm	20.00	20.00	27.70	31	34	27	26
Std. Dev.	(f)	2.04	2.51	4.1	5.6	2.4	3.82
OPyC							
Density, Mg/m^3	1.71	1.71	1.78	1.80	1.96	1.85	1.76
Std. Dev.	(f)	6.0×10^{-3}	7.12×10^{-3}	1.1×10^{-2}	(f)	6.4×10^{-3}	1.65×10^{-2}
Thickness, μm	36.00	27.00	42.56	44	30	37	36
Std. Dev.	(f)	2.98	4.12	4.5	3.9	4.71	5.54

[b] Kernels doped with Th

Table 2.3 (continued)

COATING AND KERNEL CHARACTERISTICS OF TRISO PARTICLES WHICH EXHIBITED FISSION PRODUCT REACTION WITH SiC DURING IRRADIATION

Particle Parameters	TRISO PuO_{2-x} ORNL-13-1	TRISO 3 ThO_2, PuO_{2-x} ORNL-13-2	TRISO PuO_{2-x} ORNL-13-4	TRISO 3 ThO_2, PuO_{2-x} ORNL-13-5	TRISO PuO_{2-x} ORNL-13-6	TRISO WAR $UC_{4.40}O_{1.43}$ OR 2576H	TRISO HEU UC_2 4000-307
KERNEL							
Density, Mg/m^3	10.70	10.09	10.36	9.9	10.80	3.26	Composite of 4000-302, 303, 304, 305
Diameter, μm	110	346	190	343	198	376.1	
Std. Dev.	10	31	17	23	14	10.10	
BUFFER							
Density, Mg/m^3	0.76	0.981	0.99	1.24	1.39	1.12	See 4000-302 specifications
Thickness, μm	49	94	79	91	93	53.7	
Std. Dev.	11	8	17	9	15	7.02	
IPyC							
Density, Mg/m^3	1.900	1.743	1.833	1.789	1.798	1.939	
Std. Dev.	0.01	0.0105	0.010	0.011	0.017	0.007	
Thickness, μm	19	29	32	36	24	34.57	
Std. Dev.	5	5	4	4	2	3.20	
SiC							
Density, Mg/m^3	3.219	3.216	3.202	3.220	3.201	3.200	
Std. Dev.	0.001	0.003	0.001	0.0033	0.001	0.00066	
Thickness, μm	21	37	39	30	41	35.6	
Std. Dev.	2	13	2	1	2	1.50	
OPyC							
Density, Mg/m^3	1.910	1.865	1.845	1.816	1.821	2.020	
Std. Dev.	0.020	0.009	0.015	0.0179	0.008	0.0046	
Thickness, μm	25	46	35	53	38	37.18	
Std. Dev.	5	10	4	4	4	2.60	

Table 2.4

IRRADIATION PARAMETERS FOR PARTICLES WHICH EXHIBITED FISSION PRODUCT REACTION WITH SiC DURING IRRADIATION

Test Vehicle	Position	Reactor	Fast Flux E > 29 fJ x 10^{12} n/m^2-sec.	Fast Fluence E > 29 fJ x 10^{25} n/m^2	Burnup % FIMA	Irradiation hr	Data Retrieval Number	Particle Configuration	Reference
P13Q	G2-1B	ORNL ORR	27	9.1	76	9401	6151-00-010	Rod	GA-A14174
↓	G1-3A	↓	30	10.1	77.1	9401	↓	Rod	↓
	G1-2B		31	10.5	77.3	9401		Rod	
↓	G1-3B	↓	31	10.5	77.3	9401	↓	Rod	↓
P13R	2B	GETR	60	13.3	75	6192	6151-00-035	Rod	GA-A13827
↓	2C	↓	61	13.7	75	6192	↓	Rod	↓
P13S	5C	GETR	42	9.4	66	6192		Rod	
↓	5D	↓	40	8.9	65	6192	6151-08-015	Rod	↓
P13T	1-1B4	ORNL ORR	(f)	7.67_{HTGR}	74.7	8800	6151-12-015	Rod	GA-A15608
↓	1-1B2	↓	↓	4.84_{HTGR}	69.1	↓	↓	Rod	↓
	2-4A1			4.64_{HTGR}	62.7		6151-17-025	Rod	
	1-1C4			7.67_{HTGR}	74.7		↓	Rod	
↓	1-1C1	↓	↓	3.45_{HTGR}	67.7	↓	↓	Rod	↓
HT-33	6	ORNL HFIR	73	7.25	$84.7^{(a)}/13.7^{(b)}$	2759	OR2576H	Rod	ORNL-5539
↓	19	Target G5	111.7	11.1	$84.7^{(a)}/21.9^{(b)}$	2759	OR2576H	Rod	↓
HT-34[c]	10	ORNL HFIR	(f)	7.5[c]	8.3[c]	2686	6252-14-0161-001	Loose	ORNL HTGR Base Program Monthly Progress Report Dec. 1977-Jan. 1978 ORNL/GCR/B-78/1
	11	Target C6		7.7	8.6	2686	6252-15-0161-001	Loose	
	13			8.2	9.2	2686	6252-16-0161-001	Loose	
	28			10.2	$86.7^{(a)}/20.5^{(b)}$	2686	OR2576H	Rod	
	37			9.3	$86.4^{(a)}/18.8^{(b)}$	2686	OR2576H	Rod	
	41			8.0	$85.9^{(a)}/15.9^{(b)}$	2686	OR2576H	Rod	
	44			7.2	$85.7^{(a)}/14.6^{(b)}$	2686	OR2576H	Rod	
	47			6.4	$85.5^{(a)}/13.2^{(b)}$	2686	OR2576H	Rod	
↓	50	↓	↓	5.5	$85.2^{(a)}/11.7^{(b)}$	2686	OR2576H	Rod	↓

(a) U-235 burnup

(b) U-238 burnup

(c) Calculated by ORNL

(d) Total from both reactor positions

(e) WAR-Weak-Acid resin

Table 2.4 (continued)

IRRADIATION PARAMETERS FOR PARTICLES WHICH EXHIBITED FISSION PRODUCT REACTION WITH SiC DURING IRRADIATION

Test Vehicle	Position	Reactor	Average Fast Flux E > 29 fJ x 10^{17} n/m^2-sec.	Average Fast Fluence E > 29 fJ x 10^{25} n/m^2	Burnup % FIMA	Irradiation hr	Data Retrieval Number	Particle Configuration	Reference
HRB-4	3A	ORNL HFIR RB-7	4.56	9.61	84.0[a]/23.5[b]	5855	OR-52A	Rod	ORNL-5115
HRB-11[d]	2	ORNL HFIR	(f)	4.89_{HTGR}	84.9[a]/17.8[b]	6559	OR-2460-H	↓	ORNL-5584
↓	16	VXF-13 PB-13 3 Cycles	↓	7.26_{HTGR}	86.6[a]/27.5[b]	↓	OR-2458-H	↓	↓
↓	21	RB-7 9 cycles	↓	5.68_{HTGR}	85.5[a]/21.3[b]	↓	OR-2471-H	↓	↓
HRB-12[d]	4	"	↓	5.84_{HTGR}	86[a]/22.1[b]	6602	OR-2486-H	↓	↓
HRB-12[d]	5	RB-5	↓	6.25_{HTGR}	86[a]/23.8[b]	↓	OR-2494-H	↓	↓
HRB-14	1	ORNL HFIR RB	↓	$8.3^{(c)}_{HTGR}$	8.5[h]	5124	6252-17-010	↓	GA-A15969
↓	4	↓	↓	$8.1^{(c)}_{HTGR}$	19.1[h]	↓	6155-05-020	↓	↓
↓	6	↓	↓	$7.8^{(c)}_{HTGR}$	29.5[h]	↓	6152-01-010	↓	↓
↓	8	↓	↓	$7.5^{(c)}_{HTGR}$	28.6[h]	↓	6157-08-010	↓	↓
↓	10	↓	↓	$7.1^{(c)}_{HTGR}$	27.8[h]	↓	6157-08-020	↓	↓
↓	12	↓	↓	$6.6^{(c)}_{HTGR}$	26.4[h]	↓	6157-08-010	↓	↓
↓	14	↓	↓	$6.2^{(c)}_{HTGR}$	26.1[h]	↓	6157-08-010	↓	↓
OF-2	C-2-1	ORNL ORR E-7	↓	8.5	79[a,g]/ 12.7[b,g]	8440	A615	↓	ORNL-5428

[f] Not reported

[g] Preliminary estimate

[h] Calculated at GA

Table 2.4 (continued)

IRRADIATION PARAMETERS FOR PARTICLES WHICH EXHIBITED FISSION PRODUCT REACTION WITH SiC DURING IRRADIATION

Test Vehicle	Position	Reactor	Average Fast Flux E > 29 fJ x 10^{17} n/m^2-s	Average Fast Fluence E > 29 fJ x 10^{25} n/m^2	Burnup % FIMA	Irradiation Time (hr)	Data Retrieval Number	Particle Configuration	Reference
FTE-13	2-2-2	Peach Bottom	(f)	2.23	∿43	12285	ORNL[i] 13-6	Rod	ORNL-TM-4207 GA-A15999
	2-2-6			2.26					
	2-2-9			2.56					
	2-2-12			2.22					
	2-5-9			2.56			ORNL 13-1		
	2-5-12			2.22					
	2-6-2			2.23			ORNL 13-4		
	2-6-6			2.26					
	2-6-9			2.56					
	2-6-12			2.22	10				
	2-7-6			2.26	10		ORNL 13-2		
	2-7-12			2.22	10		ORNL 13-2		
	2-8-9			2.56	10		ORNL 13-5		
FTE-14	TS8-3		∿3.3	1.24	19.3	8712	(f)	Loose	GA-A13944
	TS5-6		∿3.3	1.44	23.0		(f)	Loose	
	TS4-6		∿3.3	1.45	23.9		4161-01-030	Loose	
	2-1-7		∿3.3	1.438	23.9		4161-01-031	Rod	
FTE-15	TS8-3		∿3.0	1.90	31.0	14901	4161-01-030	Loose	
	TS5-6		∿3.0	2.02	36.5		4161-01-030	Loose	
	TS4-6		∿3.0	1.99	37.6		(f)	Loose	
	2-2-5		∿3.0	2.01	37.6		4161-01-031	Rod	
	2-1-9		∿3.0	2.02	36.5		4161-01-031	Rod	
	2-1-5		∿3.0	2.01	37.6		4161-01-031	Rod	

[i] Fabricated at ORNL, FTE-13 particle type 6

Table 2.4 (continued)

IRRADIATION PARAMETERS FOR PARTICLES WHICH EXHIBITED FISSION PRODUCT REACTION WITH SiC DURING IRRADIATION

Test Vehicle	Position	Reactor	Average Fast Flux E > 29 fJ x 10^{17} n/m^2	Average Fast Fluence E > 29 fJ x 10^{25} n/m^2	Burnup % FIMA	Irradiation Time hr	Data Retrieval Number	Particle Configuration	Reference
FTE-5	2-5-7	Peach Bottom	(f)	3.79	55.7	24832	4000-307	Rod	GA-905285
↓	3-5-2	↓	↓	2.98	50.5		4000-307	↓	↓
RTE-1	3-6-6			3.03	49.4	18358	4000-325		ORNL-5422
RTE-2	6-1-1			1.98	31.4	18641	4000-307		↓
↓	6-1-3			1.64	28.0	18641	4000-307		
	Body 3			3.1	45.2	18641	4000-307		
RTE-4	4-7-3			1.80	29.8	9930	4000-307		
↓	4-1-3			1.80	29.8	9930	4000-307		
RTE-5	3-5-6			4.13	58.3	24832	4000-307		
RTE-6	4-1-1			4.13	58.8	24832	4000-307		
RTE-7	5-5-5			0.79	13.7	6473	4000-307		
RTE-8	5-7-1	↓	↓	3.94	54.9	24832	4000-307	↓	↓

are of interest. Zirconium has been shown to be retained in both oxide and carbide kernels (Ref. 6). Cesium is generally released from the kernel, but is retained in the particle by the intact SiC layer (Ref. 7). Thus, the Cs-137/Zr-95 ratio is a good indication of the integrity of the SiC coating and can be used to monitor the impact of out-of-pile heating on the SiC layer. Particles with a Cs-137/Zr-95 ratio that deviated by $\pm 2\sigma$ from the average value were not tested. In addition, particles with Cs-137/Zr-95 ratios that differed from the calculated value by $\pm$20% were not used. Expected fission product inventories were calculated by two different computer codes: FISPROD and CURIE. FISPROD (Ref. 8) calculates heavy metal and fission product concentrations for high enriched irradiated fuel from the experimental fluence and the measured amount of any fission product. CURIE (Ref. 9) calculates the amount of a specified number of fission products and the amount of heavy metal nuclides in the chain from Th-232 to Pa-242 formed during the irradiation. This calcuation is based on the irradiation history and the initial uranium composition of the sample.

2.3 Thermal Gradient Heating

The basic methods used for thermal gradient heating are outlined in Refs. 10 and 11 and are briefly described here. It should be emphasized that this experimental technique has been applied in the characterization of amoeba migration in carbide (Ref. 10), and in ThO_2 (Ref. 11) fuels. The test temperatures and thermal gradients were established by bonding particles in a slotted graphite crucible and positioning the crucible between a graphite heating element and a cold furnace wall. A crucible consists of a graphite slab in which a vertical slot is cut. Two types of graphite were used during these tests: the tests designated, FY-78 used H-327 graphite (Great Lake Carbon Co.) and the FY-80 tests used 20/20 (Stack Pole Carbon Co.). After rough machine work, the blank crucibles were heated under vacuum at 2100°C for one hour to remove any major impurities in the graphite. Table 2.5 gives the impurities found by emission spectrocopy in both types of graphite crucibles.

Test particles were placed in individual holes drilled perpendicular to the slot, and were held in place with a matrix consisting of 25 wt % natural flake graphite flour (Asbury No. 6353) and 75 wt % binder. The binder was 5 wt % maleic acid, 45 wt % furfural alcohol, and 50 wt % methyl alcohol. The matrix was cured by heating isothermally at ∿450°C to drive off the volatile constituents of the binder.

Loaded crucibles were fired isothermally for a minimum of one hour at ≤100°C above the nominal test temperature to stabilize the matrix prior to thermal gradient heating. The crucible heating and loading configurations are shown schematically in Fig. 2.1. The temperature across a crucible was monitored at the drilled cavities shown in Fig. 2.1.b with a micro-optical pyrometer. The temperature gradient across the coated particles in the crucible was determined by assuming (1) the thermal gradient is linear through the graphite and across the slot, and (2) the thermal gradient across the particle is the same as the gradient across the drilled hole as shown in Fig. 2.1.c. The mean particle test temperature was taken as the average temperature across the particle hole diameter. Four crucibles were tested in a furnace at one time. Each crucible contained six or seven irradiated particles from a single sample and one unirradiated particle to serve as a standard.

2.4 Silicon Carbide Thinning Rate

Contact x-radiographs of each crucible were prepared before heating and at intervals when tests were interrupted. The minimum silicon carbide thickness between the outer edge of the SiC and the advancing fission product front was measured from 300x magnifications of the x-radiographs. The SiC thickness of the as-received, irradiated particles was difficult to measure because the contact radiographic image of the SiC-inner PyC interface was diffuse. For this reason, the initial SiC thickness of each particle was obtained after the first heating period when fission product accumulation at the SiC increased the clarity of the inner SiC boundary. Section 3.4.1 discusses the accuracy of the radiographic measurement and compares the amount of SiC thinning determined by radiography and by metallography.

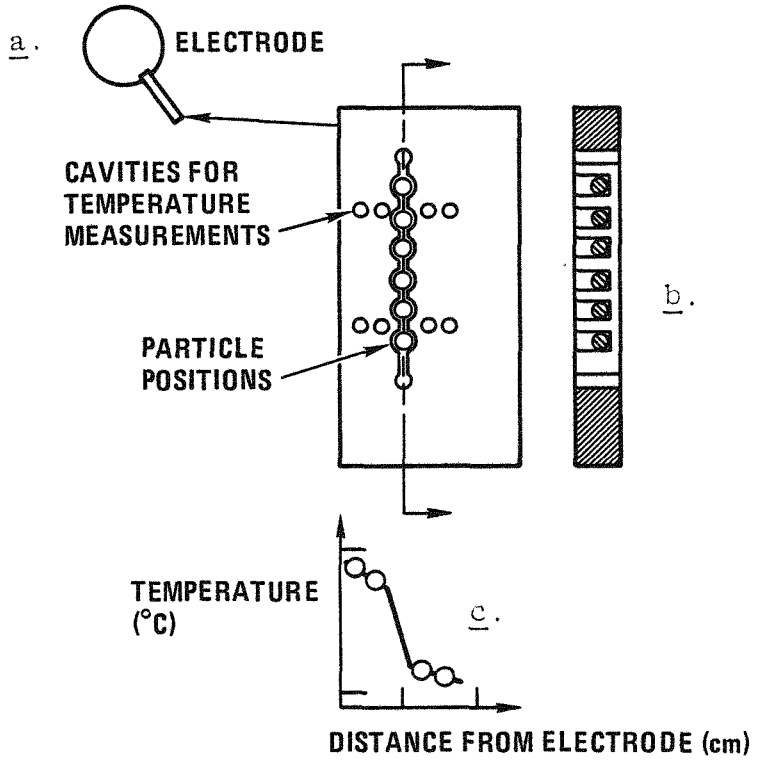

Fig. 2.1 Schematic representation of (a) heating configuration, (b) crucible containing fuel particles, and (c) thermal gradient across crucible

2.5 Fission Product Release

Fission product inventories were monitored during testing. Metallic fission product release was detected by gamma counting loaded crucibles during test interruptions. Gaseous release was detected by periodically purging the furnace atmosphere through a liquid nitrogen cooled charcoal trap and gamma counting the trap for Kr-85. Gamma-counting was done using a lithium-drifted germanium detector and either a Sigma II computer-analyzer with appropriate codes or a NDS6620 (Nuclear Data System) γ ray spectrometer. The uncertaintainty in fission product inventories measured by gamma-ray spectroscopy depends on the accuracy of the spectrometer calibration and on the specific activity of the nuclide in the sample. For fission products with high specific activities (i.e., Cs-137), calibration of the spectrometer limits the accuracy of the measurement. Calibrations using NBS standards generally result in errors of $<\pm 5\%$. Fission products with low specific activities (i.e. Ag-110m) are difficult to detect above the background noise of the Ge(Li) detector. The concentration of these fission products as measured by gamma ray spectroscopy have correspondingly larger absolute errors associated with the counting statistics. In general, Ag-110m measurements had standard deviations in the counts per minute (cpm) of approximately $\pm 20\%$.

Occasionally, particle failure occurred early during the tests. This failure could usually be attributed to interaction between the binder used to hold the particle in the crucible and the particle coatings. Silicon carbide thinning data was not obtained from any particle after coating failure was detected.

2.6 Post-test Heating Examination

After the particles were heat treated in the laboratory, the behavior of several samples was examined by standard optical metallographic techniques and by electron microprobe x-ray analysis (EMP).

To minimize exposure to irradiation, ceramography was conducted in the General Atomic hot cell. This facility is equipped with remotely operated grinding and polishing wheels and a MM5RT Leitz Research Metallograph. The metallograph is equipped with Bright field and polarized lighting. The

sample crucibles were mounted in an epoxy molding compound consisting of 71 Vol. % EPON 815 (Shell Chemical), 11 Vol. % EPON 812 (Shell Chemical) and 11 Vol. % AGE (E. V. Roberts) with 7 Vol. % DMP-30 (E. V. Roberts) as catalyst.

After ceramography, the polished samples were ultrasonically cleaned in methanol to remove any surface contamination caused by the polishing process. The samples were then examined in an ARL-EMX electron beam microprobe (Applied Research Laboratories). The EMP has three wavelength spectrometers and crystals of LiF, ADP, TAP, and pb stearate, as well as a Si(Li) x-ray energy spectrometer. The qualitative distribution of fission products in the particle was obtained from x-ray distribution patterns using the ADP and LiF crystals.

Table 2.5

EMISSION SPECTROGRAPHIC ANALYSIS OF IMPURITIES IN GRAPHITE MATERIALS USED IN OUT-OF-PILE THERMAL GRADIENT TESTS

Element	Graphite[a] Flour	Graphite Crucibles	
		78TG Experiment	80TG Experiment
Al	39.9	100	300
B	N1.3	3.0	3.0
Ba	13.3	N10.0	N10.0
Ca	N66.5	50.0	N50.0
Cu	39.9	N1.0	N1.0
Fe	26.6	30.0	N10.0
Mg	39.9	1.0	1.0
Mn	6.7	N5.0	N5.0
Ni	N6.7	N5.0	10
Si	665	75.0	30.0
Ti	6.7	50.0	7.0
V	9.3	15.0	30.0

a. Used in binder to cement particles into graphite crucible

N. Not detected at the sensitivity level shown

3. EXPERIMENTAL RESULTS

The crucibles containing the test particles were heat treated out-of-pile as described in Table 3.1. The results of radiographic and ceramographic examination of the test particles are described in Section 3.1. Section 3.2 gives fission product distributions based on electron microprobe examinations. The extent of SiC thinning as a function of time and temperature is described in Section 3.4.

3.1 Radiography and Ceramography

3.1.1 TRISO HEU UC_2

Contact X-radiographs of particles from TRISO HEU UC_2 batches 6151-17-016 and 6151-17-025 are shown in Figs. 3.1 and 3.2. Fission product distribution in each sample are typical of those observed after irradiation and after a one-hour out-of-pile thermal anneal. Figures 3.1 and 3.2 show that when irradiated TRISO UC_2 particles were heated at 1600°C and above, a random distribution of heavy metals was dispersed from the kernel into the surrounding buffer layer. In some instances, Fig. 3.2 for example, this redistribution of fission products resulted in penetration through the inner PyC and accumulation of fission products at the boundary of the SiC layer. Below 1450°C the one-hour isothermal anneal did not result in any observable fission product redistribution.

Pre-test and post-test contact X-radiographs and post-test metallography of the HEU UC_2 particles are shown in Figs. 3.3 through 3.6. A relocation of the fission products occurs during the thermal gradient anneal. Concentrations of fission products on the cool side of the heat-treated TRISO HEU UC_2 particles are evident from the radiographs. The radiographs clearly show fission products penetrating into the SiC layer after thermal gradient heating at time-averaged centerline temperatures of 1351°C, 1508°C and 1727°C.

The metallographic cross sections confirm the results obtained by contact radiography. The photomicrographs in Figs. 3.3 through 3.6 show that the fission product-SiC reactions occurred on the cool side of the particles; that no visible

Table 3.1

OUT-OF-PILE, THERMAL GRADIENT HEATING TEST PARAMETERS

Experiment Designation Number	Kernel Composition	Particle Data Retrieval Number	Time Weighted Centerline Heat Treatment Temperature °C	Time Weighted Thermal Gradient °C/cm	Total Time hr
5217-5	HEU UC_2	4413-5E	1306	260	2566
5217-5	↓	4413-5E	1460	260	575
6804	↓	4161-01-030	1551	348.5	617
6804	↓	4161-01-032-002	1525	388	617
7013	↓	4161-01-030	1692	974	87.25
7013	↓	4161-01-034-002	1704	1193	87.25
7013	↓	4161-01-032-002	1707	939	87.25
78TG 1623A1	↓	6151-17-025	1362	746	8222
78TG 1623A1	↓	6151-17-016	1351	706	8222
78TG 1773A1	↓	6151-17-016	1514	375	6396
78TG 1773A1	↓	6151-17-025	1508	420	6396
78TG 1973A1	↓	6151-17-016	1709	532	325
78TG 1973A1	↓	6151-17-025	1727	474	325
80TG 1373A1	LEU $UC_{.36}O_{1.64}$	6157-09-0120-1	1108	289	2158
↓	LEU UC_2	6151-21-0111-5	1093	231	2158
↓	LEU UO_2	6152-01-0111-3	1100	196	2158
↓	LEU UO_2*	6152-03-0111-6	1109	312	2158
80TG 1473A1	LEU $UC_{.36}O_{1.64}$	6157-09-0120-1	1204	252	2051.5
↓	LEU UC_2	6151-21-0111-5	1207	314	2051.5
↓	LEU UO_2	6152-01-0111-3	1203	295	2051.5
↓	LEU UO_2*	6152-03-0111-6	1210	354	2051.5
80TG 1623A1	LEU $UC_{.36}O_{1.64}$	6157-09-0120-1	1322	371	2253.5
↓	LEU UC_2	6151-21-0111-5	1368	590	2253.5
↓	LEU UO_2	6152-01-0111-3	1333	322	2253.5
↓	LEU UO_2*	6152-03-0111-6	1364	541	2253.5
80TG 1773A1	LEU $UC_{.36}O_{1.64}$	6157-09-0120-1	1500	522	163.5
↓	LEU UC_2	6151-21-0111-5	1510	574	163.5
↓	LEU UO_2	6152-01-0111-3	1513	602	163.5
↓	LEU UO_2*	6152-03-0111-6	1508	594	163.5
80TG-1973A1	LEU $UC_{.36}O_{1.64}$	6157-09-0120-1	1717	655	116
↓	LEU UC_2	6151-21-0111-5	1704	605	116
↓	LEU UO_2	6152-01-0111-3	1705	617	116
↓	LEU UO_2*	6152-03-0111-6	1713	615	116

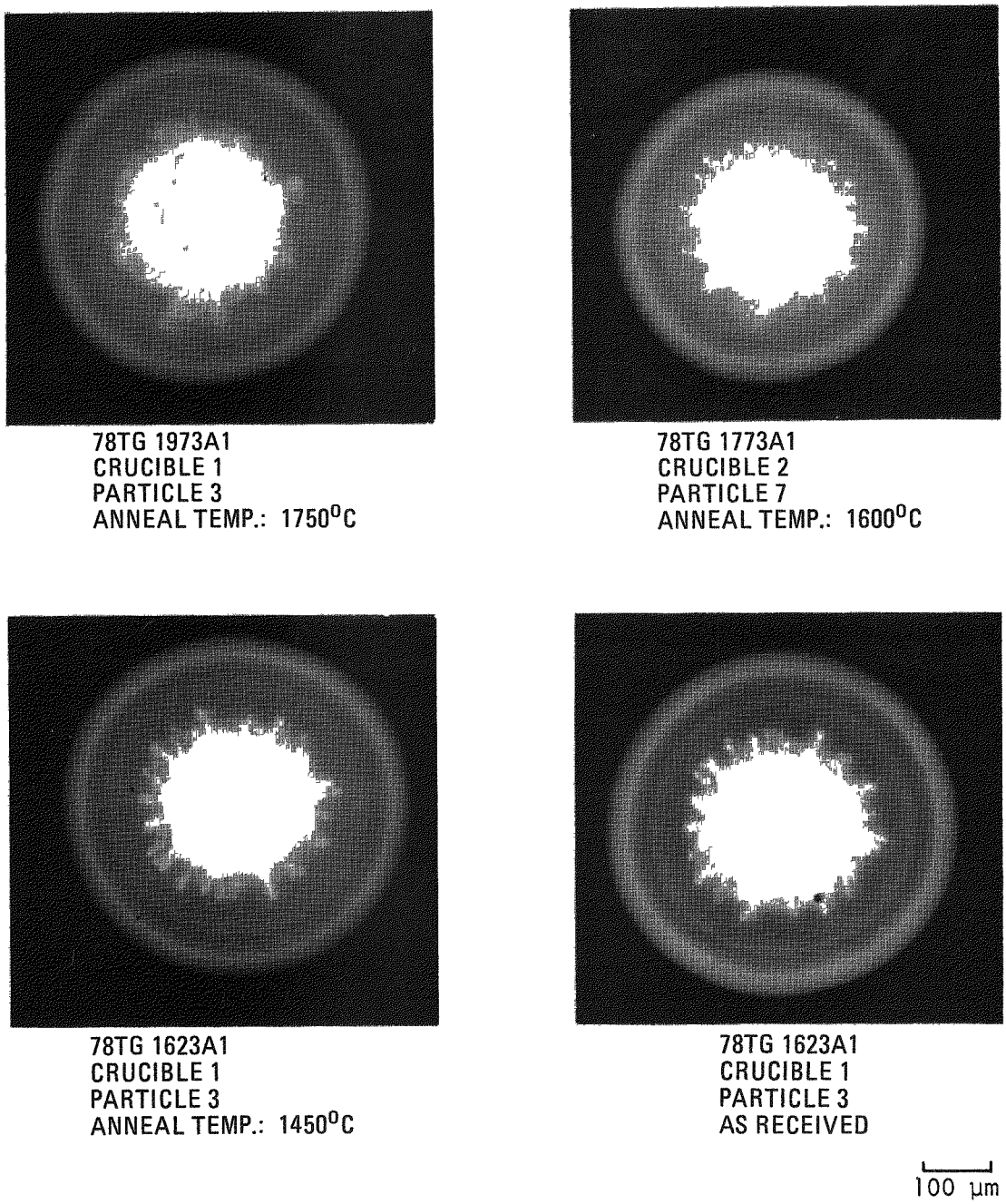

Fig. 3.1 Effect of one hour out-of-pile heat treatment on fission product distribution in irradiated TRISO HEU UC_2 (6151-17-016)

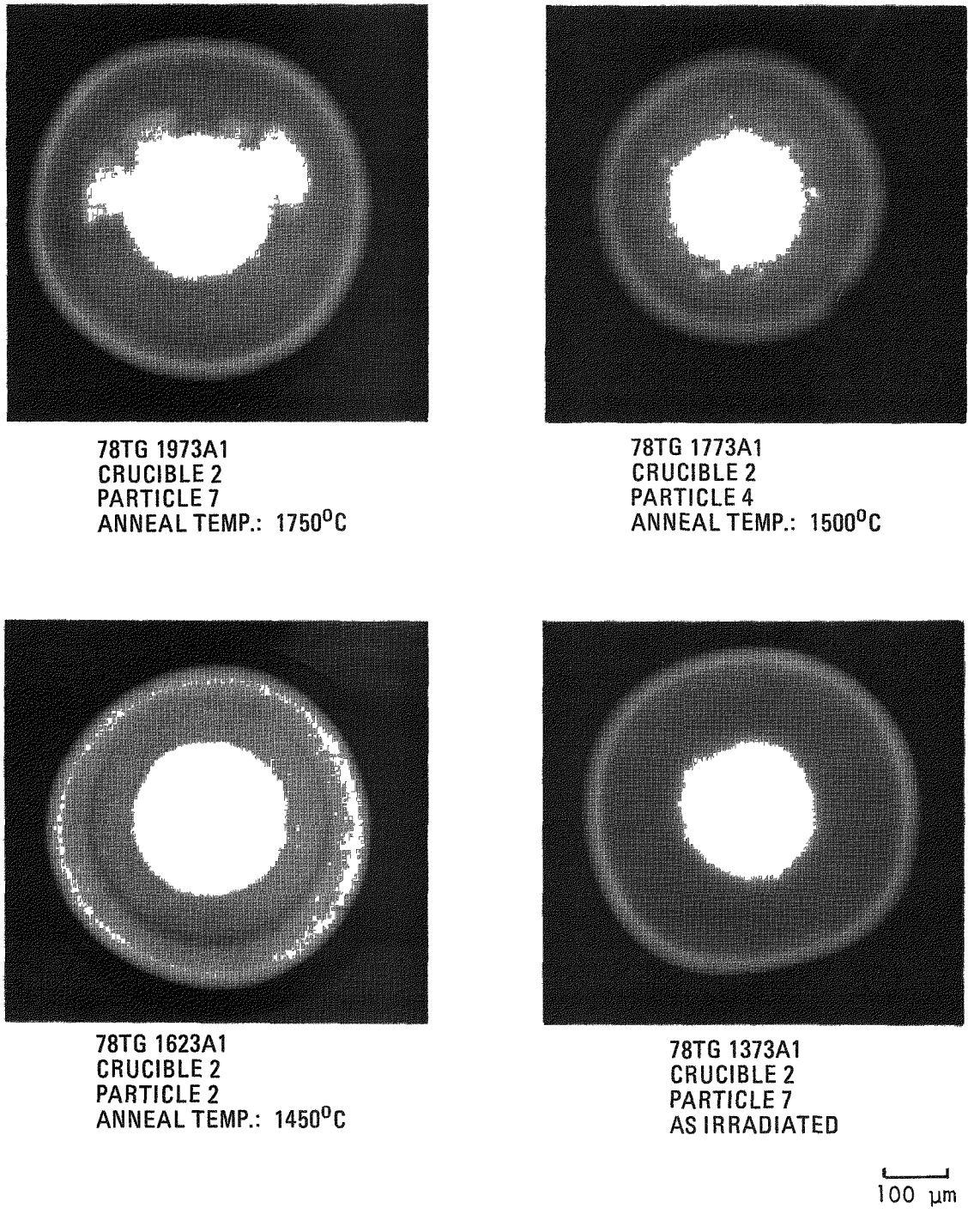

Fig. 3.2 Effect of one hour out-of-pile heat treatment on fission product distribution in irradiated TRISO HEU UC_2 (6151-17-025)

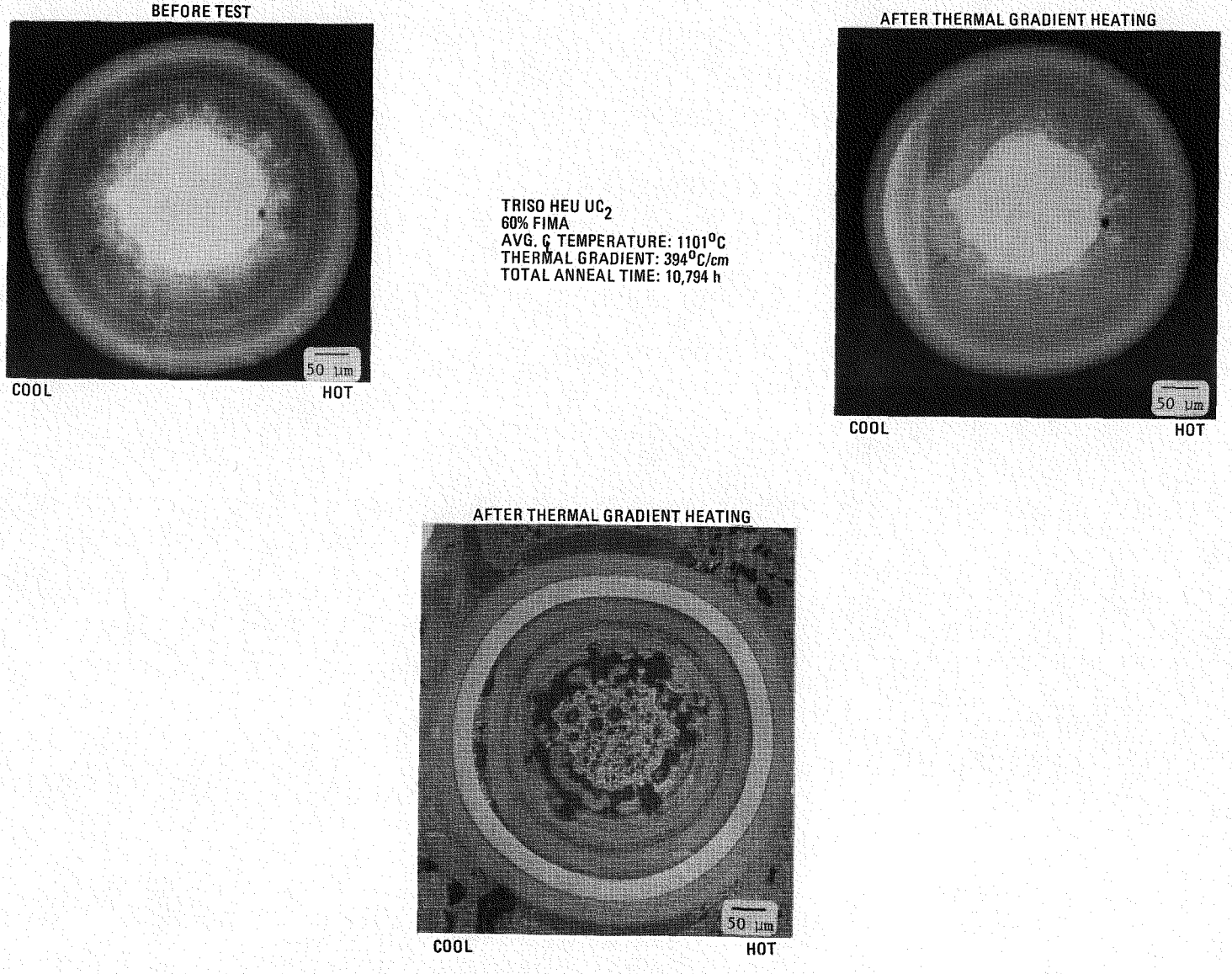

Fig. 3.3 Fission product-SiC reactions resulting from out-of-pile thermal gradient heating of TRISO HEU UC_2 at 1101°C

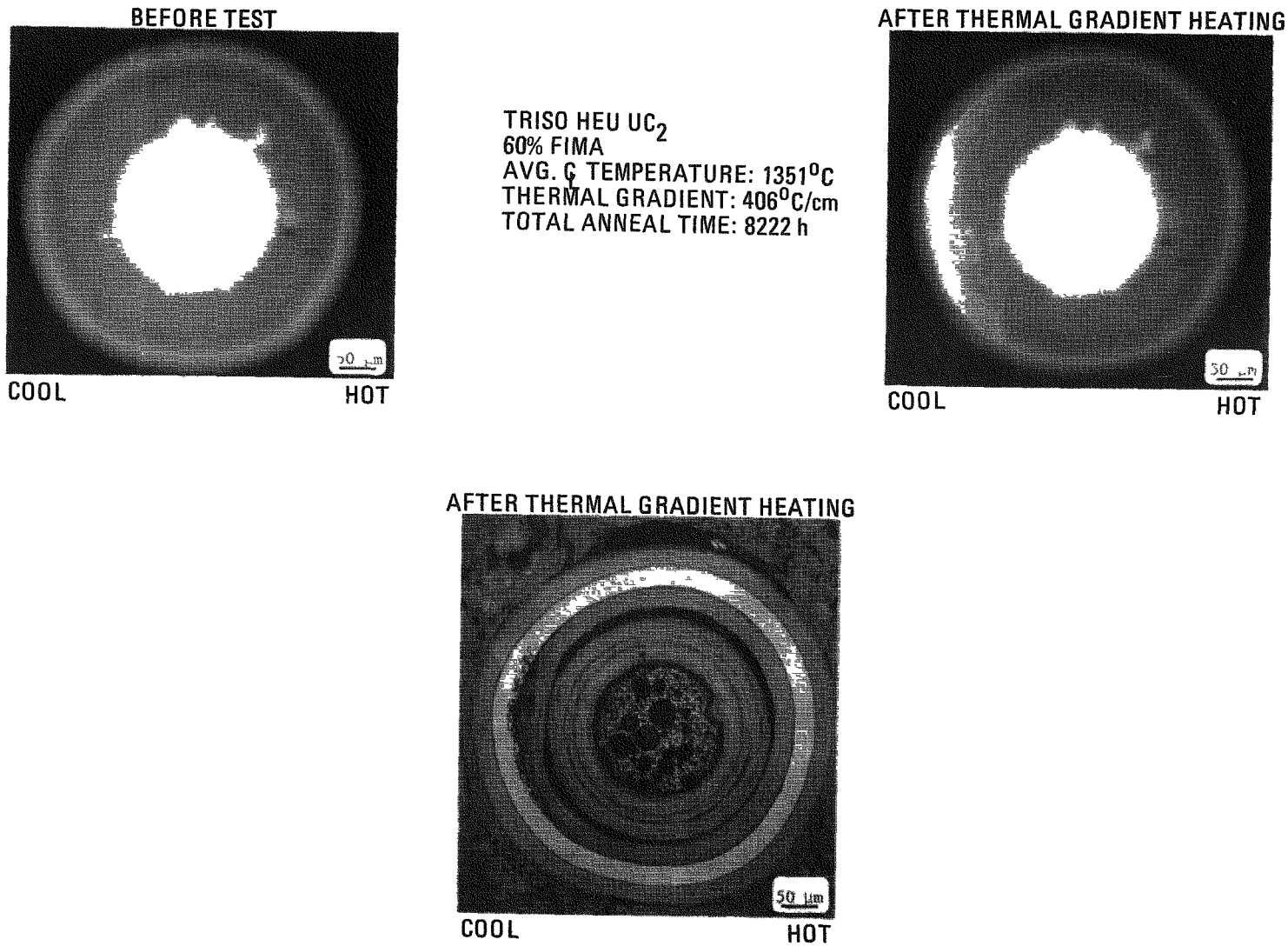

Fig. 3.4 Fission product-SiC reactions resulting from out-of-pile thermal gradient heating of TRISO HEU UC_2 at 1351°C

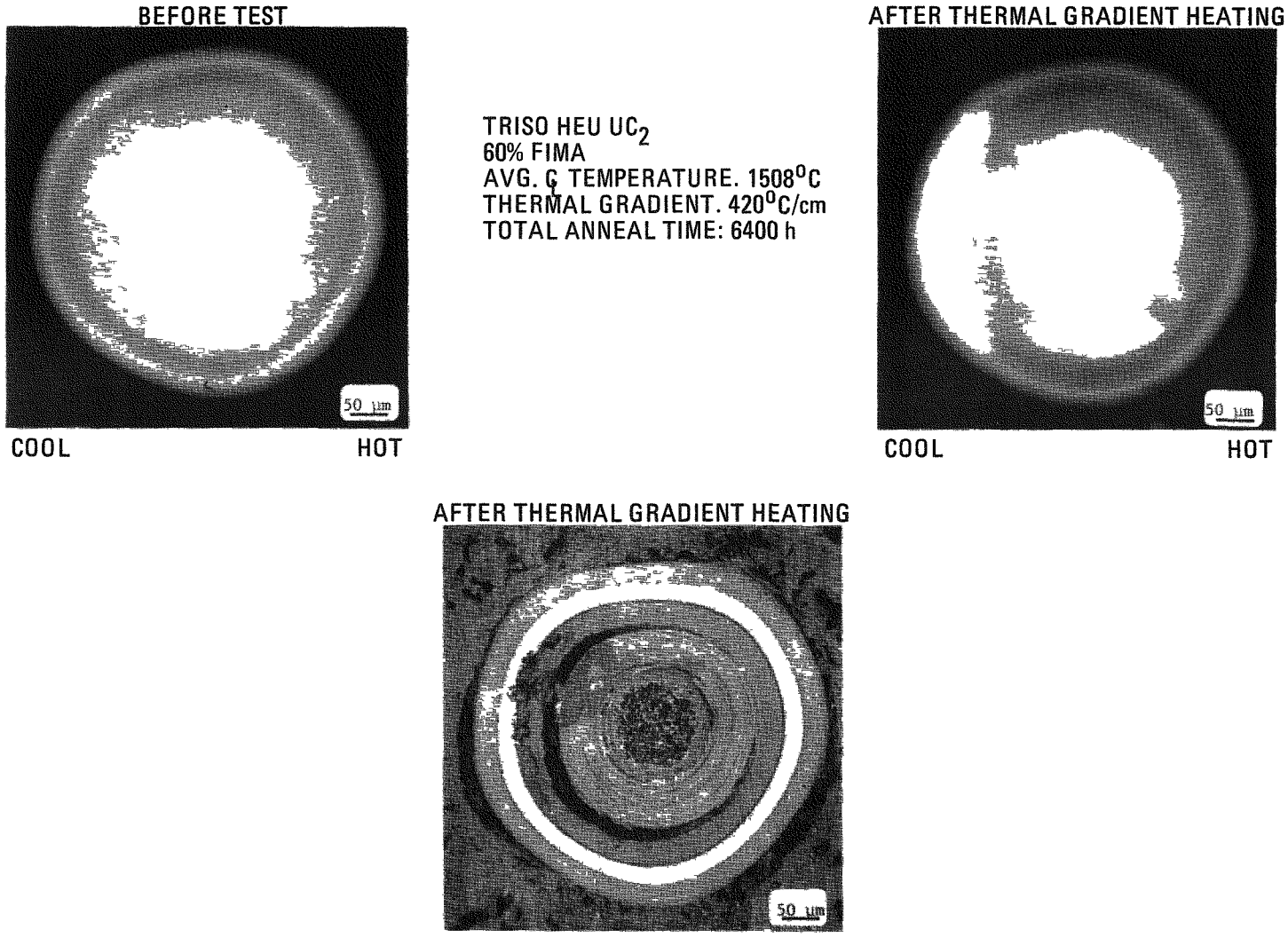

Fig. 3.5 Fission product-SiC reactions resulting from out-of-pile thermal gradient heating of TRISO HEU UC_2 at 1508°C

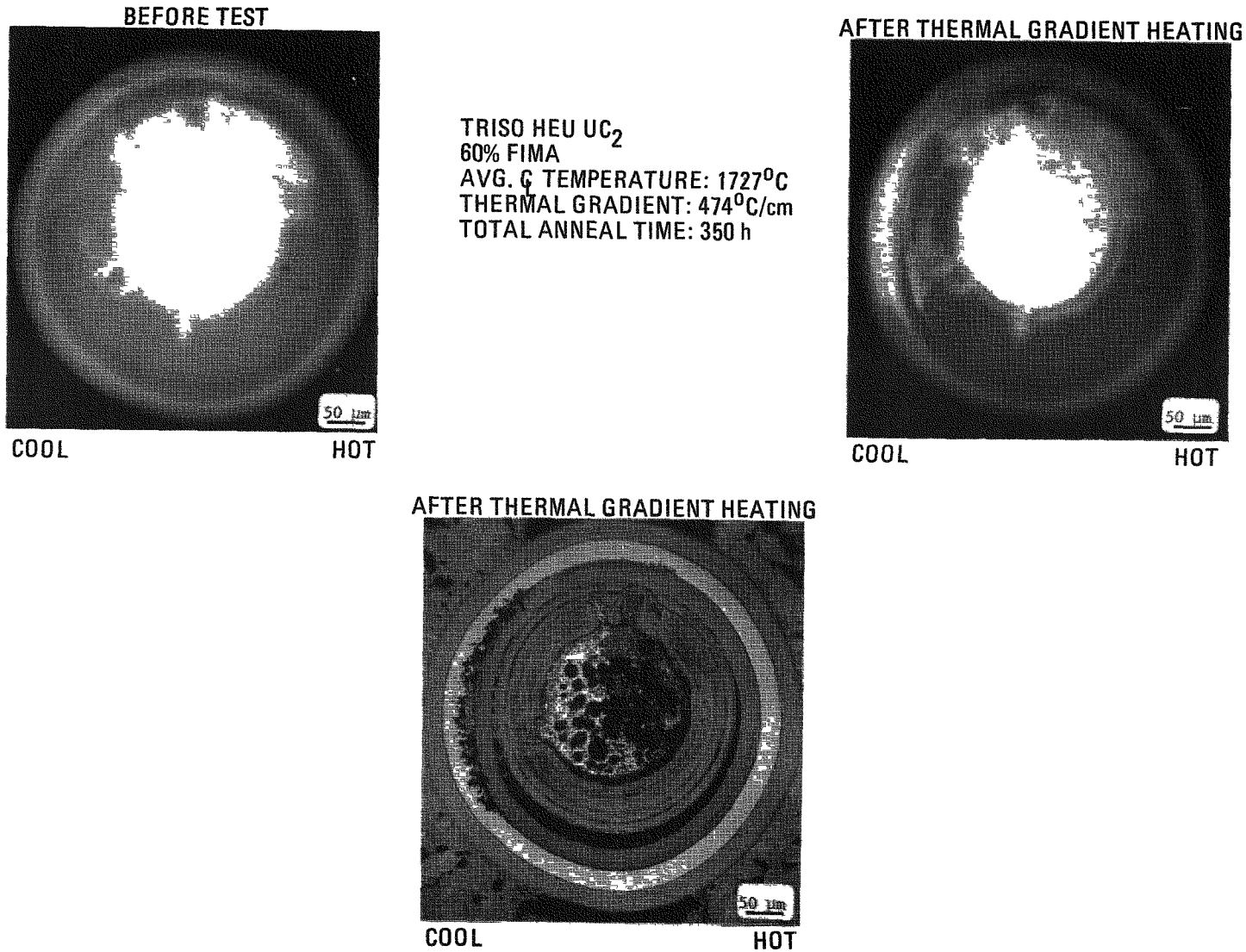

Fig. 3.6 Fission product-SiC reactions resulting from out-of-pile thermal gradient heating of TRISO HEU UC_2 at 1727°C

reactions occurred in particles tested at approximately 1100°C; and that, although the SiC thickness was reduced by reactions occurring in particles tested at higher temperatures, the SiC layer had not been breached by the reactions.

3.1.2 TRISO LEU Fissile Fuel Candidates

Figures 3.7 through 3.10 show contact X-radiographs of representative particles of each of the candidate TRISO LEU fuel types as received after irradiation and after a one-hour anneal at 1200°, 1300° and 1450°C. The radiographs of the as-received particles show that, during irradiation, fission products were not released from the kernel in sufficient quantity to be observed by X-ray radiography. This is due to the low irradiation temperatures (approximately 950°C) of the HRB-15B (Ref. 12) capsule and is consistent with the behavior of the high-enriched TRISO UC_2 which showed dispersion only after heating at >1450°C.

Fission product dispersion is evident in the TRISO LEU UC_2 and TRISO LEU $UC_{.36}O_{1.64}$ after annealing at a temperature exceeding 1200°C and 1300°C, respectively. These temperatures are significantly lower than that observed to cause dispersion in the HEU UC_2.

A slight amount of fission product dispersion was evident in the LEU UO_2 heated at 1450°C for one hour. No dispersion was detected in any of the LEU UO_2* particles after the one-hour anneal. These qualitative observations agree with earlier studies which show that rare earth fission products are not released from kernels that have an O/U ratio greater than 1.1 (Ref. 13); that is, sufficient oxygen to stabilize rare earth fission products as oxides in the kernel.

Pre-test and post-test radiographs as well as post-test photomicrographs on TRISO LEU UC_2, UO_2 and UO_2* thermal gradient annealed for 163 hours at approximately 1500°C are given in Figs. 3.11 through 3.13. Ceramography of the TRISO LEU $UC_{0.36}O_{1.64}$ was not attempted because of FY-81 funding constraints. These radiographs show that because of the thermal gradient heating, fission products accumulated on the cool side of both the TRISO LEU UC_2 and the TRISO LEU UO_2*. The SiC layer in the TRISO LEU UC_2 had been breached by the fission products.

Ceramography of the LEU particles showed three apparently different types of SiC corrosion. In the LEU UC_2, fission products had accumulated on the cool side of the particle and had reacted with the SiC. Figure 3.14 shows that the

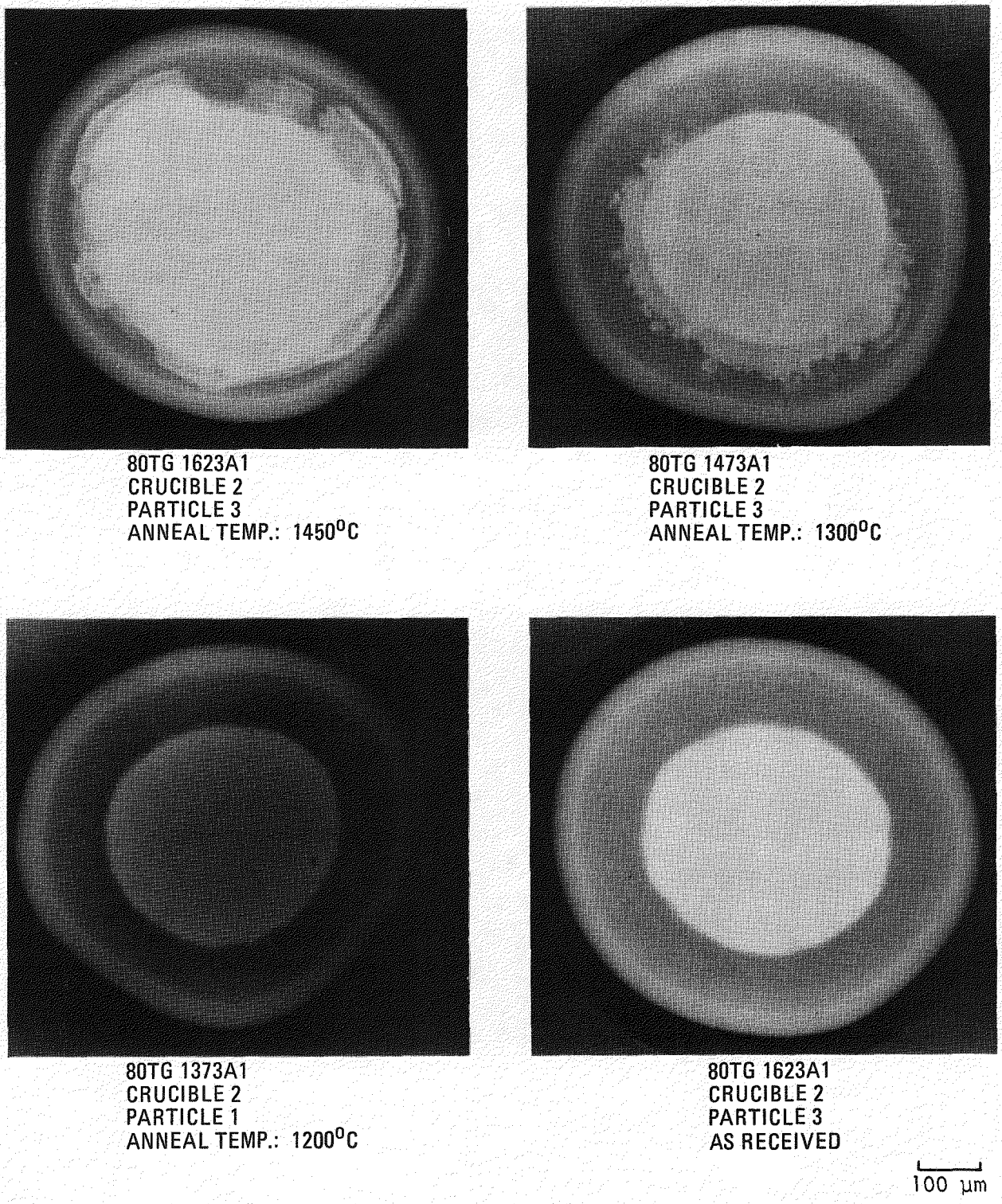

Fig. 3.7 Effect of one hour, out-of-pile heat treatment on fission product distribution in irradiated TRISO LEU UC_2 (6251-21-0111-5)

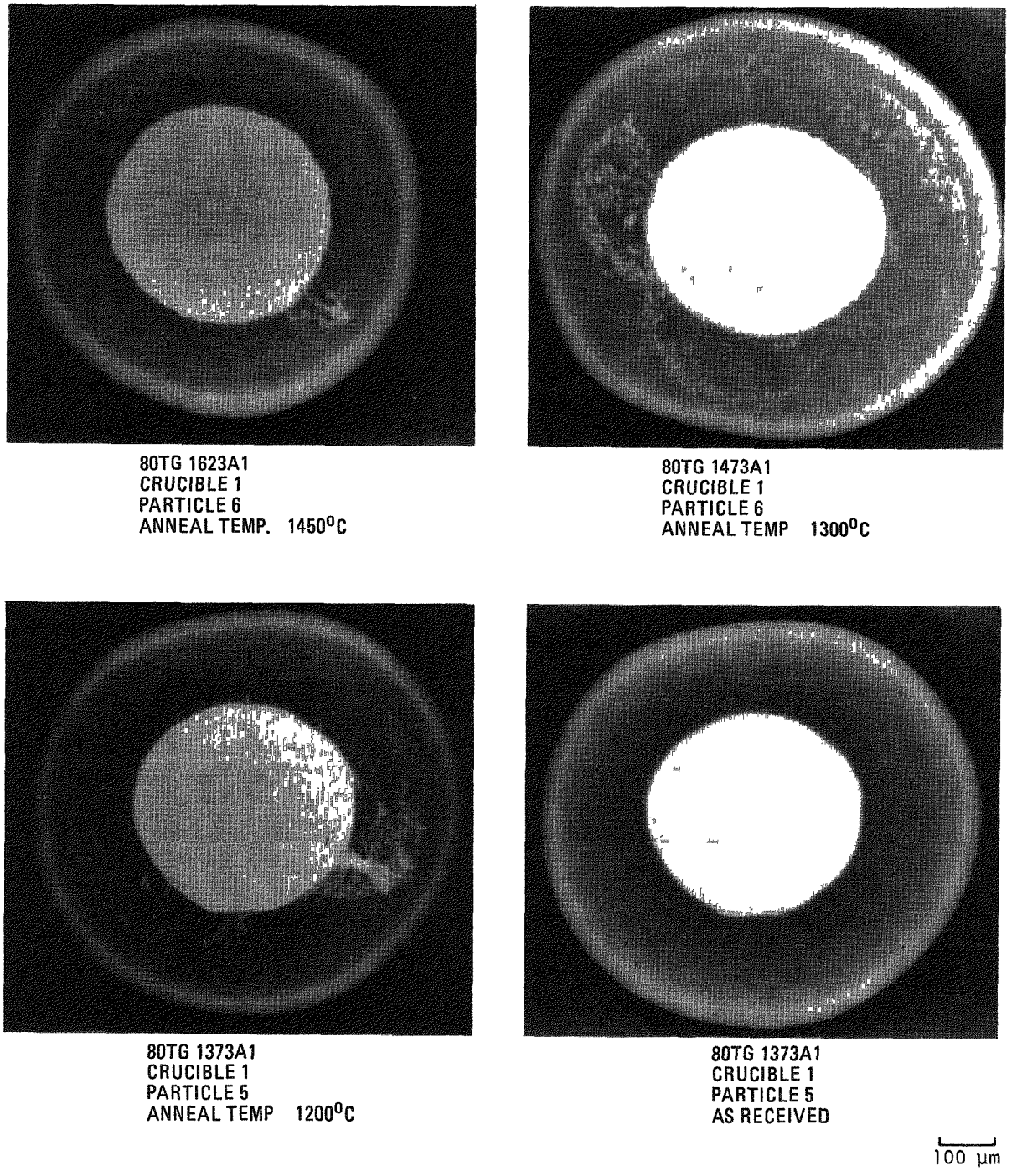

Fig. 3.8 Effect of one hour, out-of-pile heat treatment on fission product distribution in irradiated TRISO LEU $UC_{0.36}O_{1.64}$ (6157-09-0120-1)

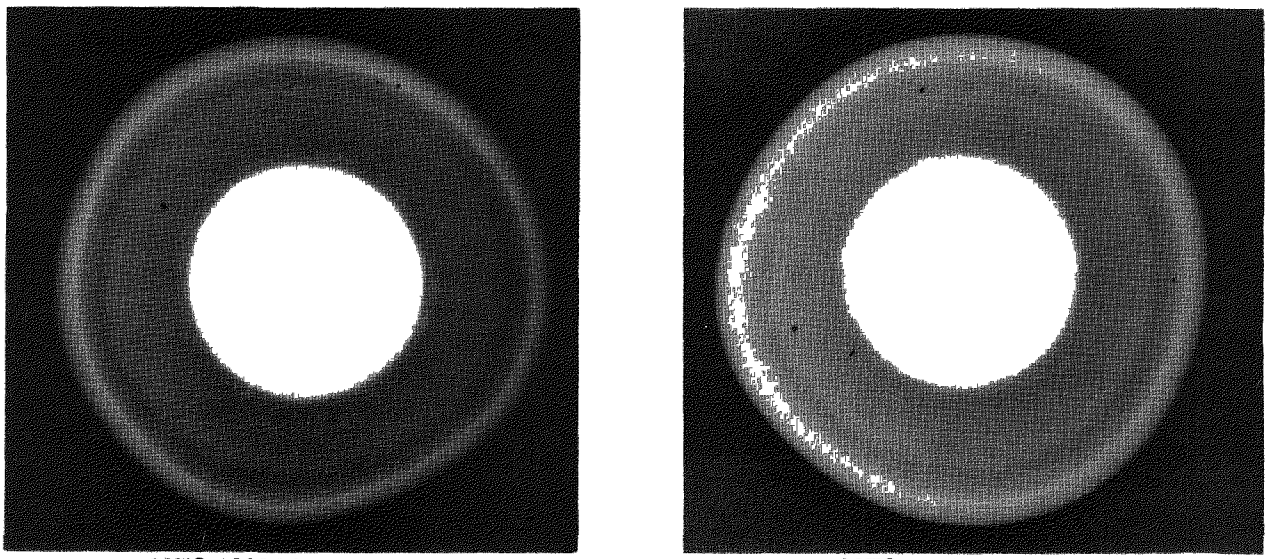

80TG 1623A1
CRUCIBLE 4
PARTICLE 1
ANNEAL TEMP.: 1450°C

80TG 1473A1
CRUCIBLE 4
PARTICLE 1
ANNEAL TEMP.: 1300°C

80TG 1373A1
CRUCIBLE 4
PARTICLE 1
ANNEAL TEMP.: 1200°C

80TG 1373A1
CRUCIBLE 4
PARTICLE 1
AS RECEIVED

100 µm

Fig. 3.9 Effect of one hour, out-of-pile heat treatment on fission product distribution in irradiated TRISO LEU UO_2 (6152-01-0111-3)

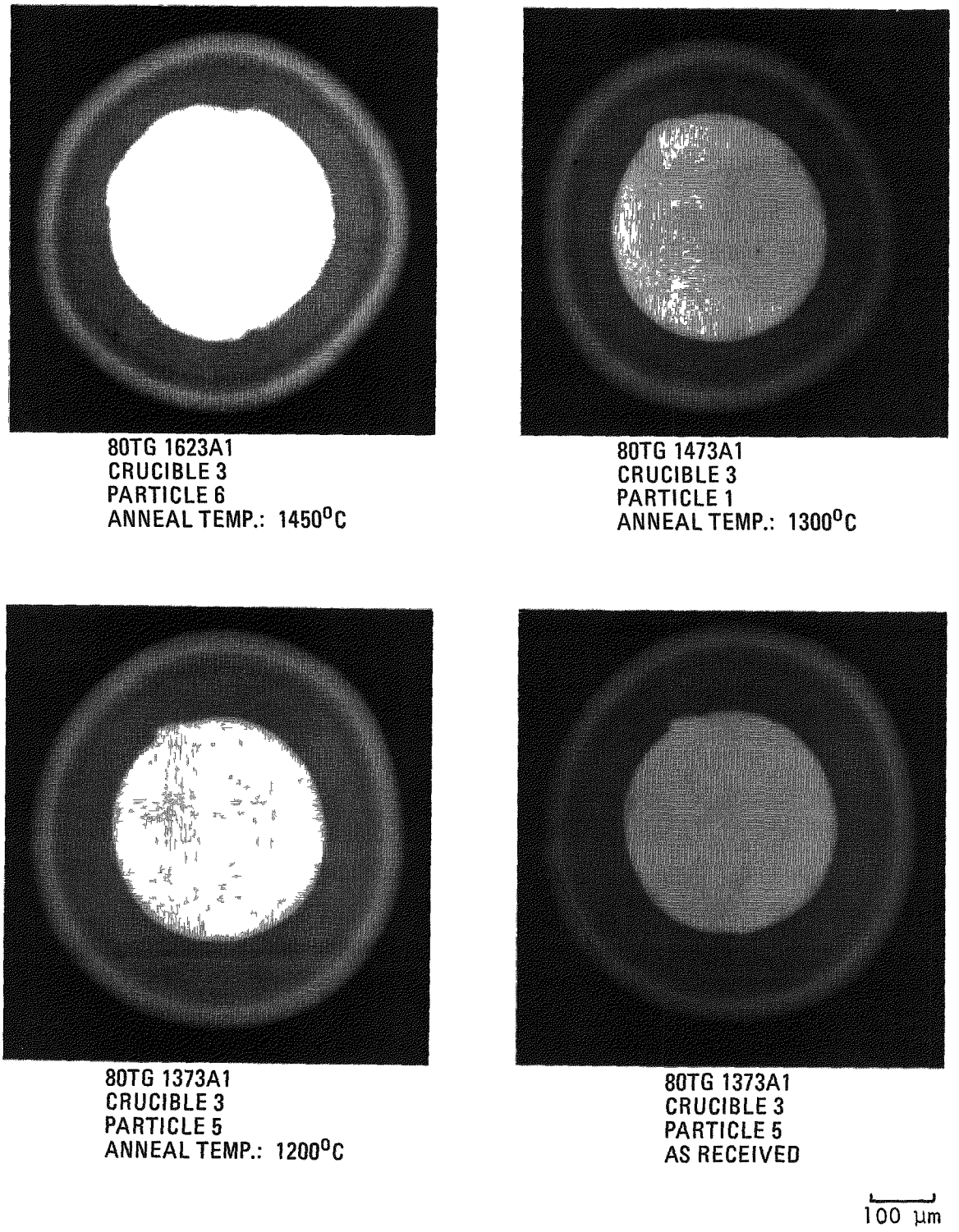

Fig. 3.10 Effect of one hour, out-of-pile heat treatment on fission product distribution in irradiated TRISO LEU UO_2* (6152-03-0111-6)

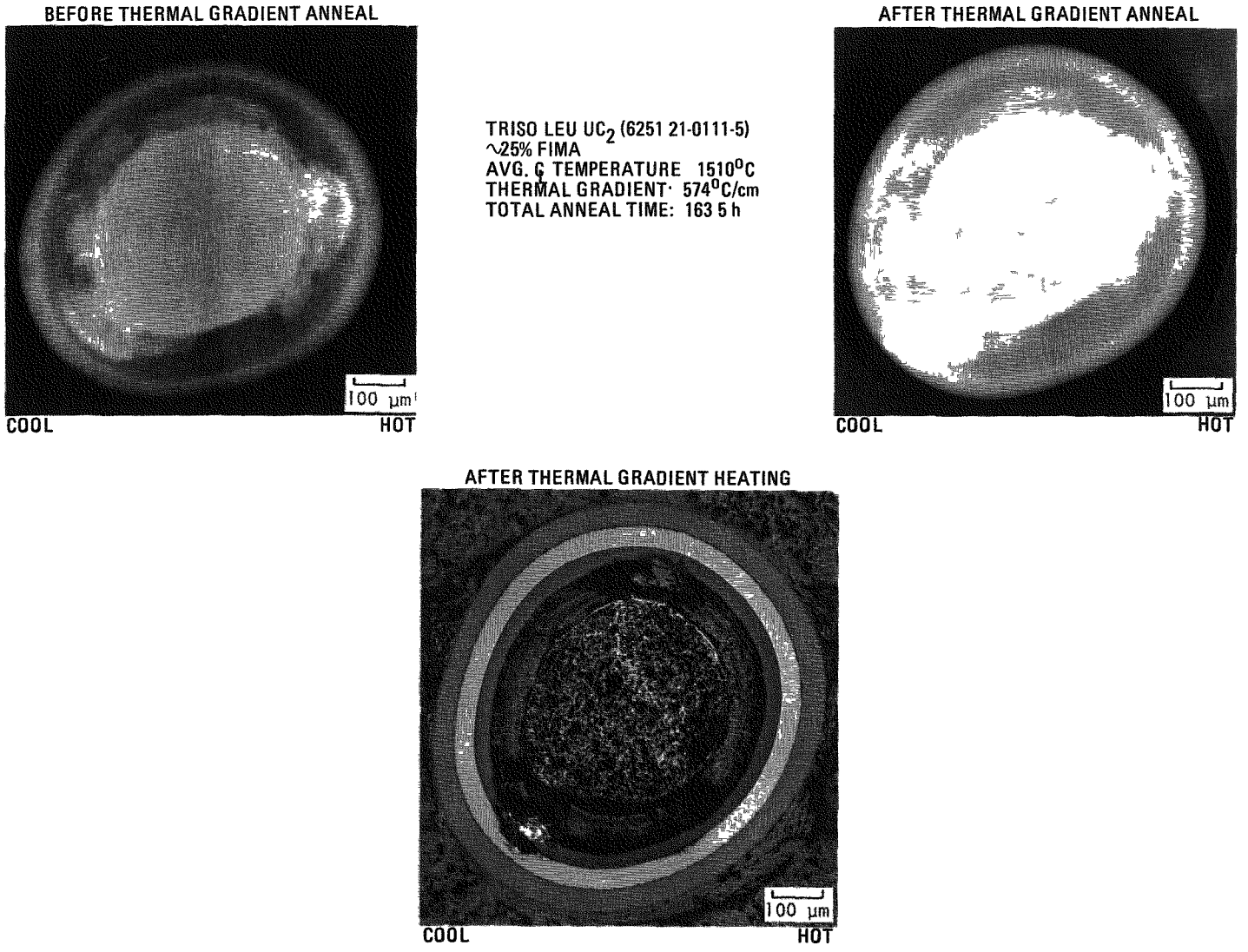

Fig. 3.11 Fission product-SiC reactions resulting from out-of-pile thermal gradient heating of LEU UC_2 at 1510°C

Fig. 3.12 Pretest and posttest radiograph and posttest photomicrograph of TRISO LEU UO_2 annealed at 1513°C in an out-of-pile thermal gradient

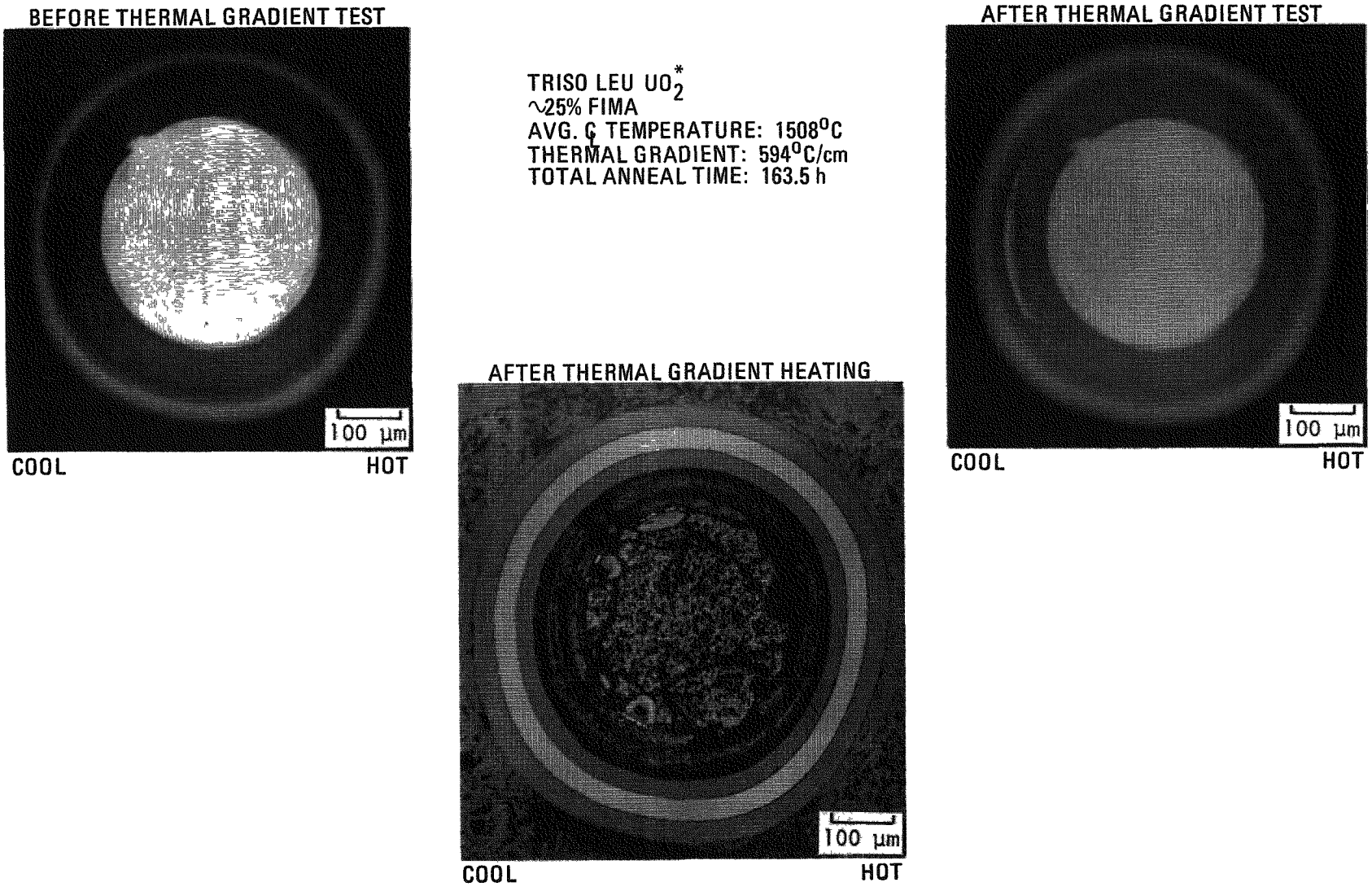

Fig. 3.13 Pretest and posttest radiographs and posttest photomicrograph of TRISO LEU UO_2* annealed at 1508°C in an out-of-pile thermal gradient

reaction caused substantial thinning of the SiC thickness. Associated with this reaction are distinct localized nodules of fission products which appear white in the photomicrographs.

The second type of SiC corrosion occurred on the hot side of the LEU UC_2 particles. This corrosion, shown in Fig. 3.14C, appears to be as small, pin-hole voids in the SiC. These voids were uniformly distributed through the SiC but only on the hot side of the particle.

The third type of SiC corrosion, shown in Fig. 3.15, occurred only in the TRISO LEU UO_2. This corrosion was observed when TRISO LEU UO_2 (Data Retrieval No. 6152-01-0111-3) was heated above 1500°C. The large voids observed in the SiC layer in Fig. 3.15 are evenly distributed around the circumference of the SiC layer. The majority of these voids occurred in the outer 50% of the SiC layer near the interface of the SiC and outer PyC layers. No fission products reacted with the SiC at the inner surface of the SiC layer in the TRISO LEU UO_2.

3.2 Electron Microprobe (EMP) Examination

To determine which fission products reacted with the SiC, electron microprobe analysis was completed on samples of TRISO HEU UC_2, TRISO LEU UC_2, TRISO LEU UO_2 and TRISO LEU UO2*. Figure 3.16 shows the areas in each particle that were studied by EMP x-ray analyses. The darkened areas in the photomicrographs are carbon accumulations on the surface of the particle caused when the electron beam swept over the area. The thin darkened lines on the UO_2 particle show where EMP line traces were obtained.

3.2.1 TRISO HEU UC_2

Electron microprobe analysis was done on samples from batch 6151-17-016 that were heated at 1508°, 1351°, and 1101°C. Figure 3.17 is a photomicrograph of the cool side of a particle heated at 1508°C for 6400 h. Superimposed on the photomicrograph is the location of the fission products found near the fission product - SiC reaction zone. Palladium and ruthenium accumulated in distinct nodules that appear white in the photomicrograph. The nodules are located at

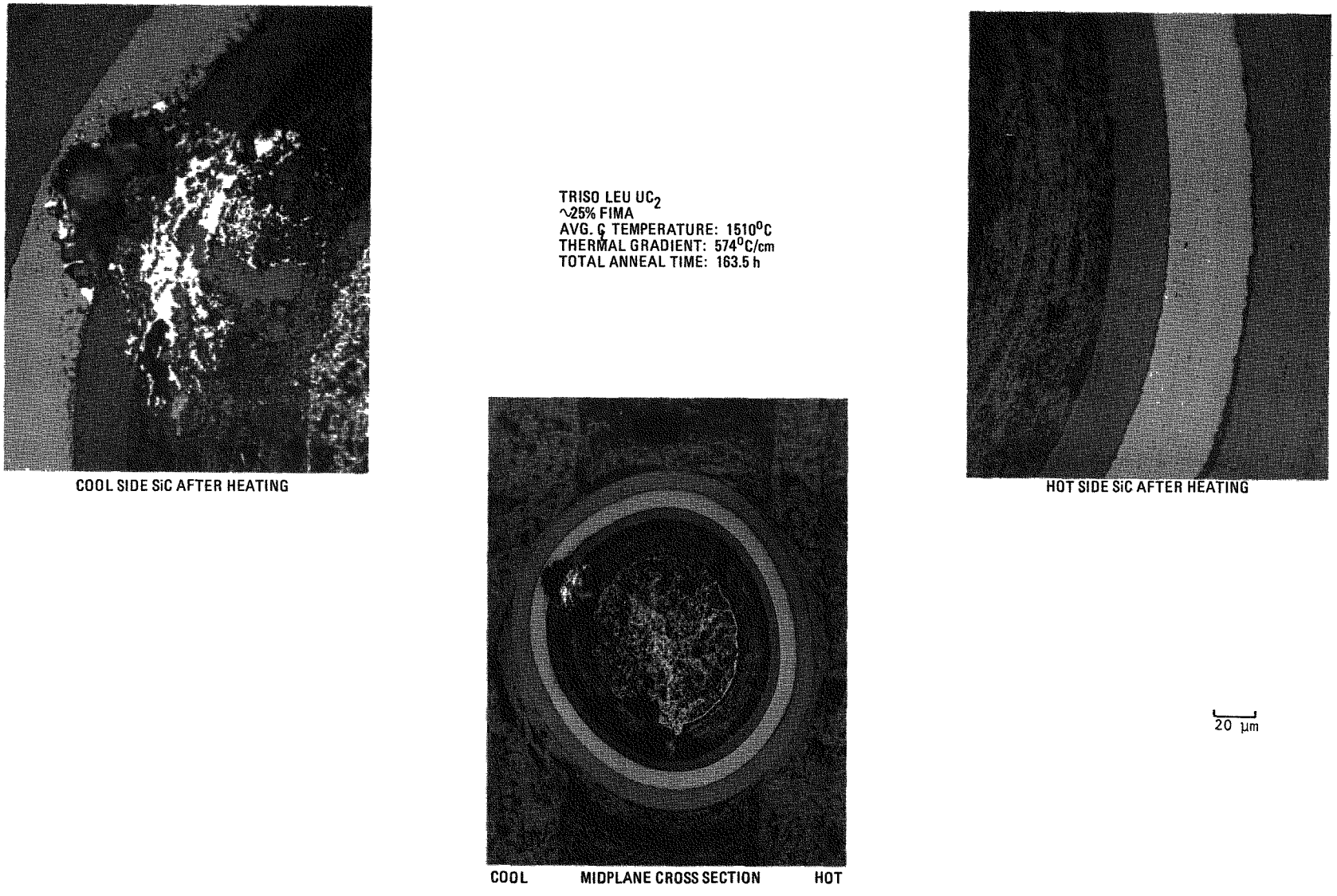

Fig. 3.14 SiC corrosion observed in TRISO LEU UC_2 after out-of-pile thermal gradient heating at 1510°C

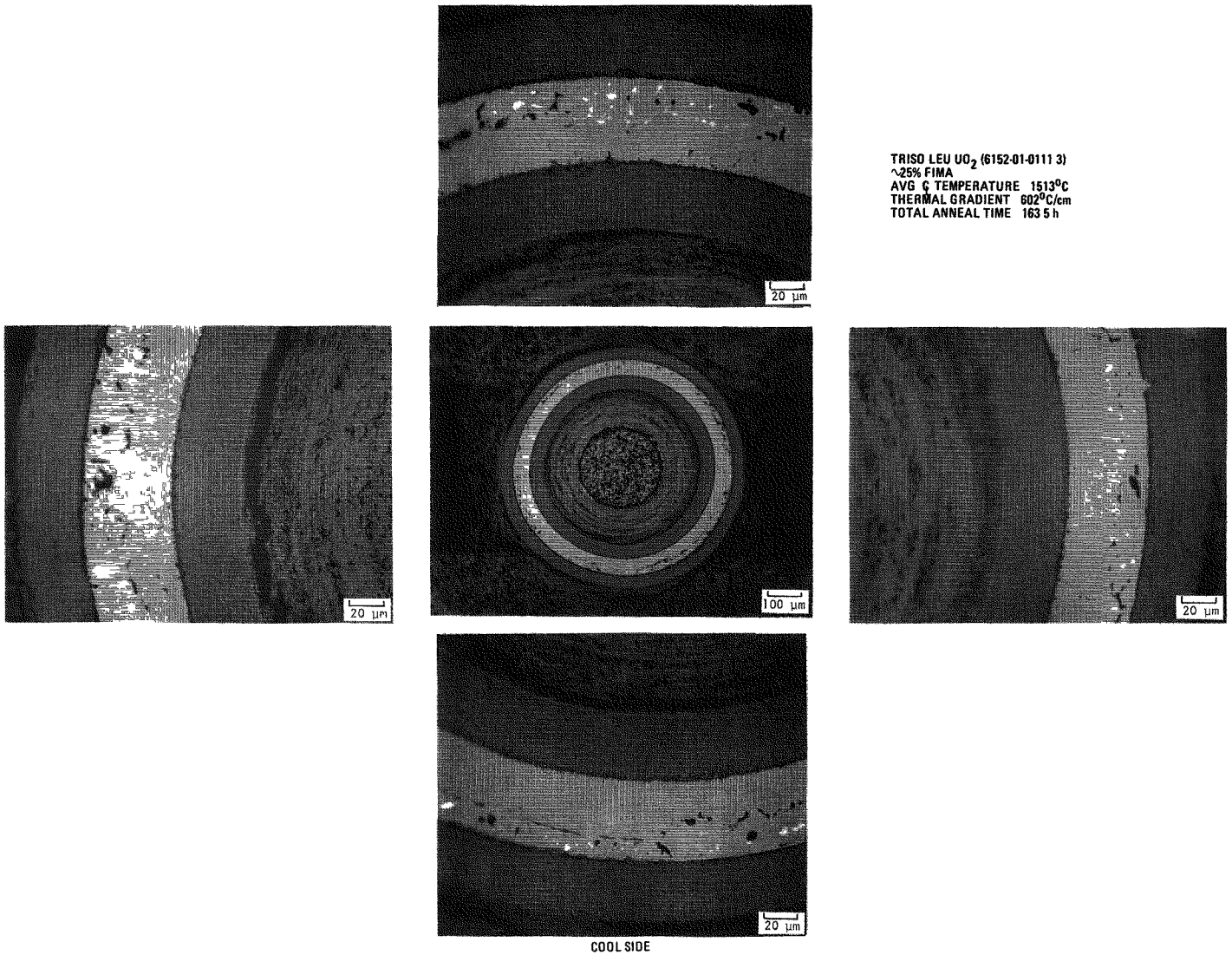

Fig. 3.15 SiC corrosion in TRISO LEU UO_2 caused by out-of-pile thermal gradient heating at 1513°C

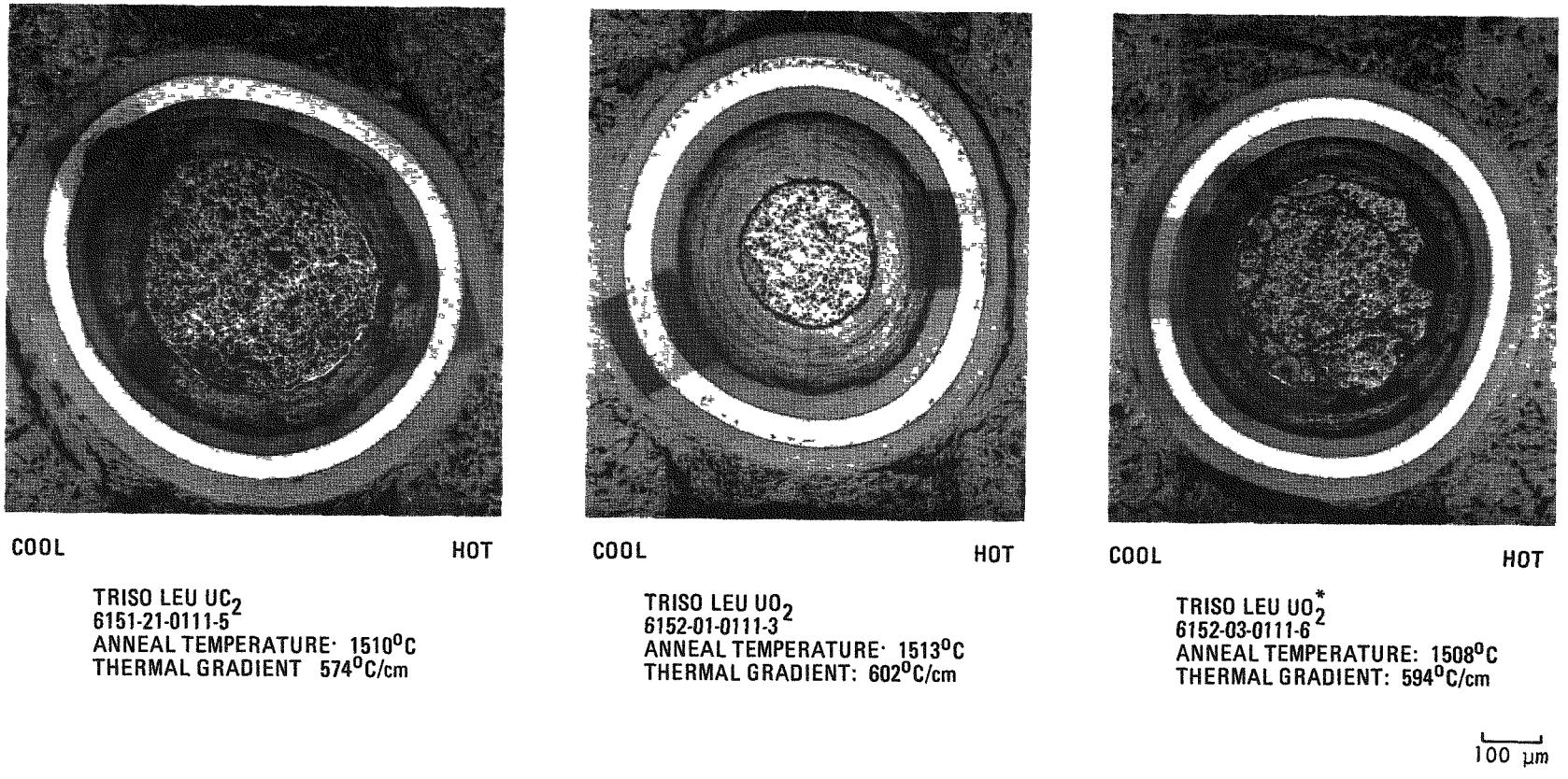

Fig. 3.16 Regions in irradiated LEU TRISO particles which were examined by electron microprobe analysis after 163.5 hr thermal gradient anneal at ∿1500°C

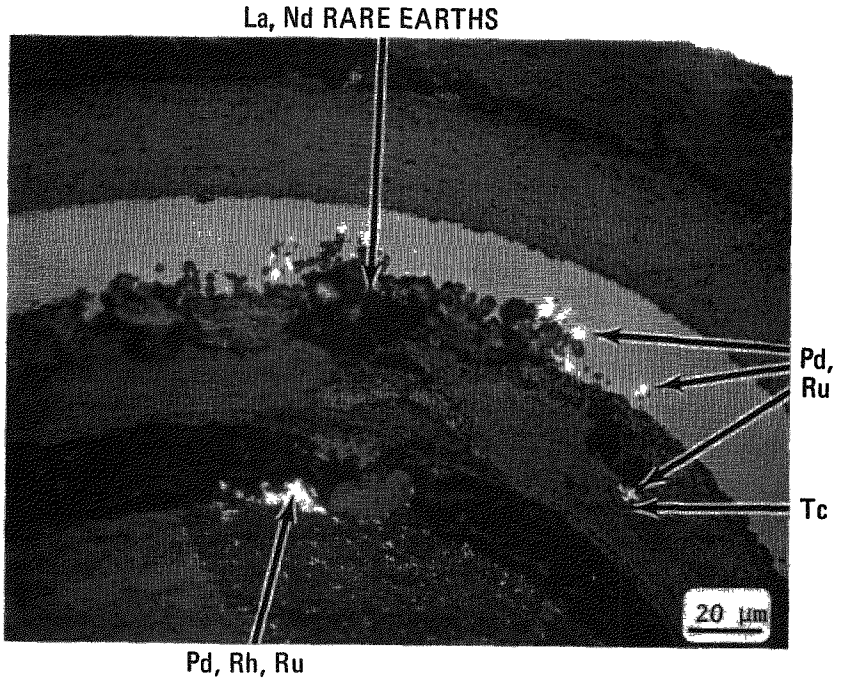

Fig. 3.17 Fission product attack on SiC layer in TRISO HEU UC_2 (60% FIMA) heated at 1508°C in an out-of-pile thermal gradient test

the leading edge of the reaction zone in the SiC. Rare earth fission products are also concentrated in the reaction zone but are not associated with the white phases that contain palladium and ruthenium.

Figures 3.18 and 3.19 show photomicrographs and electron microprobe results obtained on TRISO HEU UC_2 fuels tested at 1351° and 1101°C. General observations are qualitatively the same as those discussed for Fig. 3.17.

Line scans were also made from the kernel through the SiC to show, in a more precise way, the actual locations of palladium, rare earths, and silicon. Samples from particles tested at 1101° and 1351°C are shown in Figs. 3.20 and 3.21. The results show that the depths of palladium and rare earth (neodymium) penetration into the SiC are the same. They also suggest some palladium and rare earth penetration occurred at 1101°C even though no visible reactions occurred.

3.2.2 TRISO LEU Fissile Fuel Candidates

Electron microprobe analysis was completed on samples of TRISO LEU UC_2 (6151-21-0111-5), UO_2 (6152-01-0111-3) and UO_2* (6152-03-0111-6). Due to the FY-87 funding constraint, the sample of TRISO LEU $UC_{0.36}O_{1.64}$ (6157-09-0120-1) was not mounted and sectioned. These particles had been heated for 163.5 hours in a thermal gradient at approximately 1500°C.

3.2.2.1 TRISO LEU UC_2. EMP X-ray analysis of the LEU UC_2 showed fission product behavior similar to that obtained with HEU UC_2: U, Ru, Rh, Pd and rare earth elements were found in the zone of SiC attack (Fig. 3.22).

Silicon had been transported from the SiC and accumulated in the inner PyC associated with concentrations of the above elements.

X-ray distribution patterns for the hot side of a LEU UC_2 particle heated at 1514°C are shown in Fig. 3.23. Uranium had migrated into the inner pyrocarbon but had not reached the SiC. The only fission product found on the hot side was a small amount of Nd located at the inner surface of the SiC.

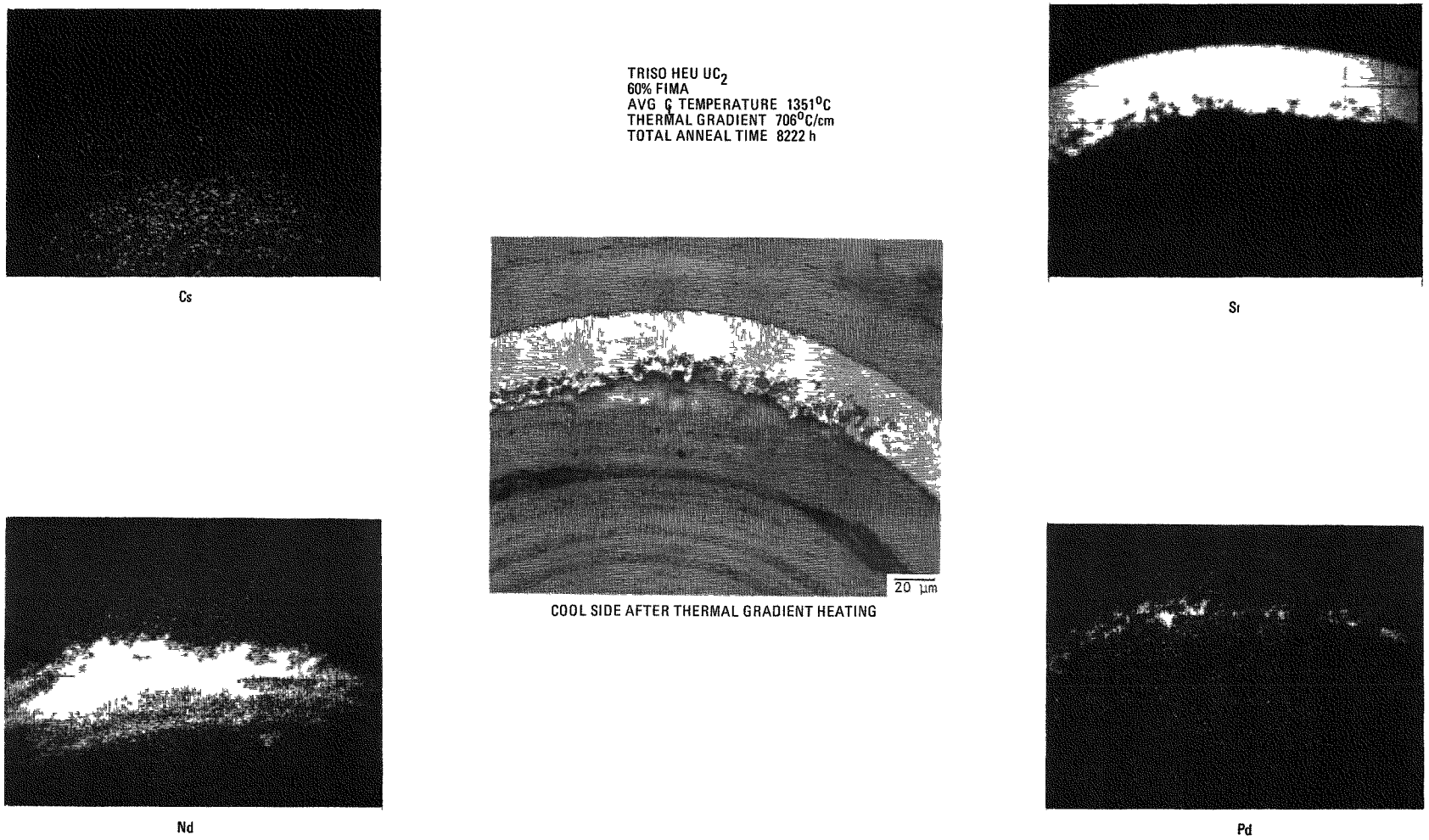

Fig. 3.18 Fission product distribution near SiC attack resulting from out-of-pile thermal gradient heating of TRISO HEU UC_2 at 1351°C

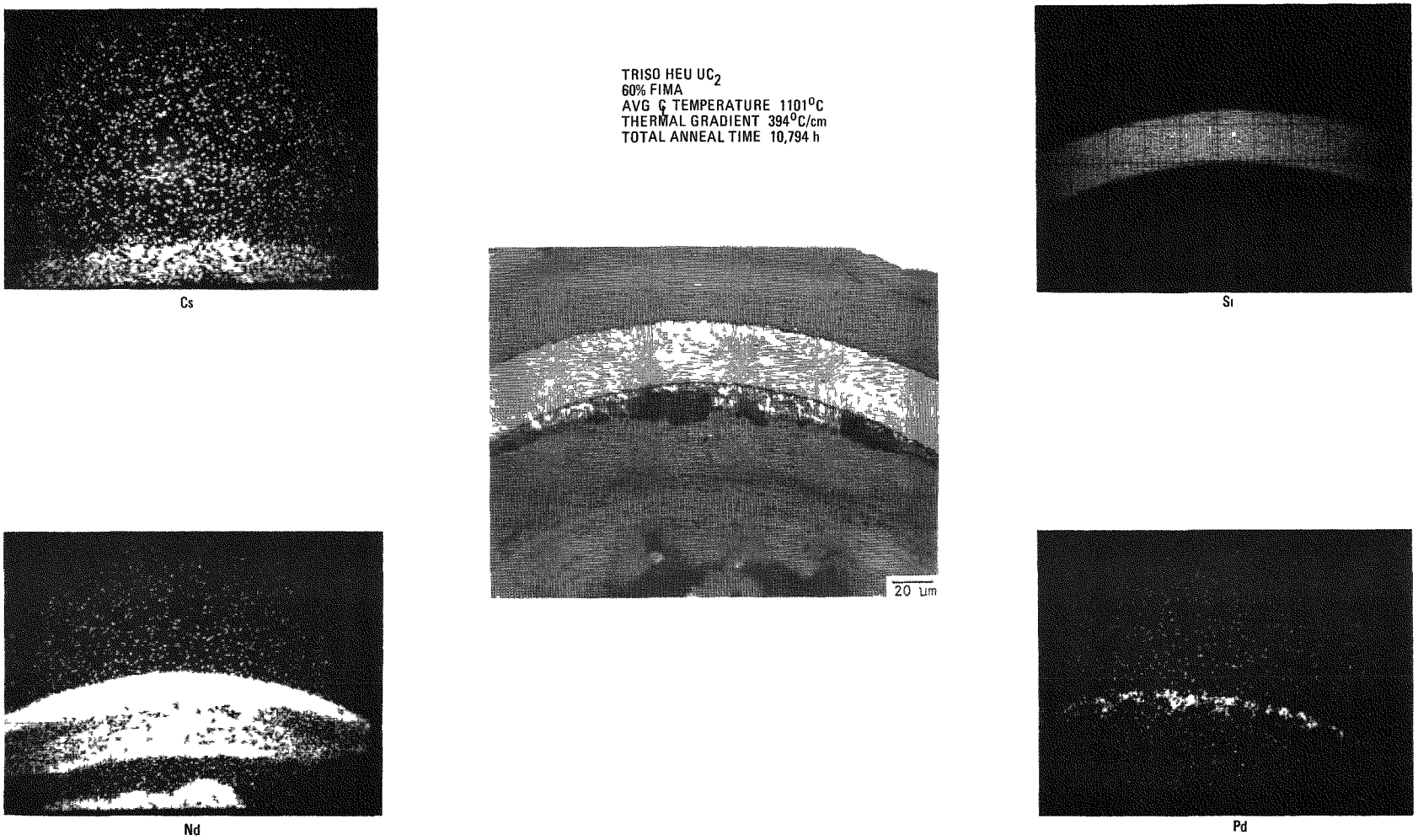

Fig. 3.19 Fission product distribution near SiC attack resulting from out-of-pile thermal gradient heating of TRISO HEU UC_2 at 1101°C

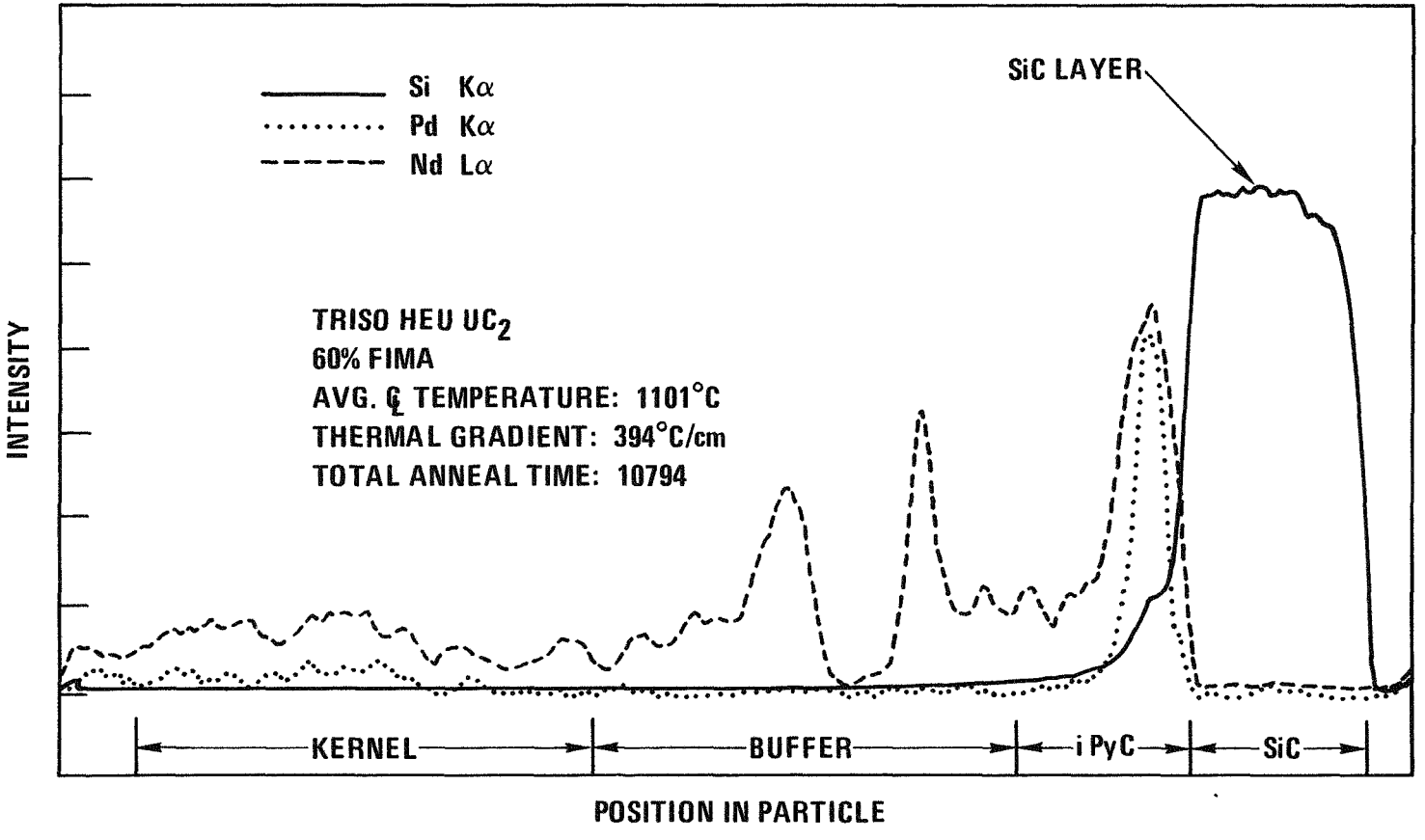

Fig. 3.20 Electron microprobe line scans across SiC for HEU UC_2 (60% FIMA) annealed 10,763 hr. at 1101°C

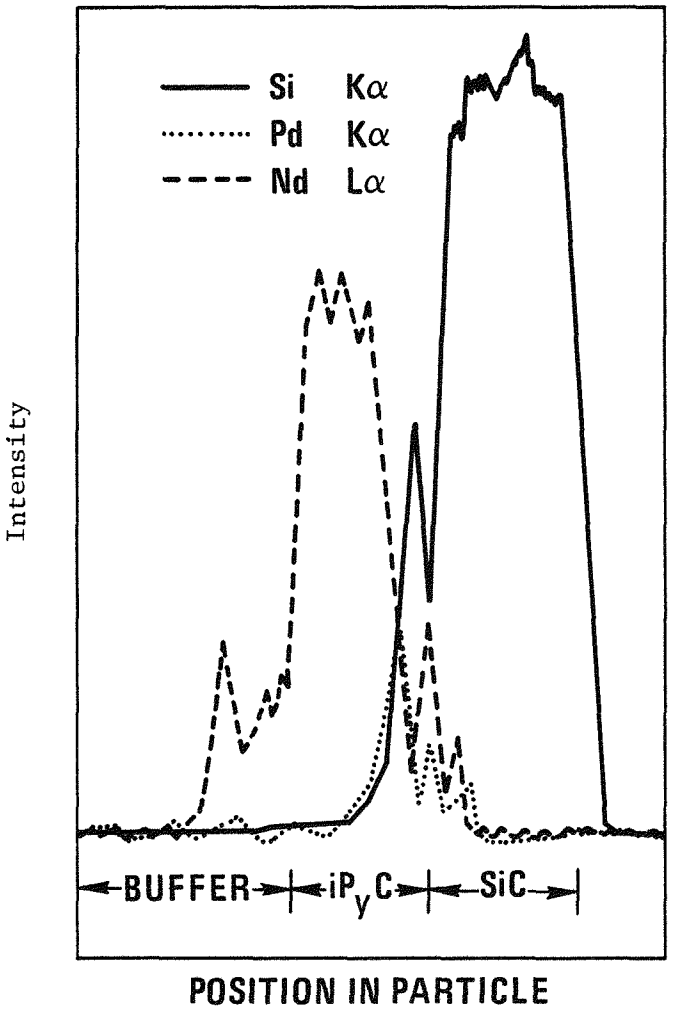

Fig. 3.21 Nd, Pd, and Si profiles measured by electron microprobe on TRISO HEU UC_2 (60% FIMA) particles annealed 8222 hr. at 1351°C

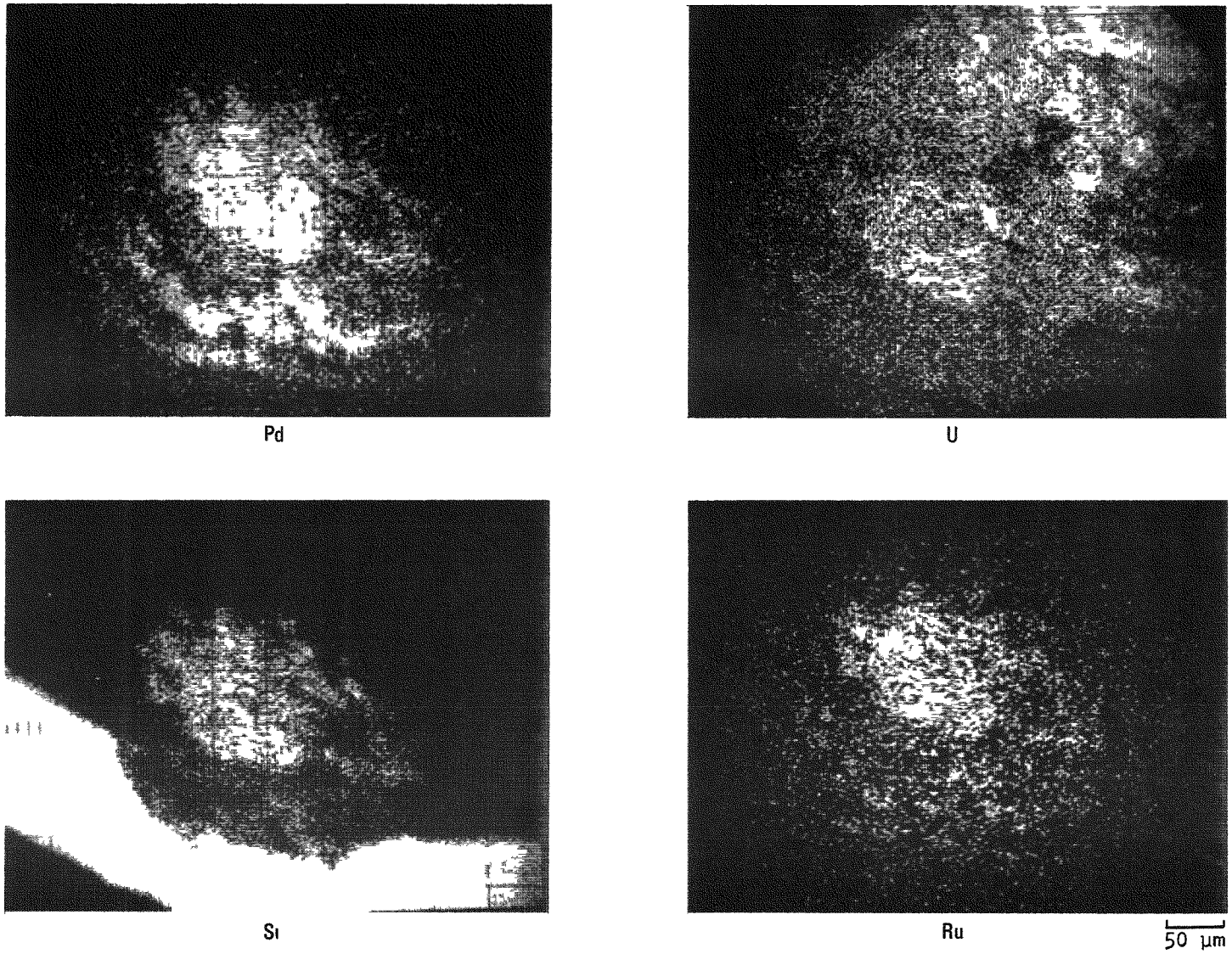

Fig. 3.22 Fission products in the SiC corrosion zone after heating TRISO LEU UC_2 at 1510°C for 163.5 hr

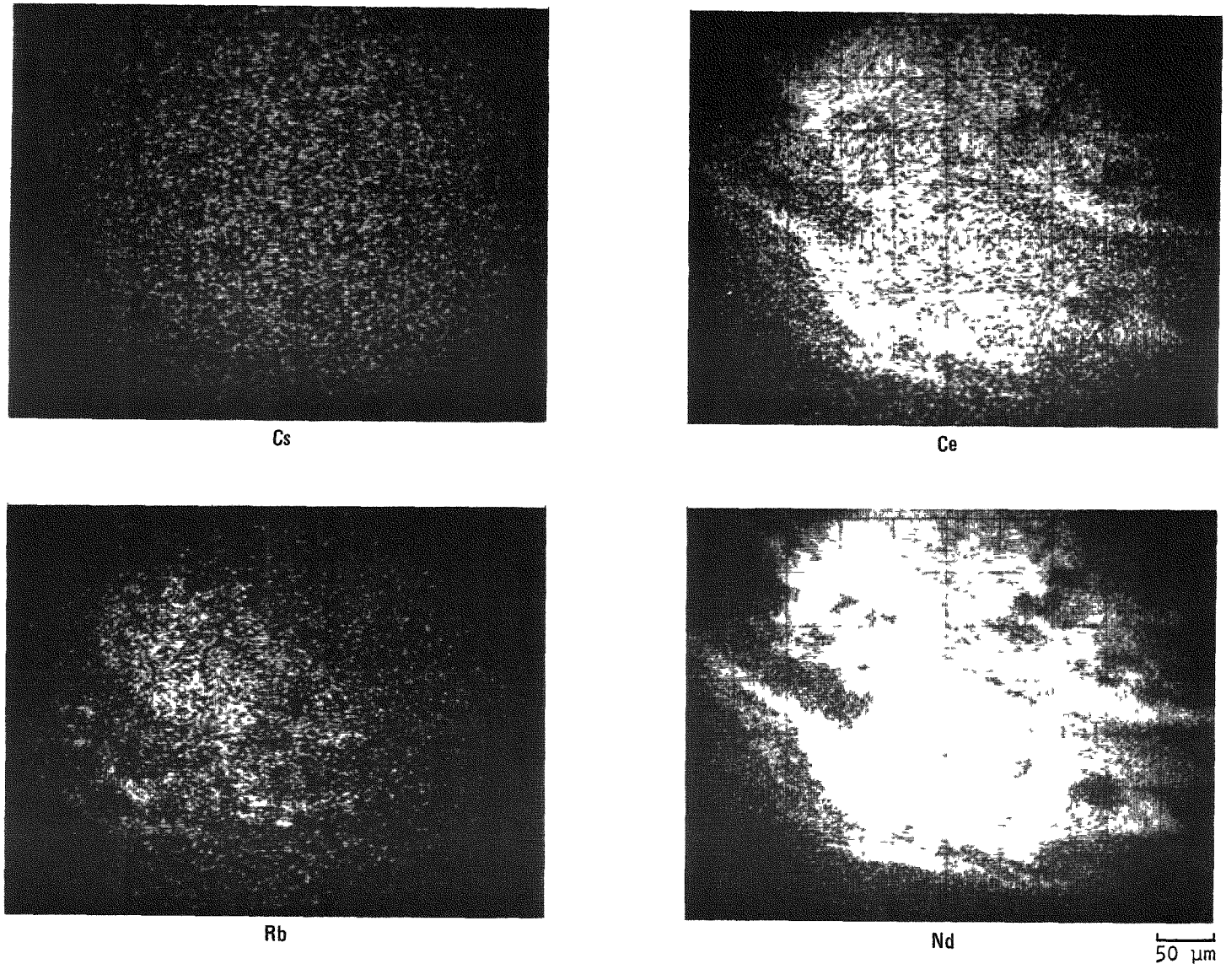

Fig. 3.22 Fission products in the SiC corrosion zone after heating TRISO LEU UC_2 at 1510°C for 163.5 hr (continued)

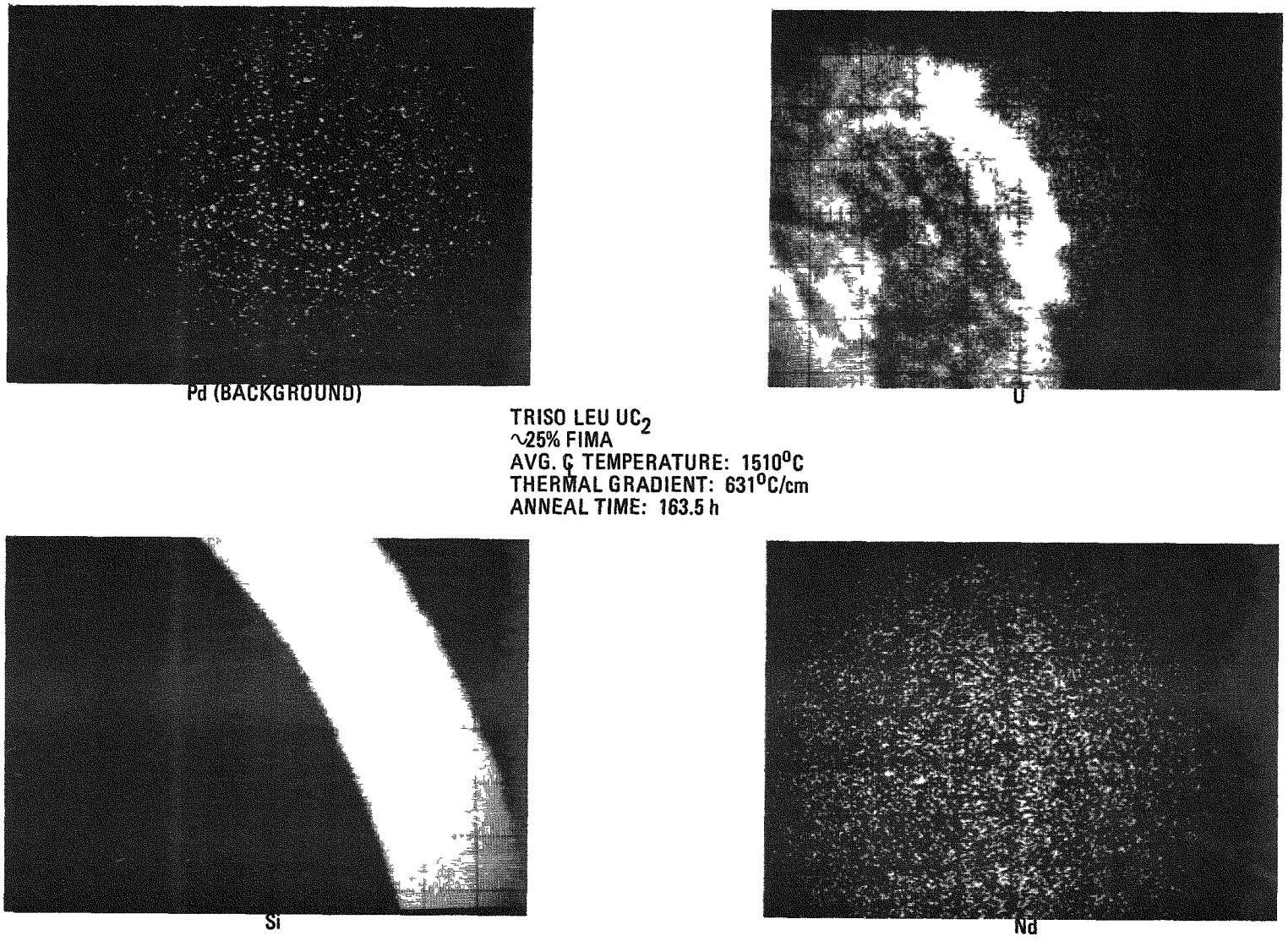

Fig. 3.23 Metal distribution on hot side of TRISO LEU UC_2 particle heated in a thermal gradient at 1514°C

An attempt was made to identify the chemical form of the fission products found on the cold side of the particle. The atom fractions of Si, U, Ru, Rh, Nd, Pd and C were measured in two regions. The first region, designated X_1-X_y in Fig. 3.24 was bound by the original SiC thickness and included the area of fission product corrosion of the SiC. The second region, designated by .1 - .4, was the white phase in the inner PyC in which the fission products had concentrated. The atomic ratios are given in Table 3.2.

3.2.2.2 TRISO LEU UO_2

Figure 3.25 shows EMP X-ray distribution patterns for Si and Pd on the hot and cool side of the particles after heating at 1513°C. Although the SiC had numerous holes (Fig. 3.15), Pd had accumulated at the SiC surface on both the hot and cool sides of the particle. Nd, Ce, Ag, Sr, Ru, Rh, Co, U and Mo could not be detected near the SiC layer. EMP determination of the Pd/Si ratio at the SiC boundary indicated that Pd had reacted with the silicon to form Pd_3Si. In addition the white metallic inclusions in the SiC layer of the TRISO LEU UO_2 were shown by EMP to be ∿100% silicon.

3.2.2.3 TRISO LEU UO_2*

Irradiated, thermal gradient annealed, LEU UO_2* exhibited fission product distributions similar to the LEU UO_2. Pd was the only fission product found at the SiC interface, and it was found only on the cool side of the particle. Si and Pd line traces across the SiC are shown in Figure 3.26. These traces show that Pd has diffused at least 2/3 of the way through the SiC even though no visual SiC corrosion has occurred.

3.3 Fission Product Release

Fission product - SiC reactions could penetrate the SiC layer if allowed to continue long enough at high enough teperatures or lead to premature cracking of the SiC in regions where the cross section was reduced by the reactions. In either case, cesium release would be expected and could be used as a SiC failure criterion. Noble gases, on the other hand, are retained in the particle by the intact outer PyC layer. Thus noble gas release indicates failure of both the outer PyC and the SiC layers. Ag release from particles is also of interest because of the influence of silver release on activity in the

Table 3.2

ATOMIC RATIO OF ELEMENTS FOUND IN THE VICINITY OF THE SiC CORROSION IN TRISO LEU UC_2

Site	C/Pd	Si/Pd	U/Pd	Ru/Pd	Rh/Pd	Nd/Pd	Ce/Pd	La/Pd
.1	66	8.1	.36	7.4	.51	.56	.05	.03
.2	22	9.6	.32	5.1	.64	.37	.05	.03
.3	22	9.9	.36	4.6	.51	.38	.09	.04
.4	32	11.4	.65	7.3	.25	.32	.05	.04
X1	2	19	.20	2.1	.55	.37	.08	.02
X2	13	6.1	.86	2.1	.56	.37	.08	.45
X3	54	4.1	1.06	4.0	.68	59	.06	.41
X4	4	18	.15	2.0	.59	.44	.05	.03

primary circuit and the attendant implications to maintenance of the reactor. Silver release has also been observed from particles that have successively retained cesium (Ref. 14).

Thus Cs-137, Kr-85 and Ag-110m were monitored during the out-of-pile thermal gradient heating tests to determine the integrity of the particle coatings.

3.3.1 TRISO HEU UC_2

Cesium-137 inventories of the TRISO HEU UC_2 particles were monitored by gamma counting the samples during periodic test interruptions. The variation in Cs-137 inventory with time is shown for each test in Figs. 3.27 through 3.30. The results show that no detectable cesium release occurred during 10,763 h at ∿1100°C, 8222 h at 1350°C, or 6400 h at ∿1500°C. This suggests that fission products did not penetrate the SiC or lead to mechanical failure of the SiC and is consistent with metallography, X-ray, and electron microprobe analyses of the samples. One of the samples heated at 1709°C for 348.5 h released ∿15% of its inventory after 100 to 150 h at temperature (Fig. 3.30). This is equivalent to one failed particle. The other sample showed no cesium release, implying no SiC failure.

3.3.2 TRISO LEU Fissile Fuel Candidates

The fraction of Cs-137, Kr-85 and Ag-110m released from the LEU fuel samples during the out-of-pile thermal gradient tests are given in Table 3.3 Cs-137 release was observed from the LEU UO_2 samples that were heated at 1500°C. The release fractions include Cs-137 that was released during the one hour carbonizing anneal. The 1773A1 tests were fired at ∿1600°C and LEU UO_2 released ∿7% of its initial Cs-137. The UO_2 particles in the 1973A1 test were annealed at 1700°C and ∿58% of the Cs-137 was lost. The high release of Cs-137 from the LEU UO_2 samples was unexpected, since HEU UC_2 tested for 6400 hours at 1500°C did not release Cs-137 (see 3.3.1).

Release of Kr-85 indicates failure of the outer PyC layer. Table 3.3 shows that even though Cs-137 was released from the LEU UO_2 samples at 1500°C and 1700°C, the outer PyC was still intact and capable of retaining Kr-85.

Table 3.3

RELEASE FRACTIONS FOR SAMPLES OF LEU
FISSILE FUEL HEATED IN OUT-OF-PILE THERMAL GRADIENT TESTS

Parameter	Experiment				
	1373A1	1473A1	1623A1	1773A1	1973A1
Accumulated Hours	2158	2051.5	2253.5	163.5	116
Test Temperature, °C					
UC_2	1093	1207	1368	1510	1704
$UC_{0.36}O_{1.64}$	1108	1204	1322	1500	1717
UO_2	1100	1203	1333	1513	1705
UO_2*	1109	1210	1364	1508	1713
Cs-137 Release Fraction					
UC_2	0.0	0.06	.05	0.01	.04
$UC_{0.36}O_{1.64}$	0.0	0.07	0	0.05	.04
UO_2	0.0	0.09	.14	0.65	.9
UO_2*	0.01	0.09	.06	0.0	.04
Kr-85 Release Fraction per experiment	0	0	0	0	10^{-4}
Ag-110M Release Fraction[(a)]					
UC_2	.10	0.11	.10	0.16	1
$UC_{0.36}O_{1.64}$	.14	0.32	.35	0.21	.23
UO_2	.16	0	.23	0.82	1
UO_2*	.08	0.30	.22	0.03	.37

(a) Based on initial particle counts.

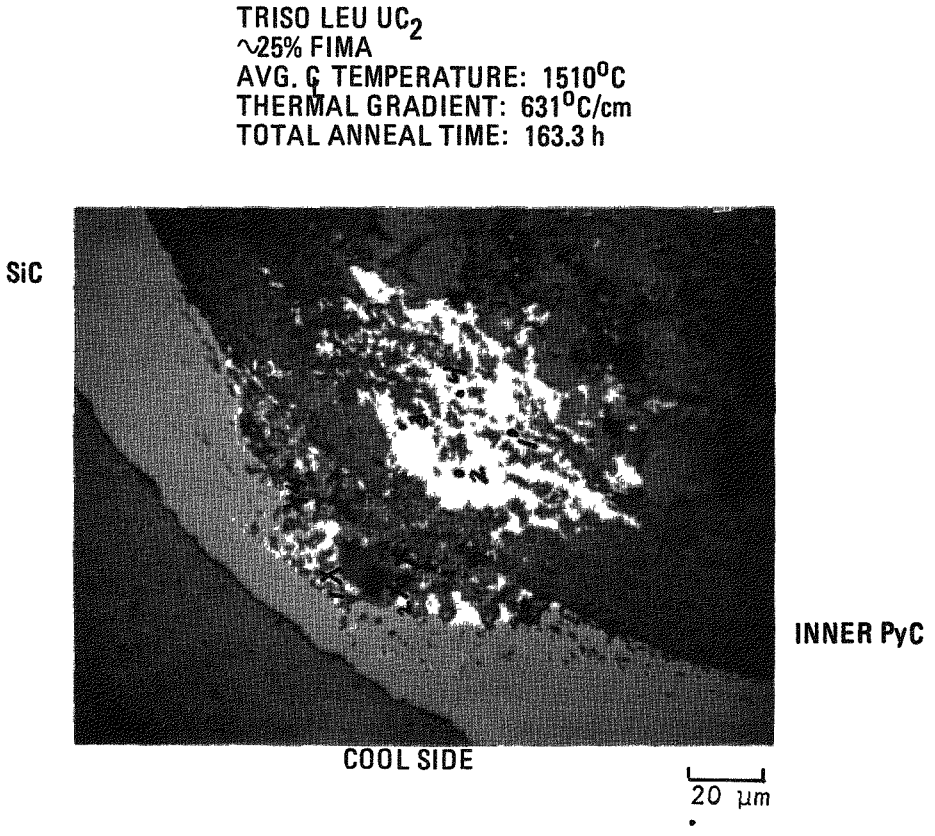

Fig. 3.24 Specific regions in TRISO LEU UC_2 where elemental ratios were determined by electron microprobe X-ray analysis

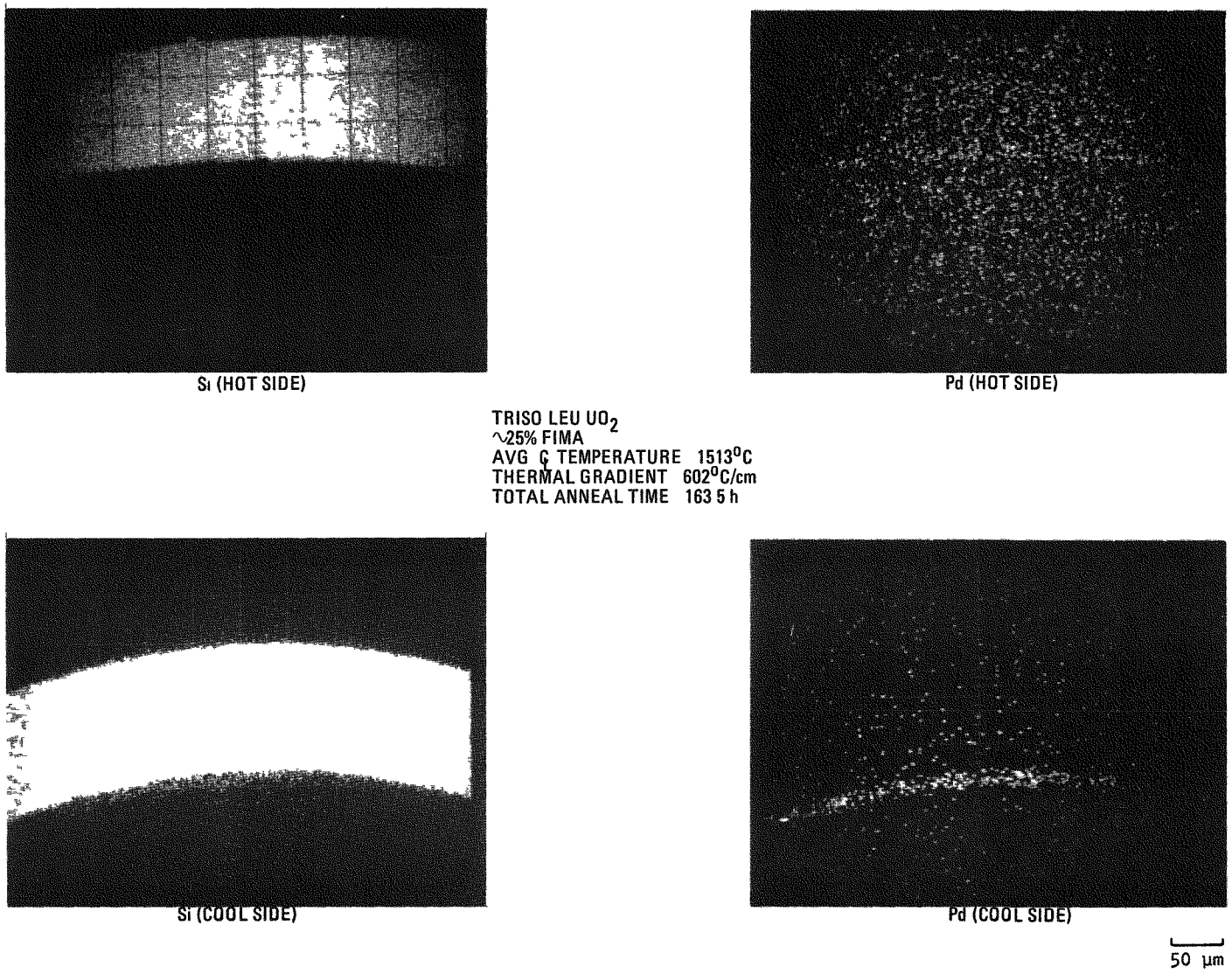

Fig. 3.25 Distribution of Pd at inner surface of SiC on hot and cool side of TRISO LEU UO_2 annealed in a thermal gradient at 1513°C

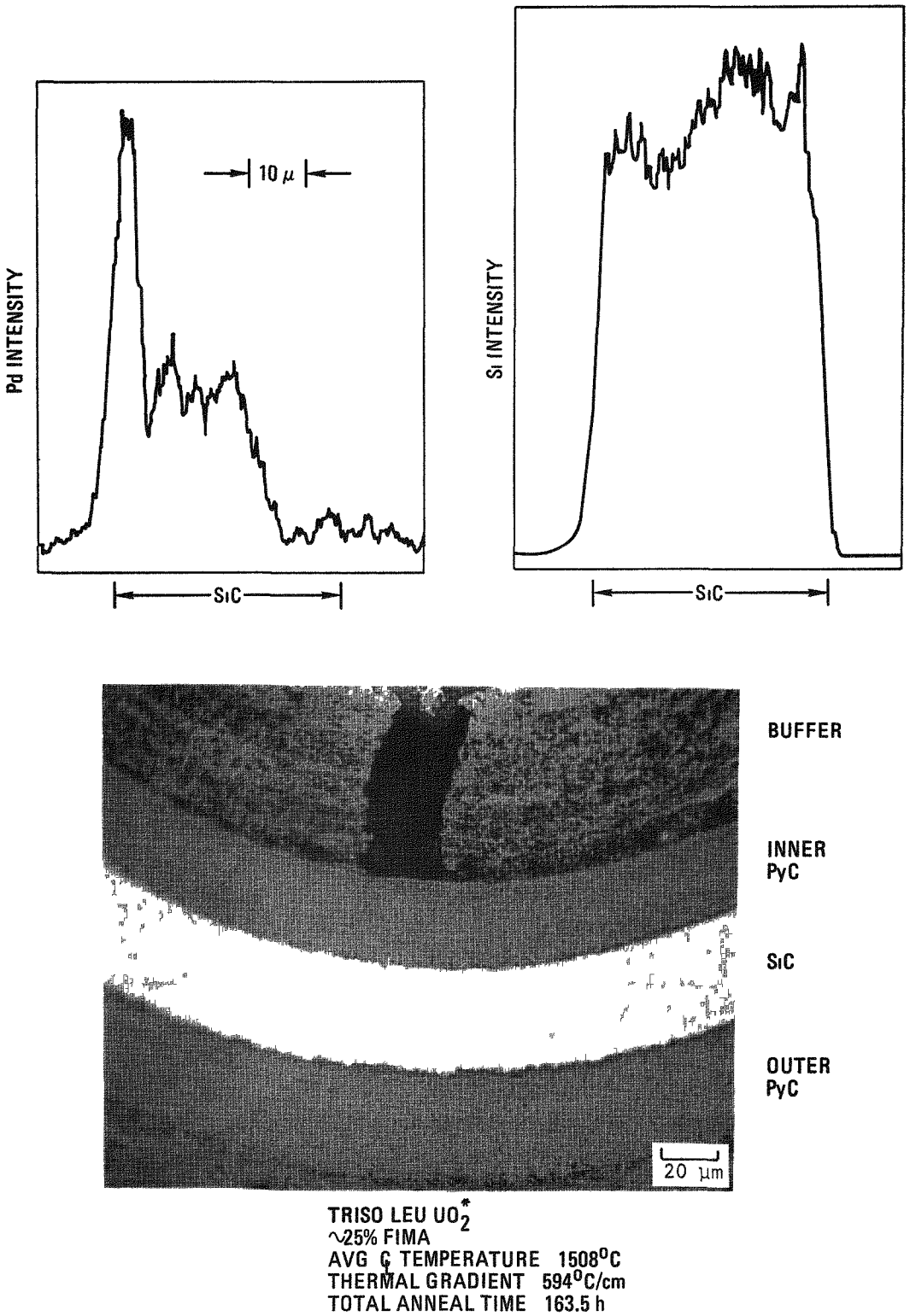

Fig. 3.26 Electron microprobe line scans across SiC for LEU UO_2* after heating out-of-pile for 163.5 hr at 1508°C

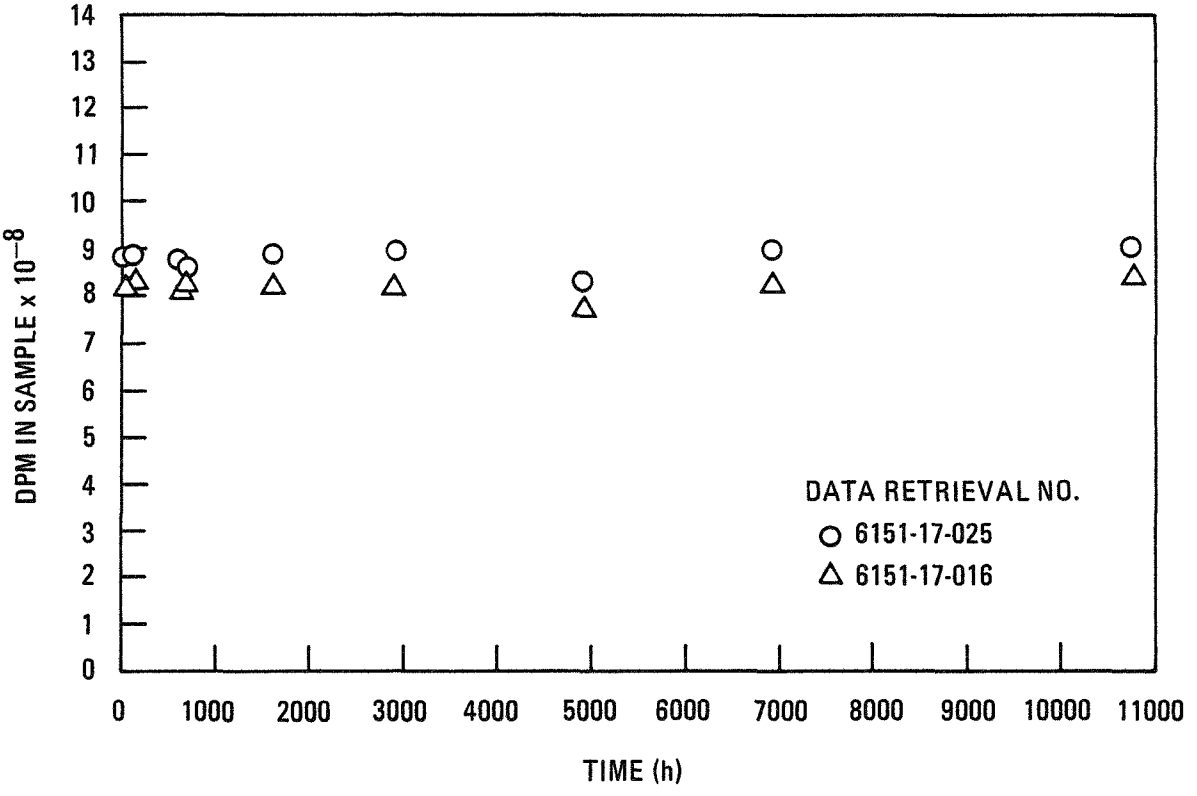

Fig. 3.27 Variation in the Cs-137 content of TRISO HEU UC_2 particles heated in a thermal gradient at 1101°C

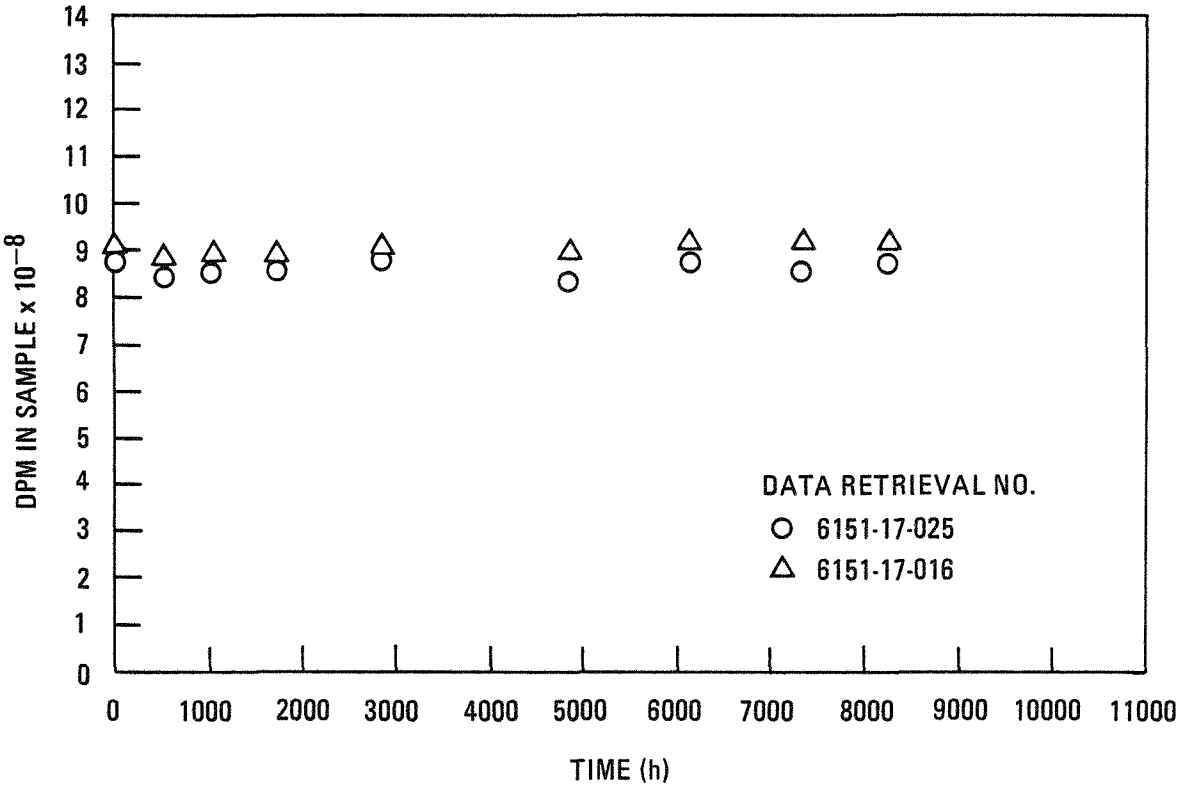

Fig. 3.28 Variation in the Cs-137 content of TRISO HEU UC_2 particles heated in a thermal gradient at 1351°C

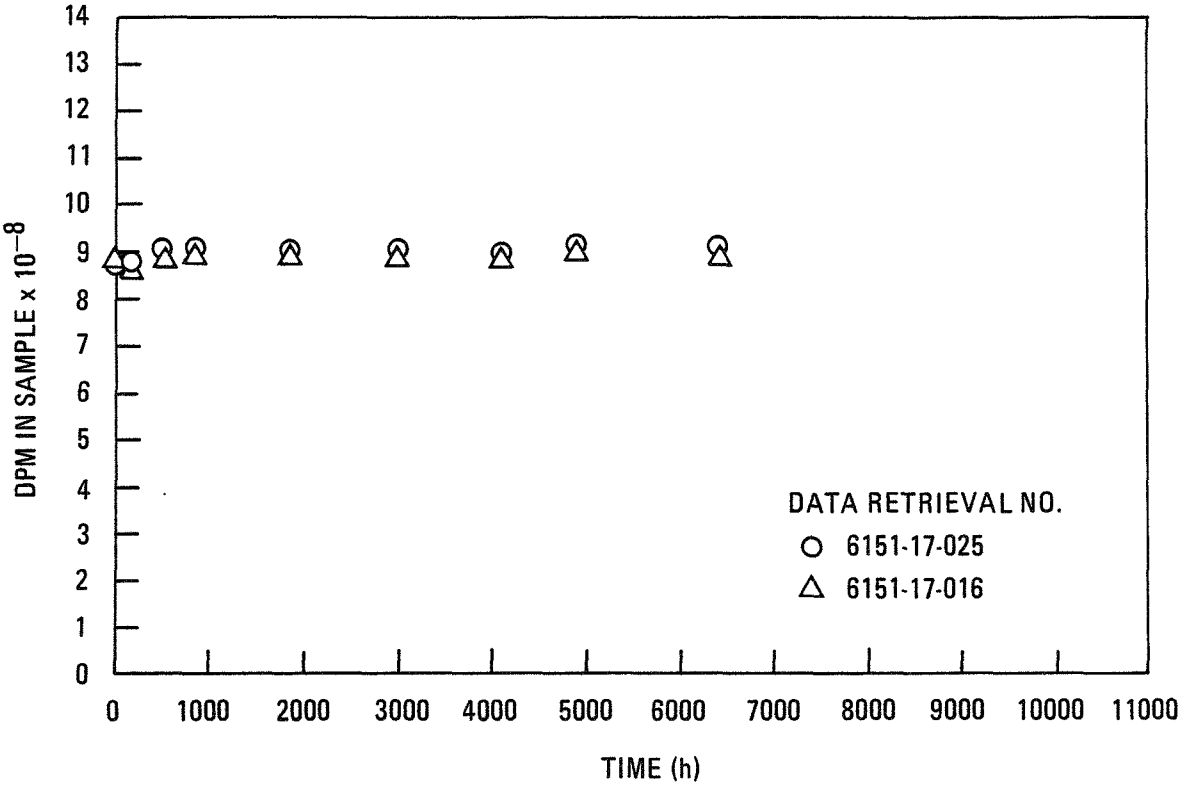

Fig. 3.29 Variation in the Cs-137 content of TRISO HEU UC_2 particles heated in a thermal gradient at 1508°C

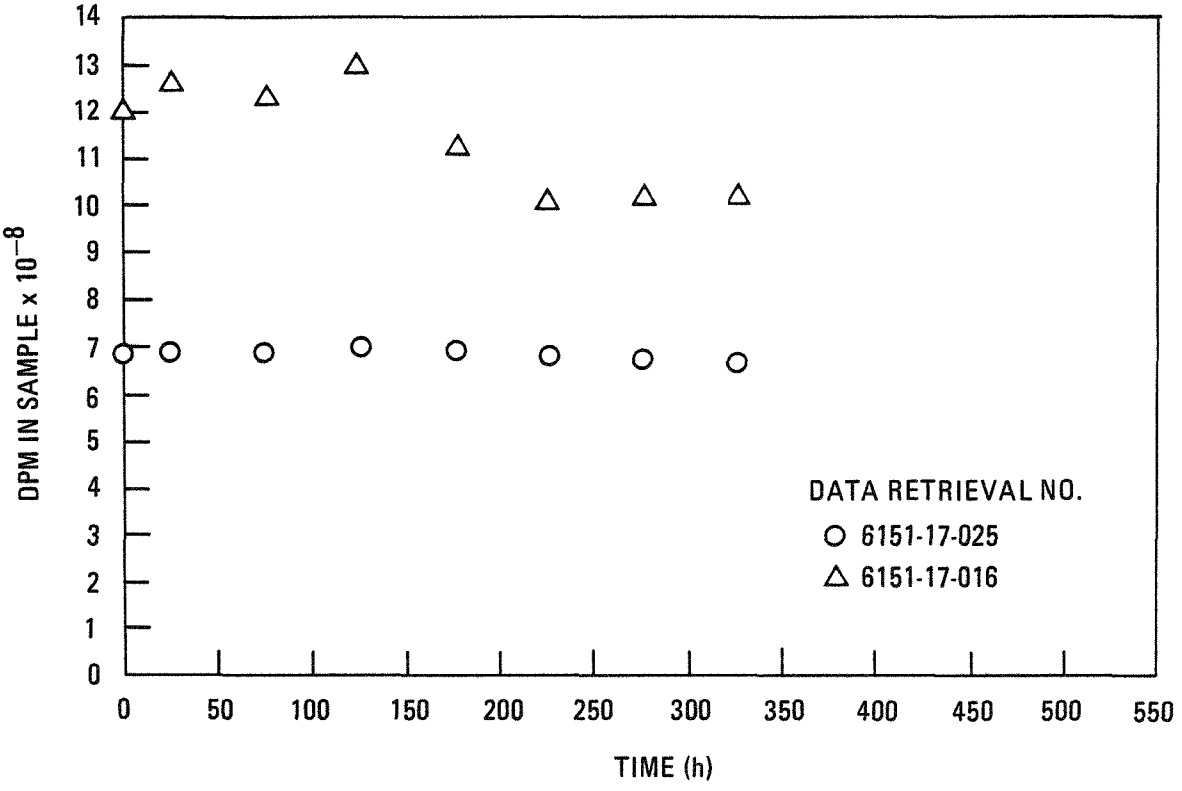

Fig. 3.30 Variation in the Cs-137 content of TRISO HEU UC_2 particles heated in a thermal gradient at 1709°C

Ag-110m was released from all the LEU particles. Since Ag was released in many experiments when neither Cs-137 or Kr-85 was released, Ag migration through the SiC probably occurred by diffusion and not by corrosive chemical attack.

3.4 Rate of SiC Thinning

3.4.1 TRISO HEU UC_2

The decrease in SiC thickness caused by fission product reactions in TRISO HEU UC_2 is given as a function of time for different reaction temperatures in Tables 3.4 through 3.7. The final thickness changes, which were obtained from contact X-radiographs, were compared to changes in SiC thickness measured during the post test metallographic examinations.

Metallographic values and end-of-test radiographic values are shown in Table 3.8. A comparison of the data determined by X-ray analysis and by metallography shows that below ~1350°C both techniques give approximately the same change in SiC thickness. At 1508° and 1709°C, metallographic measurement of the visible penetration of the SiC coating shows greater values than measured by the X-ray technique. The radiographic technique does not measure the penetration depth unless the concentration of fission products in the corrosion zone is sufficiently high. Although it has not been proven, at temperatures $\gtrsim$1500°C, the rare earth elements appear not to have penetrated the SiC in sufficient concentration to allow radiographic measurement of the maximum penetration. Although changes in SiC thickness measured by metallographic techniques are somewhat larger than those obtained from X-ray analysis, the X-ray values were used as differences remain small relative to the data scatter.

3.4.2 TRISO LEU Fissile Fuels

The change in the thickness of the SiC layer was measured using a radiographic procedure. This technique relies on accumulating rare earth elements in the fission product - SiC reaction zone. Since rare earths are not easily released from UO_2 kernels, (Ref. 13) this technique cannot be used to follow SiC reactions in UO_2. In particles that have $O/U \geq 1$, end-of-test metallography is conducted to measure the extent of SiC thinning.

TABLE 3-4

CHANGE IN SiC THICKNESS CAUSED BY FISSION PRODUCT - SiC REACTIONS IN TRISO HEU UC_2 (60% FIMA) AT APPROXIMATELY 1100°C

Data Retrieval No.	Crucible No.	Temp. (°C)	Time (h)	1(a)		2		3		4		5		6		7		8		Average	
				t(b)	Δt(c)	t	Δt	t	Δt	t	Δt	t	Δt	t	Δt	t	Δt	t	Δt	Δt	σ
6151-17-016	1	1101	0	Unirradiated		34.5		33		32		32.5		32.5		32		32.5			
			96			31	3.5	33	0	32	0	32.5	0	32.5	0	(d)	--	32	0.5	0.67	1.4
			624			32.5	2	33	0	32	0	32	0.5	32.5	0	32.5	0	32	0.5	0.43	0.73
			694			32.5	2	33	0	32	0	32	0.5	32.5	0	32	0	32	0.5	0.43	0.73
			1,596			32.5	2	32	0	31	1	32	0.5	32.5	0	31.5	0.5	32	0.5	0.64	0.69
			2,886			32.5	2	32	1	31	1	32	0.5	31	1.5	31.5	0.5	32	0.5	1.0	0.58
			4,898			33	1.5	32	1	31	1	32	0.5	32.5	0	31.5	0.5	33	0	0.64	0.56
			6,940			32.5	2	32	1	31	1	31.5	1	32.5	0	31	1	33	0	0.86	0.69
			10,763			32	2.5	31.5	1.5	31	1	32	0.5	30.5	2	30.5	1.5	31.5	1	1.4	0.67
6151-17-025	2	1106	0	29.3		27		Unirradi-		28		26.5		24.5		27		26			
			96	28.7	0.6	27	0	ated		28	0	26.5	0	24.5	0	26.5	0.5	(d)	--	0.18	0.29
			624	29.5	0	26.9	0.3			28.7	0.3	26.5	0	24.5	0	26.5	0.5	25	1	0.27	0.39
			694	30	0	28	0			(d)	--	(d)	--	(d)	--	26.5	0.5	25	1	0.38	0.48
			1,596	30.5	0	26.5	0.5			27.5	0.5	24.5	2	24.5	0	26.5	0.5	25	1	0.64	0.69
			2,886	30.5	0	26.5	0.5			29	0	24.5	2	24.5	0	25.8	1.2	25	1	0.67	0.77
			4,898	30.5	0	26	1			30	0	24.5	2	24.5	0	25	2	25	1	0.86	0.90
			6,940	27	2.3	27	0			28.5	0	24.5	2	24.5	0	24.7	2.3	26	0	0.94	1.2
			10,763	28.8	0.5	26.5	0.5			28.5	0	24	2.5	24.5	0	24.5	2.5	25.5	0.5	0.93	1.1

(a) Particle number.

(b) t = measured SiC thickness, μm.

(c) Δt = change in SiC thickness, μm.

(d) X-ray out of focus.

TABLE 3-5
CHANGE IN SiC THICKNESS CAUSED BY FISSION PRODUCT - SiC REACTIONS IN TRISO HEU UC_2 (60% FIMA) AT APPROXIMATELY 1350°C

Data Retrieval No.	Crucible No.	Temp. (°C)	Time (h)	1[a]		2		3		4		5		6		7		8		Average	
				t[b]	Δt[c]	t	Δt	t	Δt	t	Δt	t	Δt	t	Δt	t	Δt	t	Δt	Δt	σ
6151-17-016	1	1351	0	Unirradiated		34.5		32.5		32.5		32		35		37		35.5			
			523			30	4.5	32.5	0	30	2.5	30	2	32	3	32	5	31	4.5	3.1	1.8
			1048			29	5.5	31	1.5	28.5	4	28	4	30	5	32	5	30	5.5	4.4	1.4
			1711			28	6.5	31	1.5	28.5	4	26	6	29.5	5.5	(d)	--	27	8.5	5.3	2.4
			2818			28	6.5	31	1.5	27.5	5	23.5	8.5	28.5	6.5	(d)	--	27	8.5	6.1	2.6
			4833			28	6.5	30	2.5	26	6.5	22.5	9.5	28.5	6.5	32	5	27	8.5	6.4	2.3
			6106			23.5	11	27	5.5	20	12.5	20	12	26	9	29	8	26.5	9	9.6	2.4
			7313			25.5	9	29.5	3	20	10.5	21.5	10.5	24.5	10.5	(d)	--	26.5	9	9.1	3.2
			8222			25	9.5	28	4	22.5	10	16.5	15.5	21	14	(d)	--	26.5	9	10.3	4
6151-17-025	2	1361	0	Unirradiated		26		28		31		27.5		31		27		27			
			523			25.5	0.5	25	3	(e)	--	(e)	--	(e)	--	(e)	--	(e)	--	1.8	1.8
			1048			25.5	0.5	25	3	27.5	3.5	23.5	4	27.5	3.5	23.5	3.5	27	0		
			1711			25	1	24.5	3.5	27.5	3.5	23.5	4	22.5	8.5	19.5	7.5	28	0	4	3.1
			2818			24	2	23	5	25.5	5.5	23.5	4	21	10	19.5	7.5	26	1	5	3.1
			4833			24	2	24	4	25	6	23.5	4	20.5	10.5	16.5	10.5	26.5	0.5	5.4	3.9
			6106			23	3	24	4	25	6	22.5	5	18.5	12.5	10	17	24	3	7.2	5.4
			7311			22.5	3.5	23.5	4.5	24	7	22	5.5	18.5	12.5	(f)	--	22.5	4.5	6.3	3.3
			8222			22.5	3.5	22.5	5.5	23	8	21.5	6	18	13	16.5	10.5	21	6	7.5	3.3

[a] Particle number.

[b] t = measured SiC thickness, μm.

[c] Δt = change in SiC thickness, μm.

[d] X-ray out of focus.

[e] X-ray too bright - poor contrast.

[f] No X-ray.

TABLE 3-6
CHANGE IN SiC THICKNESS CAUSED BY FISSION PRODUCT - SiC REACTIONS IN TRISO HEU UC_2 (60% FIMA) AT APPROXIMATELY 1500°C

Data Retrieval No.	Crucible No.	Temp. (°C)	Time (h)	1[a]		2		3		4		5		6		7		8		Average	
				t[b]	Δt[c]	t	Δt	t	Δt	t	Δt	t	Δt	t	Δt	t	Δt	t	Δt	Δt	σ
6151-17-025	1	1508	0	26		26		24		28.5		24.5		Unirradiated		29		28			
			139	24	2	21	5	21	3	27.5	1	22	2.5			24.5	4.5	26	2	2.8	1.4
			494	24	2	17	9			26.5	2	22	2.5			17	12	24.5	3.5	5.2	4.3
			825	22	4	14.5	11.5			25	3.5	20.5	4			13.5	15.5	24	4	7.1	5.1
			1855	16.5	9.5	14	12			26	2.5	18	6.5			(d)		(d)		7.6	4.1
			2980	15.5	10.5	12.5	13.5			26	2.5	18	6.5			10	19	23.5	4.5	9.4	6.2
			4055	14.5	11.5	12.5	13.5			26	2.5	17	7.5			7	22	16.5	11.5	11.4	6.5
			4888	14	12	9	17			24	4.5	7	17.5			0	29	14	14	15.7	8.1
			6396	13	13	5	21			24	4.5	7	17.5							14	7.1
6151-17-016	2	1514	0	33		34.5		Unirradiated		33.5		33		34.5		32.5		31.5			
			139	31	2	31.5	3			31.5	2	27.5	5.5	33.5	1	28.5	4	30	1.5	2.7	1.6
			494	29.5	3.5	31	3.5			30	3.5	29	4	31	3.5	27.5	5	28	3.5	3.8	0.6
			825	28	5	28	6.5			28.5	5	27.5	5.5	31	3.5	24	8.5	27.5	4	5.4	1.7
			1855	25.5	7.5	24.5	10			27.5	6	24.5	8.5	31	3.5			25	6.5	7	2.2
			2980	20	13	23.5	11			25.5	8	23	10	28	6.5			18	13.5	10.3	2.8
			4055	21.5	11.5	23.5	11			21.5	12	23	10	27	7.5			18	13.5	10.9	2
			4888	20.5	12.5	21.5	13			21.5	12	21.5	11.5	25	9.5					11.7	1.4
			6396	20.5	12.5	21.5	13			21.5	12	21.5	11.5	25	9.5					11.7	1.4

[a] Particle number.

[b] t = measured SiC thickness, μm.

[c] Δt = change in SiC thickness, μm.

[d] X-ray out of focus.

TABLE 3-7

CHANGE IN SiC THICKNESS CAUSED BY FISSION PRODUCT - SiC REACTIONS IN TRISO HEU UC_2 (60% FIMA) AT APPROXIMATELY 1700°C

Data Retrieval No.	Crucible No.	Temp. (°C)	Time (h)	1[a]		2		3		4		5		6		7		8		Average	
				t[b]	Δt[c]	t	Δt	t	Δt	t	Δt	t	Δt	t	Δt	t	Δt	t	Δt	Δt	σ
6151-17-016	1	1709	0	34		32		33.5		Unirradiated		35.5				Failed on		33			
			24	30.5	3.5	30.5	1.5	30	3.5			30	5.5	(d)		fire run		27.5	5.5	3.9	1.7
			73	29	5	28.5	3.5	26	7.5			28	7.5					26	7	6.1	1.8
			123	28.5	5.5	25.5	6.5	22.5	11			25.5	10					22.5	10.5	8.3	2.7
			174.5	28.5	5.5	(d)	--	14.5	19			25	10.5					19.5	13.5	12.1	5.7
			225	22	12	21	11	10	23.5			(d)	--					(d)	--	14.8	7.7
			275	17.5	16.5	(d)	--					17.5	18					(d)	--	17.3	1.1
			325	(d)	--	16.5	15.5											16.5	16.5	16	0.7
6151-17-025	2	1727	0	27.5		Failed on		25		27.5		Unirradiated		30.5		28.5		28.5			
			24	25	2.5	fire run		22.5	2.5	23	4.5			28.5	2	25	3.5	22	6.5	3.6	1.7
			73	25	2.5			19.5	5.5	23	4.5			25.5	5	23.5	5			4.5	1.2
			123	21.5	6			17.5	7.5	21	6.5			22.0	8.5	20	8.5			7.4	1.1
			174.5	21.5	6.5			16.5	8.5	18.5	9			14	16.5	18.5	10			10.1	3.8
			225	21	6.5			13	12	17.5	10			9	21.5	14	14.5			12.9	5.6
			275	20	7.5			12	13	16	11.5			7	23.5	(d)				13.9	6.8
			324	20	7.5			12	13					7	23.5	10	18.5			15.6	6.9

[a] Particle number.

[b] t = measured SiC thickness, μm.

[c] Δt = change in SiC thickness, μm.

[d] X-ray out of focus.

Table 3.9 gives the change in the SiC thickness observed by radiography for the LEU UC_2 sample. The particles being tested at 1093°C were inadvertently heated at ∿1600°C for less than 20 hr. During an additional 646 hr at 1083°C the SiC in one particle of the six tested was completely penetrated by the fission product SiC reaction. Neglecting this one particle, the change in SiC thickness is 2.9 $\pm$ 1.5 μm. Tests on HEU UC_2 at 1100°C showed no SiC attack after 1100 hr.

TABLE 3-8
COMPARISON OF METALLOGRAPHIC AND X-RAY TECHNIQUES

Data Retrieval No.	Temp. (°C)	Crucible No.	Particle No.	Initial SiC Thickness (μm)		SiC Thickness After Reaction (μm)		Change in SiC Thickness (μm)	
				Metallography	X-ray	Metallography	X-ray	Metallography	X-ray
6151-17-016	1351	1	3	34.7	32.5	25.2	28.0	9.5	4.5
			4	31.5	32.5	15.5	22.5	16.0	10.0
			5	31.7	32.0	17.3	16.5	14.4	15.5
			6	32.6	35.0	22.5	21.0	10.1	14.0
			$\bar{X}$	32.6	33.0	20.1	22.0	12.5	11.0
			σ	1.5	1.4	4.5	4.7	3.2	4.9
6151-17-025	1361	2	2	28.2	26.0	21.0	22.5	7.2	3.5
			3	26.2	28.0	21.5	22.5	4.7	5.5
			6	29.5	31.0	18.0	18.0	11.5	13.0
			7	25.2	27.0	18.5	16.5	6.7	10.5
			$\bar{X}$	27.3	28.0	19.8	19.9	7.5	8.1
			σ	1.9	2.2	1.8	3.1	2.9	4.4
6151-17-025	1508	1	1	27.8	26.0	6.5	13.0	21.3	13.0
			5	25.6	24.5	5.25	7.0	20.4	17.5
			8	30.8	28.0	11.9	14.0	18.9	14.0
			$\bar{X}$	28.1	26.2	7.9	11.3	20.2	14.8
			σ	2.6	1.8	3.5	3.8	1.2	2.4
6151-17-016	1709	1	1	32.3	34.0	11.7	17.5	21.0	16.5
			2	33.8	32.0	7.0	16.5	26.8	15.5
			3	33.7	33.5	5.0	12.5	28.7	21.0
			5	36.4	35.5	13.5	17.5	22.9	18.0
			6	32.0	38.0	2.5	3.0	29.5	35.0
			$\bar{X}$	33.6	34.6	7.9	13.4	25.8	21.2
			σ	1.7	2.3	4.5	6.2	3.7	8.0
6151-17-016	1101	1	2	32.0	34.5	30.7	32	1.3	2.5
			3	30.9	33	30.4	32	0.5	0.5
			4	31.6	32	29.0	31	2.6	1.0
			5	31.6	32.5	28.0	32	3.6	1.5
			6	32.6	32.5	31.0	30.5	1.6	2
			$\bar{X}$	31.7	32.9	29.8	31.5	1.9	1.5
			σ	0.6	1.0	1.3	0.7	1.2	0.8

Table 3.9

CHANGE IN SILICON CARBIDE THICKNESS CAUSED BY FISSION PRODUCT - SiC REACTIONS IN TRISO LEU UC_2 (~25% FIMA)

Data Retrieval Number	Crucible Number	Temperature °C	Time hr.	1[a]		2		3		4		5		6		7		Average	
				t[b]	Δt[c]	t	Δt	t	Δt	t	Δt	t	Δt	t	Δt	t	Δt	Δt	σ
6151-21-0111-5	2	1093	1201	40	--	43	--	38.5	--	36.5		38	--	39		Unirradiated		--	--
			1512	38	2	40	3	35.5	3.0	36.5	0	36	2	35.5	3.5			2.25	1.25
			2158[d]	38	2	40	3	35	3.5	35.5	1.0	33	5	2.0	37			2.9	1.5
6151-21-0111-5		1207	0	40	--	36.5	---	39	--	37	--	37	--	37	--			--	--
			224	41.5	--	36	--	42	--	39	--	40.5	--	38.5	--			--	--
			535.5	41	--	36.5	--	40	--	38	--	38.5	--	38	--			--	--
			1088.5	38	2	37	--	38	1	34	3	37	--	37	--			1.0	1.26
			2051.5	37	3	35	1.5	38	1	34	3	35	2	35	2			2.1	.8
6151-21-0111-5		1368	0	40	--	40	--	37.5	--	38	--	38	--	38	--			--	--
			526	36.5	3.5	37.5	2.5	17	20.5	28	10	34.5	3.5	36	2			7.0	7.2
			764.5	32	8	35	5	14	23.5	29.5	8.5	34	4	34	4			8.8	7.4
			1174.5	32	8	31	9	13	24.5	27	11	28	10	24	14			12.8	6.1
			2253	23	17	27	13	7	30.5	17	21	18	20	24	14			19.25	6.4
6151-21-0111-5		1510	0	37	--	37.5	--	41	--	39	--	38	--	38	--			--	--
			92.5	31	6	10	27.5	38.5	2.5	38.5	0.5	19	19	10	28			13.9	12.5
			163.5	7	30	5	32.5	23	18	29	10	5	33	3	35			26.4	10.1
6151-21-0111-5		1704	0	38.5	--	38.5	--	38.5	--	38.5	--	38.5	--	38.5	--			--	--
			10	46	--	34	4.5	34	4.5	44	--	35	3.5	35	3.5			2.7	2.1
			36	26	12.5	24	14.5	31	7.5	(e)	--	26	12.5	30	8.5			11.1	3.0
			81	12	26.5	19	19.5	17	21.5	30	8.5	(e)	--	(e)	--			19.0	7.6
			116	13	25.5	(f)	--	(f)	--	(f)	--	(f)	--	(f)	--			--	--

(a) Particle number

(b) t = measured SiC thickness, μm

(c) Δt = change in SiC thickness, μm

(d) Includes <24 hr. at ~1600°C

(e) X-radiograph out of focus

(f) No distinct fission product front

4. DISCUSSION

4.1 Reacting Fission Products

A number of fission products have been associated with SiC-fission product reactions in TRISO fuel. These include the rare earth metals (cerium, neodymium, lanthanum, samarium, praseodymium, and europium); palladium, ruthenium, and rhodium of the platinum family; and strontium. Generally speaking, SiC-fission product reactions occur in two modes. The first is temperature gradient dependent and is attributed to rare earth-SiC reactions on the inner surface of the cooler side of SiC coatings. Many examples of this mode of attack can be found in the literature (Refs. 15, 16, 17). The second mode of attack appears as localized reaction sites and may be independent of temperature gradient. Although this mode of attack is generally attributed to palladium, evidence of ruthenium-, rhodium-, strontium-, and silver- SiC reactions has also been noted (Refs. 18, 19). The results of microprobe work on samples of irradiated HTGR fuel heated in out-of-pile thermal gradients were given in Section 3.2. These results agree with microprobe analysis of samples irradiated in capsule and fuel test elements, as discussed above.

The concentration of several of these fission products which affect SiC integrity is dependent on the isotopic composition of HTGR fuel. This occurs because the ratio of the fissioning isotopes (U-235, Pu-239, Pu-241) differs as the uranium enrichment changes and because the fission product yields from each isotope are not the same.

Smith (Ref. 20) and Lindemer (Ref. 21) have calculated the effect of change in isotopic composition from HEU (93% enriched U-235) to LEU (19.5% enriched U-235) HTGR fuel. At peak burnup (~25% FIMA), the fission products that have greater inventories in typical LEU fuel particles are Mo, Ru, Rh, Pd, Ag and Cd. Of these, Ag, Pd and Cd are affected most by the change from HEU to LEU. Assuming a 200 μm HEU kernel and a 300 μm LEU kernel, there is approximately 11 times more Ag and 4.5 times more Pd and Cd in a LEU particle than in a HEU particle. There are, however, still more rare

earth elements than either Ag, Pd or Cd.

4.2 Influence of Kernel Composition

The composition of the kernel may indirectly affect the rates of fission product-SiC reactions by affecting the release of Pd and other fission products from the kernel. Obviously, if fission products were completely retained in the kernel, no reactions could occur at the inner surface of the SiC.

Extensive microprobe work has been done concerning the release of fission products from various kernel compositions (Refs. 13, 22, 23, 24, 25). Tiegs has reviewed that data (Ref. 26) at ORNL and has concluded that the rare earth fission products are released from kernels with $O/U \leq 1.1$ and migrate down the temperature gradient to the cool side of the particle. With higher O/U ratios the rare-earth metals are retained in the kernel (Ref. 13).

Pd, however, is not significantly retained in the kernel of any U-C-O composition. In irradiated kernels of dense LEU UO_2, PuO_{2-x}, and 2 $ThO_2 \cdot PuO_{2-x}$, some Pd was tied up in noble metal inclusions but most of the Pd had been released from the kernel and resided at the SiC coating (Refs. 25, 27).

Kernels which are less than theoretically dense do not retain any amount of Pd. In LEU and HEU UC_xO_y kernels made from low-density, weak acid resins, no holdup of Pd was apparent (Ref. 28). SiC attack associated with palladium and strontium was observed in LEU DRAGON TRISO UO_2 which had an 80% theoretically dense kernel (Ref. 18). After irradiation for 1 year at 1550°C to 4% FIMA, Pd, Ru and Rh were found along with Sr at the inner PyC-SiC interface. It was suggested that these elements might have catalyzed the Sr-SiC reaction. It can be inferred from this discussion that fission product Pd is of most concern, and that variations of kernel composition do not affect the release of Pd from the kernel.

4.3 Time Dependence of SiC-Fission Product Reactions

Reactions at high temperature may take many courses and forms depending on the reactants, the temperature, and the elapsed time of reaction. Kinetic studies of solid-state reactions usually relate the amount of reaction, (α), to the time of reaction in an equation of the form

$$F(\alpha) = kt \tag{1}$$

where the function $F(\alpha)$ depends on the mechanism controlling the reaction. Many forms of $F(\alpha)$ have been derived depending on what process is assumed to be controlling the rate of the reaction (Ref. 29). If, for example, the reaction products remain at the reaction surface as a continuous, compact layer, the reaction rate is often governed by solid-state transport through the increasing thickness of the layer. Kinetically, the reaction rate decreases with time. When lattice diffusion through the compact layer predominates, the reaction kinetics follow the well known parabolic rate equation in which the rate is inversely proportional to the thickness of the product layer, x,

$$\frac{dx}{dt} = \frac{k_p}{x} \tag{2}$$

where t is the time, and k_p is the parabolic rate constant.

Integration of eq. 2 within limits t_{i-1} and t_i leads to eq. 3:

$$X_i^2 - X_{i-1}^2 = 2\, k_p\, (t_i - t_{i-1}) \tag{3}$$

During out-of-pile testing, $t_{i-1} = 0$ and $X_{i-1} = 0$ because at the start of the thermal anneal no product layer has been formed. For this special case, Equation 3 reduces to an expression in which the extent of reaction is proportional to the square root of the time,

$$x = k_p'\, t^{0.5} \tag{4}$$

where

$$k_p' = (2\, k_p)^{0.5}$$

Solid-state reactions which are not controlled by transport through a product layer often do not slow down until one of the reactants is depleted. This type of reaction mechanism can result in a rate equation of the type

$$\frac{dx}{dt} = k_\ell \tag{5}$$

where k_ℓ is the linear rate constant. The extent of reaction, then becomes directly proportional to time:

$$x = k_\ell t \tag{6}$$

The original model used to calculate changes in SiC thickness during core design studies (prior to CY-80) assumed that the reaction rate at a given temperature was constant with time (eq. 6) and therefore, the decrease in SiC thickness was linear with time. This "linear" model was based upon data collected from out-of-pile testing of irradiated fuel at temperatures $\geq$1300°C, and from results obtained during postirradiation examination of accelerated irradiation experiments. Each out-of-pile test was conducted at constant temperature and initial fission product concentration and allowed determination of the change in SiC thickness with time and temperature. The accelerated irradiation data included the effects of fission product concentrations and temperatures ($\geq$1400°C) that vary with time; however, the resulting change in SiC thickness could only be measured at one time point (i.e. the end of the irradiation). The single time point precludes any direct empirical verification of the fundamental kinetic expression from the irradiation data.

The changes in SiC thickness as a function of test time during the FY-78 thermal gradient heating tests on irradiated TRISO HEU UC_2 are given in Table 3.4 through 3.7. Comparison of these results with the original linear model, shows that the original linear model overpredicts the change in SiC thickness for samples heated out-of-pile at $\leq$1500°C (Ref. 30). Figure 4.1 gives the

change in SiC thickness and the 90% confidence bound (1.8σ) on the mean change in thickness caused by fission product-SiC reaction at 1500°C in an out-of-pile thermal gradient test. Also included is the change predicted by the original model. It is quite apparent that the original model does not reflect the actual rate-time behavior of SiC thinning.

A reanalysis of the data results in a better description of the out-of-pile tests at temperatures $\leq$1500°C (Ref. 31). This analysis assumed that the change in SiC thickness was proportional to the square root (Eq. 4) of the anneal time. Figure 4.2 demonstrates the validity-of-the assumption that for the UC_2 samples studied, the change in SiC thickness caused by out-of-pile fission product attack on the SiC layer was proportional to the square root of time, when the temperature was $\lesssim$1500°C.

When the reaction temperature was >1500°C, Fig. 4.3 shows that the out-of-pile reaction can be described by either a linear time dependence or by a square root time dependence. This agrees with high temperature work by Lindemer in which the rate of change in SiC thickness caused by interaction of LaC_2 and NdC_2 was found to be time independent between ∿1500°C and ∿1700°C (Ref. 32).

The purpose of any out-of-pile study is to obtain data to support a predictive model which can be shown to be valid during fuel irradiations. Since the change in SiC thickness during the irradiation tests was only measured at one time point, neither the linear or square root model has a firm basis for calculations of SiC thinning during irradiation. There is evidence that palladium is diffusing out of TRISO particles during the out-of-pile testing. Kaae has observed that the solubility and diffusivity of Pd in SiC are relatively high and therefore Pd is lost from particles during thermal annealing (Ref. 33). Our out-of-pile thermal gradients tests provide additional evidence for Pd diffusion through SiC. Figure 3.26 shows electron microprobe line traces for Si and Pd across the SiC in LEU TRISO UO_2*. This sample had been irradiated to ∿25% FIMA at ∿950°C and then heated at ∿1500°C for 163.5 hr during

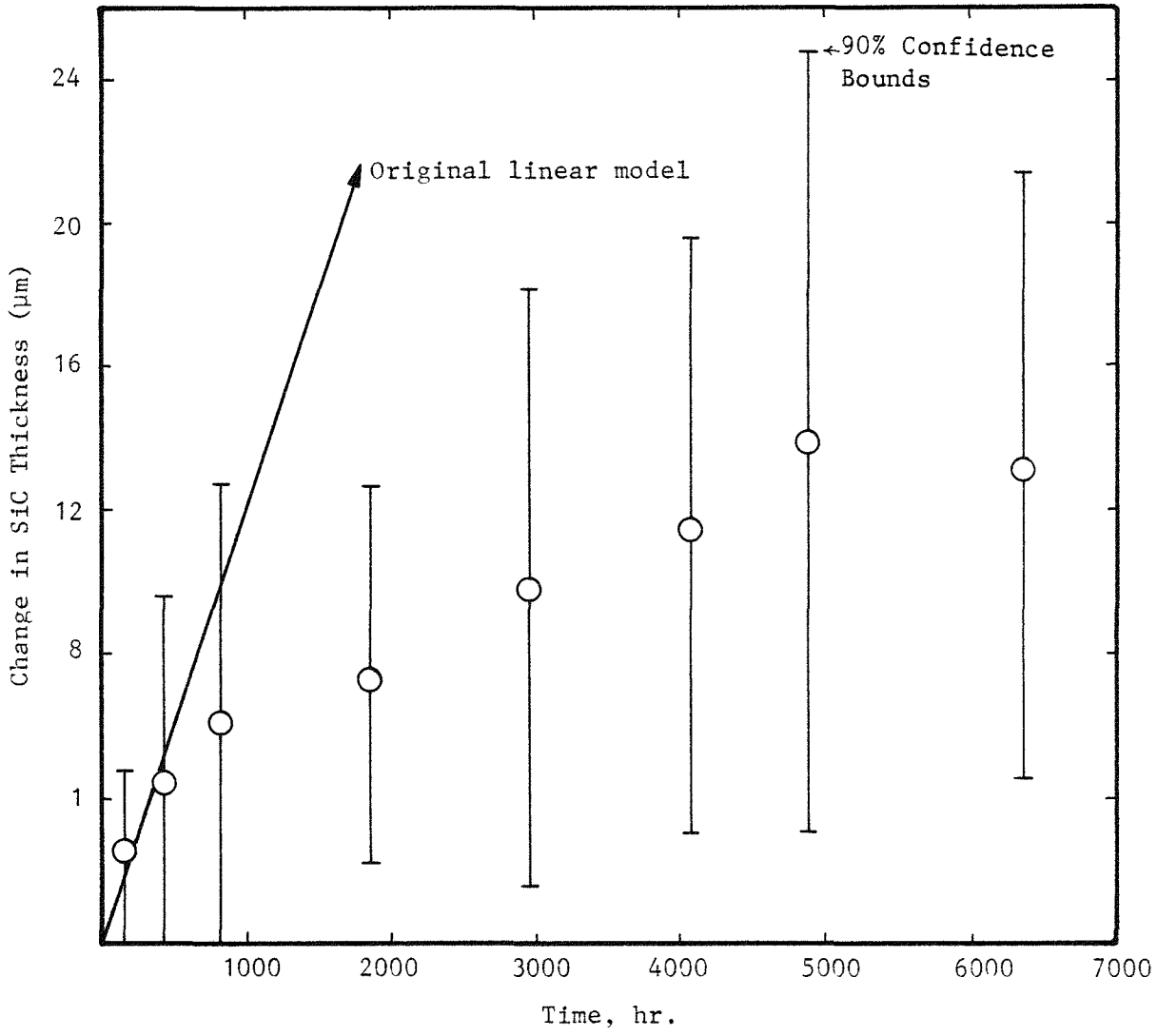

Fig. 4.1 Comparison of the observed change in SiC thickness with time to that predicted at 1500°C using the CY-80 linear model for SiC-fission product reaction

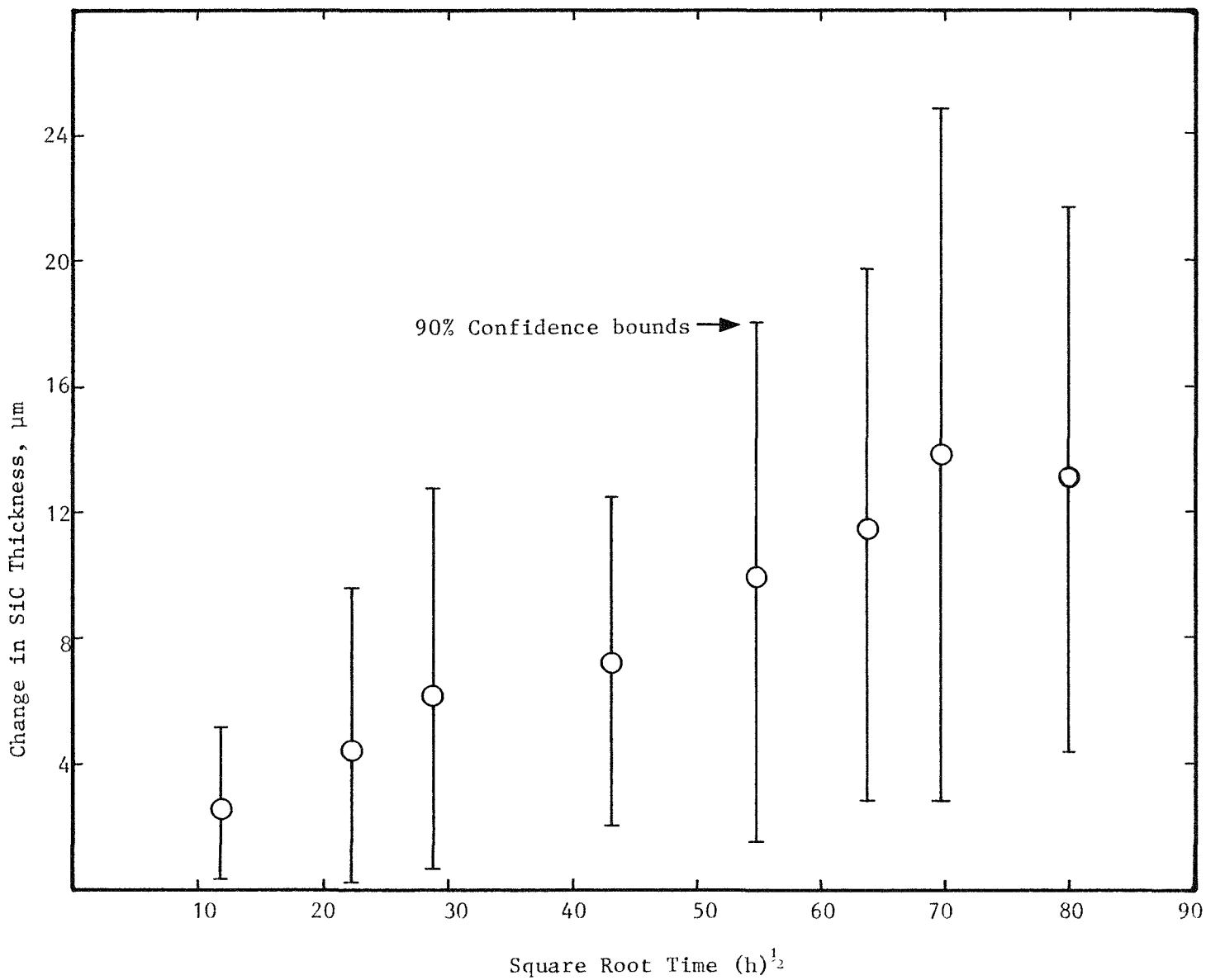

Fig. 4.2 Change in SiC thickness as a function of square root time for HEU UC_2 heated at 1511°C in out-of-pile thermal gradient test

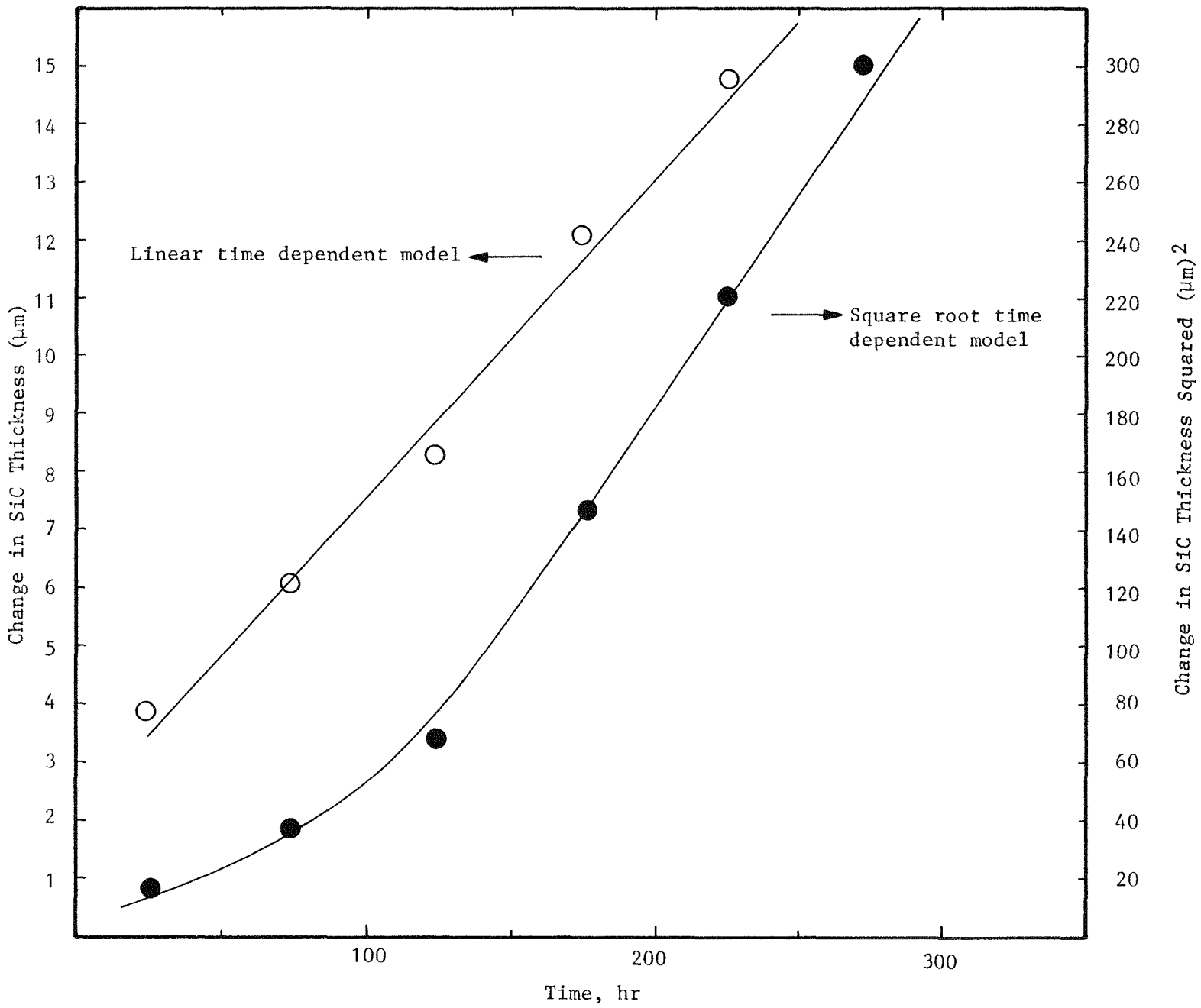

Fig. 4.3 Time dependence of fission product-SiC reactions in TRISO HEU UC_2 (6151-17-016) during out-of-pile thermal gradient testing at 1709°C

an out-of-pile test. Comparison of the locations of Pd and Si shows that the Pd has diffused at least 2/3 of the way through the SiC. The photomicrograph of the SiC in the region of the line traces shows no Pd corrosion of the SiC. If, indeed, Pd is being released from the particles during the out-of-pile tests, then the concentration of Pd in the particle decreases with time. Kaae has suggested that this decreasing Pd source causes the apparent square root time dependence for the out-of-pile tests. During irradiation, the concentration of Pd in a particle does not decrease with time but in fact increases because it is continuously being generated by fissioning. Neither model has yet been shown to be the best description of the time dependence of in-pile fission product-SiC reactions.

4.4 Temperature Dependence

The rate constants for SiC thinning caused by fission product - SiC reactions defined by eqs. 2 and 5 are given as a function of 1/T in figure 4.4 assuming the linear time dependence model; and in figure 4.5, assuming the square root time dependence model. These figures show that both models for fission product-SiC reactions generally follow the Arrhenius relationship with temperature

$$k = A \exp(-Q/RT) \tag{7}$$

where

k = proportionality constant defined by eqs. 2 and 5, μm/hr or μm^2/hr
A = preexponential factor, μm/hr or μm^2/hr
Q = activation energy J/mole
R = gas constant, 8.314 J/mole-K
T = temperature, K

The 50% confidence lines shown in the figures were obtained by a least squares fit of ℓn k versus 1/T. The 90% confidence bounds are for the estimation of the rate constant for a single observed temperature (Ref. 34).

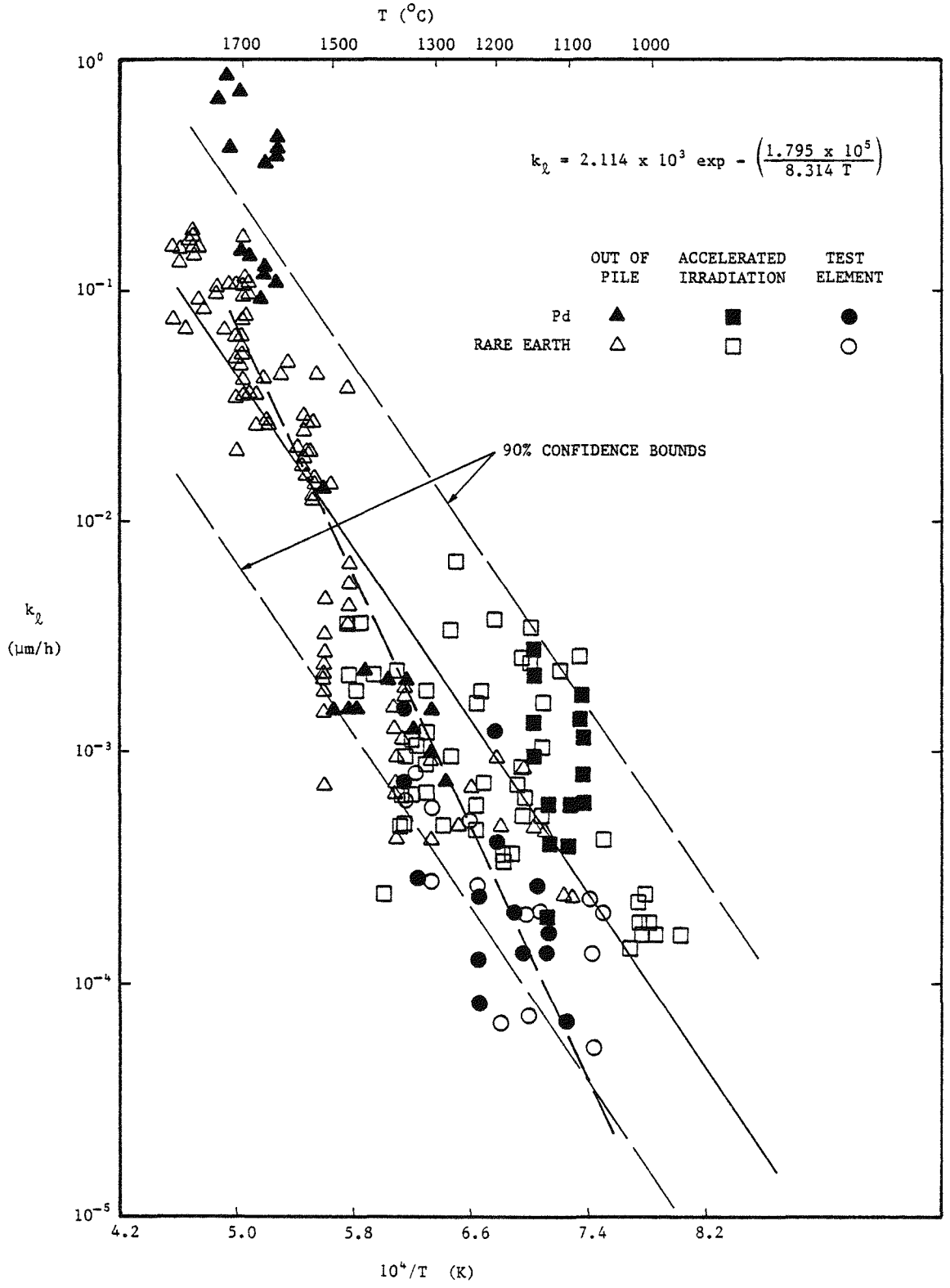

Fig. 4.4 Temperature dependence of fission product-SiC reaction rate constant for linear time dependence model

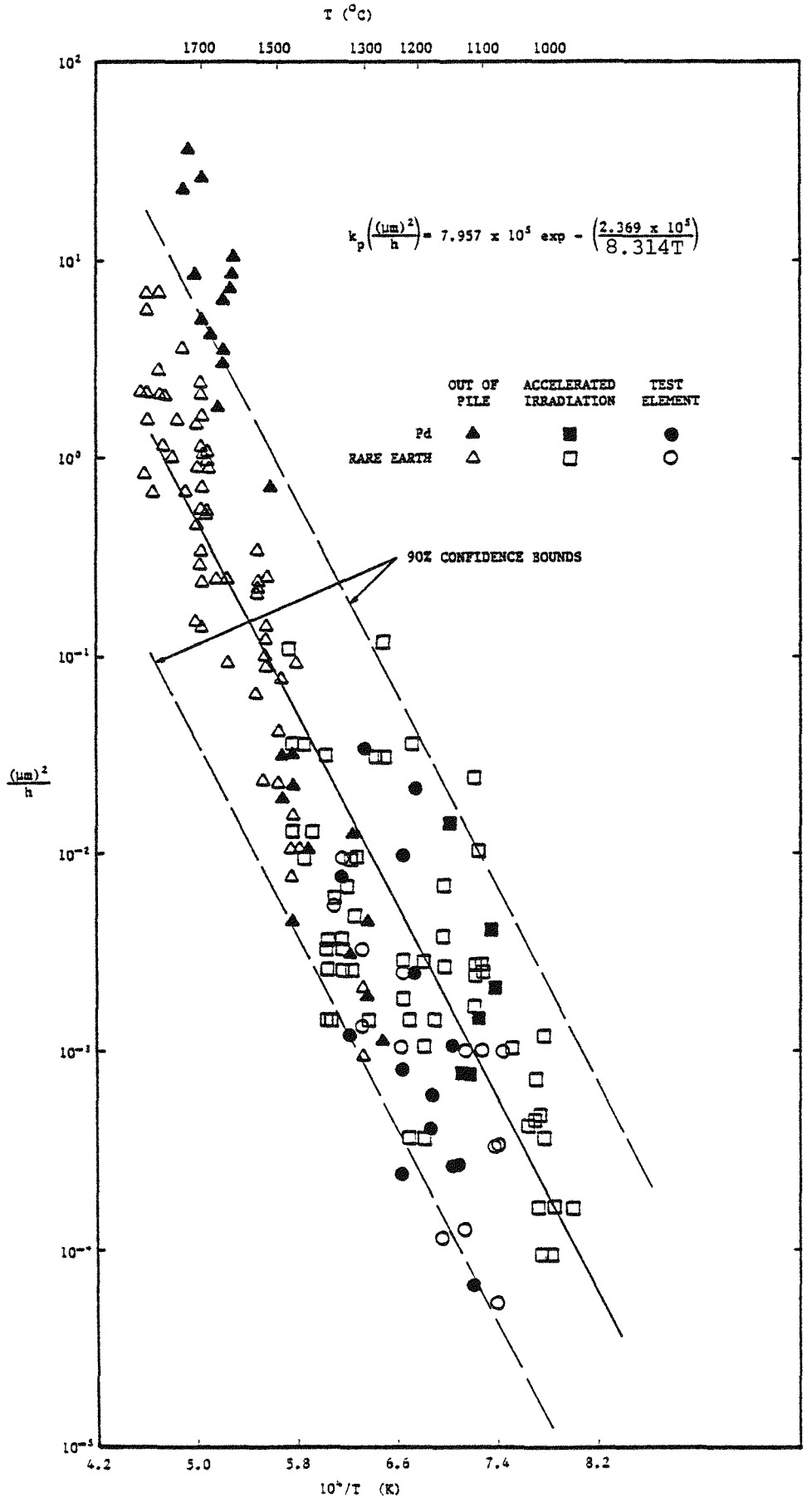

Fig. 4.5 Temperature dependence of fission product-SiC reaction rate constant for square root time dependence model

For the linear time dependence model

$$A_\ell = 2.114 \times 10^3 \ \mu m/hr$$

$$Q_\ell = 1.795 \times 10^5 \ J/mole \pm 0.081 \times 10^5 \ J/mole$$

and for the square root time dependence model

$$A_p = 7.957 \times 10^5 \ \mu m^2/hr$$

$$Q_p = 2.369 \times 10^5 \ J/mole \pm 0.114 \times 10^5 \ J/mole$$

The correlation coefficients for both Arrhenius plots (0.8751 for the linear model; 0.8613 for the square root model) are similar and thus do not allow any conclusion as to which time dependence is correct. In compiling the data for figures 4.4 and 4.5 no distinction was made between in-pile and out-of-pile data; rare earth or Pd attack; accelerated or real time irradiations; or between HEU and LEU fuel.

The data used in the Arrhenius plots are given in Tables 4.1-4.7 and include measurements of SiC thinning from the following types of experiments:

(1) out-of-pile thermal gradient tests at ORNL by Lindemer, et. al., on SiC interaction with NdC_2 and LaC_2 (Refs. 21 and 32) and with Pd (Ref. 21) in SiC coated kernels doped with simulated fission products

(2) out-of-pile thermal gradient tests at ORNL by Lauf on Pd-SiC interaction in SiC coated particles with Pd doped kernels (Ref. 19)

(3) out-of-pile thermal gradient tests on irradiated HEU UC_2 conducted at GA by Smith (Ref. 17)

(4) in-pile irradiation testing of TRISO HTGR fuel during accelerated capsule tests from data obtained by Tiegs, et. al., at ORNL (Ref. 26) and by various experimenters at GA

(5) in-pile irradiation testing of TRISO HTGR fuel during real time irradiation testing from the Peach Bottom test element program (Refs. 35 and 36)

The temperatures used in the Arrhenius plots for the out-of-pile data are those given in the documents cited in the tables. For the in-pile data, however, the temperatures used were activation energy weighted. Activation energy weighting defines an effective temperature, $T_{eff.}$, at which the irradiation can be considered to have taken place and accounts for the fact that the irradiations were non-isothermal. Activation energy weighting of non-isothermal data is appropriate for chemical reactions or for processes in which the rate is an exponential function of temperature (i.e. diffusion). A computer program was written which calculated $T_{eff.}$ from the time-temperature history for each irradiation experiment using equation 8

$$e^{-Q/RT_{eff.}} = \frac{\sum_i \Delta t_i e^{-Q/RT_i}}{\sum_i \Delta t_i} \qquad (8)$$

where Q is the Arrhenius activation energy and Δt_i is the length of time that the sample was at temperature $T_i(K)$. Equation 8 is analogous to the well known statistical formula for calculating the weighted mean of a population (Ref. 37). To use equation 8, the Activation Energy, Q, for the fission product-SiC reaction was needed. Since this is determined from the

Arrhenius plot, an iterative procedure was used to arrive at the best value. Initially, the out-of-pile data, which was obtained isothermally, was used to calculate Q. This Q was used to weight the temperatures of the in-pile data and then the out-of-pile and in-pile data were combined to compute a new Q. This procedure was repeated until Q did not change on successive runs.

When possible, the time-temperature history of the in-pile samples was taken from computer outputs of the thermal analysis of the capsule and test element experiments. In some instances, however, the thermal analyses were not available. For capsule HRB-14, only rods 2, 10, and 17 had detailed thermal analysis. An estimate of $T_{eff.}$ for the other rods which showed SiC attack was obtained from a linear interpolation of $T_{eff.}$ for rods 2, 10 and 17 based on their relative location in the reactor. No attempt was made to account for different fuel types and thus different fission heat rates. Temperature data for HRB-4, HRB-5, HRB-11, HRB-12 and for P13Q were taken from plots of the irradiation temperature versus the irradiation time given in the postirradiation examination reports. Temperatures for particles in capsules P13R, P13S, and HT-33 were calculated by eqs. 9 and 10 from the location of the particle within the fuel rod (Ref. 15)

$$T = T_{c.\ell.} - bx^2 \tag{9}$$

$$b = \frac{T_{c.\ell} - T_s}{r^2} \tag{10}$$

where

$T_{c.\ell.}$ = fuel rod centerline temperature
x = distance of particle from fuel rod centerline
T_s = fuel rod surface temperature
r = radius of fuel rod

The final activation energy weighted temperatures for both the linear and square root time dependence models are given along with the linear time weighted vol. average temperature in tables 4.2-4.3.

Two sources of error in the SiC thinning rate are prevalent in the irradiation data. The first is intrinsic in the ceramographic technique used to measure the extent of SiC corrosion in the particles: unless the grinding and polishing coincides exactly with the position of maximum SiC corrosion, the measured amount of SiC thinning is biased low. The magnitude of this error is very difficult to estimate and depends on the care with which the ceramographic grinding was completed.

The second source of error is in the uncertainty in the temperature of the particle during irradiation. Young has identified three primary sources of error in the method used for the thermal analysis of the P13Q capsule (Ref. 3). The root mean square of these errors was calculated to be approximately $\pm$100°C.

Another uncertainty in the reaction temperature is caused by the fact that there is a thermal gradient across a fuel rod; with the center hotter than the edges. With the exception of P13R and P13S, postirradiation examination of fuel rods done by General Atomic did not record the location in the fuel rods of the particles that had fission product-SiC attack. Thus it is not known whether peak fuel rod temperature, fuel rod surface temperature or fuel rod volume averaged temperature is the best estimate of reaction temperature. As mentioned earlier, postirradiation examination of P13R and P13S did include particle locations, and the particle temperature was calculated using the location, the rod centerline temperature and assuming a parabolic temperature profile across the rod. The location of the particles in which SiC thinning was observed was, on the average, 56% of the way between the rod centerline and the rod surface. This is approximately the location of the volume average temperature and thus, activation energy weighted, volume

average temperature were used for most of the data in the Arrhenius plots. For the FTE-13 samples, however, the maximum fuel rod temperature was used since SiC thinning data was taken only from particles at the fuel rod centerline.

4.5 Comparison of Measured and Predicted SiC Penetration in Peach Bottom Test Element Fuel for Linear and Square Root Time Dependence Models

Saurwein has calculated the nominal SiC penetration (50% confidence) for samples of HTGR fuel used in Peach Bottom test elements (Ref. 38). This calculation used the Arrhenius activation parameters discussed in the previous section and compared both the linear and square root time dependence models.

The nominal SiC penetration, ΔSiC_N, was calculated based on temperature histories obtained for the Peach Bottom test elements using the TREVOR code. For the linear model,

$$\Delta SiC_N = \sum_{i=1}^{N} \Delta t_i \, A_\ell e^{-Q_\ell/RT_i} \qquad (11)$$

where the symbols are defined for eq. 8. To calculate the penetration using the square root model, the Arrhenius expression was substituted into eq. 3 and eq. 3 was rearranged to give

$$\Delta SiC_N = \sqrt{\sum_{i=1}^{N} \Delta t_i \, A_p e^{-Q_p/RT_i}} \qquad (12)$$

The 90% confidence range was calculated by propagating the error associated with the Arrhenius fit along with a $\pm$ 130°K uncertainty in the test element temperature.

The results of this calculation are given in Table 4.8, and show that both models overpredict the amount of SiC thinning observed in the test element samples. Both models predict fairly well the observed penetration at temperatures $\lesssim$1100°C. However, as the temperature of the sample increases the linear model considerably overpredicts the penetration. At effective temperatures >1300°C, the ratio of predicted penetration to measured penetration is $\sim$6 for the linear model. The square root model also overpredicts at temperature >1100, but not as severly as does the linear model. When $T_{eff.}$ >1300, the predicted penetration is about twice the measured value.

A linear time dependence model developed from the out-of-pile data and the test element data does predict the penetration observed in the test elements. The model, shown as a dashed line in Fig. 4.4, has the following Arrhenius constants:

$$Q = 2.608 \times 10^5 \pm 0.013 \times 10^5 \text{ J/mole}$$

$$A = 4.515 \times 10^5 \text{ μm/hr}$$

In order to use this model, it would be necessary to rationalize why the accelerated irradiation data exhibits rates of SiC - fission product attack much greater than real time irradiations. This could be justified by the following considerations: (1) neutron flux enhancing the reaction rate, (2) fuel samples used in the capsule tests which were contaminated or had inferior coatings. The effect of neutron fluence on SiC - fission product corrosion was studied by Grübmeier (Ref. 39). He found that fast neutrons cause a change in the SiC and that a high neutron fluence can be accompanied by strong SiC corrosion. Substantial fuel performance gains could be realized, i.e. a factor of 2-20 reduction in reaction rates between 1300° and 900°C, if additional empirical evidence is developed to support a linear model based on exclusion of accelerated capsule data (refer to dashed line in Fig. 4.4)

Table 4.1

SiC PENETRATION OBSERVED DURING OUT-OF-PILE THERMAL GRADIENT HEATING TESTS OF TRISO HTGR FUEL AT GENERAL ATOMIC

Experiment Designation Number	Data Retrieval Number	Irradiation Test	Out-of-Pile Time Weighted Temperature °C	Out-of-Pile Test Time hr	Change in SiC μm	Rate		Reference
						μm/hr x 10^4	μm/$\sqrt{hr}$ x 10^2	
5217-5[a]	4413-5E	P13L	1306	2541	2.3	9.05	4.56	GA-905239/1
			1306	5549	2.3	4.14	3.09	
			1306	5549	2.3	4.14	3.09	
			1306	5549	2.7	4.87	3.62	
			1306	5549	5.1	9.19	6.85	
			1460	575	3.0	52.2	12.5	
			1460	575	3.7	64.3	15.4	
			1460	575	2.5	43.4	10.4	
			1460	575	2.1	36.5	8.76	
6804[a]	4161-01-030	FTE-14 TS5-6	1551	617	11.4	185	45.9	
			1551	617	11.8	191	47.5	
			1551	617	12.1	196	48.7	
			1551	617	14.8	240	59.6	
			1551	617	10.9	177	43.9	
			1551	617	12.2	198	49.1	
			1551	617	12.2	198	49.1	
7013[a]	4161-01-030	FTE-14 TS3-6	1692	87.25	6.9	791	73.9	
			1692	87.25	6.9	1029	95.3	
			1692	87.25	9.8	1123	105	
			1692	87.25	9.3	1066	99.6	
/013[a]	4161-01-034 -002	P13P CIP2	1704	87.25	6.7	768	71.7	
			1704	87.25	8.0	917	85.6	
			1704	87.25	8.4	963	89.9	
			1704	87.25	8.4	963	89.9	
			1704	87.25	9.4	1077	101	
7013[a]	4161-01-032 -002	P13P CIP4	1707	87.25	5.5	630	58.9	
			1707	87.25	3.5	401	37.5	
			1707	87.25	5.1	585	54.6	
			1707	87.25	4.6	527	49.2	
			1707	37	6.3	1703	104	
6804[a]	4161-01-032 -002	P13P CIP4	1525	331	9.2	278	50.6	
			1525	617	7.5	122	30.2	
			1525	617	9.5	154	38.2	
			1525	617	7.9	128	31.8	
			1525	617	8.7	141	35.0	

[a] Data on which original linear model was based.

Table 4.1 (continued)

SiC PENETRATION OBSERVED DURING OUT-OF-PILE THERMAL GRADIENT HEATING TESTS OF TRISO HTGR FUEL AT GENERAL ATOMIC

Experiment Designation Number	Data Retrieval Number	Irradiation Test	Out-of-Pile Time Weighted Temperature °C	Out-of-Pile Test Time hr	Change in SiC μm	Rate		Reference
						μm/hr x 10^4	μm/$\sqrt{hr}$ x 10^2	
78TG[b]	6151-17-025	HB2 T250	1362	8222	3.5	4.26	3.86	GA-905239/1
				8222	5.5	6.69	6.07	
				8222	8.0	9.73	8.82	
				8222	6.0	7.30	6.62	
				8222	13	15.8	14.3	
				8222	10.5	12.8	11.6	
				8222	5.5	6.69	6.07	
78TG[b]	6151-17-016	HB5 T210	1351	8222	9.5	11.6	10.5	
				8222	4.5	5.47	4.96	
				8222	10	12.2	11.0	
				8222	15.5	18.9	17.1	
				8222	14	17.0	15.4	
				8222	9	10.9	9.93	
78TG[b]	6151-17-025	HB2 T250	1508	6396	13	20.3	16.3	
				6396	21	32.8	26.3	
				6396	4.5	7.04	5.63	
				6396	17.5	27.4	21.9	
				6396	29	45.3	36.3	
				6396	14	21.9	17.5	
78TG[b]	6151-17-016	HB5 T210	1514	6396	15.5	24.2	19.4	
				6396	13	20.3	16.3	
				6396	12	18.8	15.0	
				6396	11.5	18.0	14.4	
				6396	9.5	14.9	11.9	
				6396	13.5	21.1	16.9	
78TG[b]	6151-17-025	HB2 T250	1727	275	11.5	418	69.3	
				375	7.5	200	38.7	
				375	13	347	67.1	
				375	23.5	627	121.4	
				375	18.5	493	95.5	
78TG[b]	6151-17-016	HB5 T210	1709	275	16.5	600	99.5	
				275	26.0	945	156.8	
				325	15.5	477	86.0	
				325	23	708	128	
				325	17.5	538	97.1	
				325	16.5	508	91.5	

[b] Data used to support square root time dependence

Table 4.2

SiC PENETRATION OBSERVED DURING ACCELERATED IRRADIATION TESTING OF TRISO HTGR FUEL

Data Retrieval Number	Irradiation Test	Position	Irradiation Temperature[c] °C	Activation Energy Weighted		Irradiation Time hr.	PIE	Decrease in SiC Thickness µm	Rate		Reference
				Linear Model °C	Square Root Model °C				µm/hr. x 10^4	µm/$\sqrt{hr.}$ x 10^2	
6151-12-015	P13T	1-1B4	1215	1227	1231	8800	GA	5	5.68	5.33	GA-A15608
		1-1B2	1177	1190	1194			5	5.68	5.33	W.J. Scheffel private communication
		2-4A1	995	1018	1027			2	2.27	2.13	
			995					2	2.27	2.13	
			995					2	2.27	2.13	
6151-17-025	P13T	1-1C4	1215	1227	1231			4	4.55	4.26	
		1-1C1	1177	1190	1194			3	3.41	3.20	
6151-00-010	P13Q	G2-1B	932	936	938	9401		5	5.32	5.16	GA-A14174
		G1-3A	1105	1113	1114			4	4.25	4.13	
								10	10.6	10.3	
								10	10.6	10.3	
								5	5.32	5.16	
								5			
								5			
								5			
								5			
								15	16.0	15.5	
6151-00-010	P13Q	G1-2B	1161	1163	1164	9401		6	6.38	6.19	
								8	8.51	8.25	
6151-00-010	P13Q	G1-3B	1161	1163	1164	9401		5	5.32	5.16	
6151-00-035	P13R	2B[a]	1037	1053	1058	6192		2.5	4.04	3.18	GA-A13827
			1000	1015	1021			<1	<1.61	<1.27	
6151-00-035	P13R	2C[a]	981	996	1002			<1.0	<1.61	<1.27	
			954	971	977			<1.0	<1.61	<1.27	
			977	992	997			<1.0	<1.61	<1.27	
			994	1008	1013			1.5	2.42	1.91	
			1038	1050	1055			<1.0	<1.61	<1.27	
			979	994	1000			<1.0	<1.61	<1.27	
6151-00-035	P13S	5C[a]	1321	1356	1372			3.0	4.84	3.81	
			1274	1311	1326			5.5	8.88	6.99	
			1332	1367	1382			1.5	2.42	1.91	
			1274	1311	1326			4.0	6.46	5.08	
			1325	1360	1375			3.0	4.84	3.81	
			1330	1365	1380			4.0	6.46	5.08	
			1243	1282	1297			3.0	4.84	3.81	
			1249	1288	1303			3.0	4.84	3.81	

[a] Calculated temperature using time weighted fuel rod centerline temperature and hyperbolic temperature profile across rod.

Table 4.2 (continued)

SiC PENETRATION OBSERVED DURING ACCELERATED IRRADIATION TESTING OF TRISO HTGR FUEL

Data Retrieval Number	Irradiation Test	Position	Irradiation Temperature °C [c]	Activation Energy Weighted		Irradiation Time hr	PIE	Decrease in SiC Thickness µm	Rate		Reference
				Linear Model °C	Square Root Model °C				µm/hr x 10^4	µm/ hr x 10^2	
6151-00-035	P13S [a]	5C	1327	1362	1377	6192	GA	4.5	7.27	5.72	GA-A13827
			1298	1335	1350			1.5	2.42	1.91	
			1331	1366	1381			14.0	22.6	17.8	
6151-08-015	P13S [a]	5D	1299	1336	1351	6192		4.0	6.46	5.08	
			1312	1349	1365			6.0	9.69	7.62	
			1307	1343	1359			6.0	9.69	7.62	
			1237	1276	1291			6.0	9.69	7.62	
			1278	1316	1331			7.5	12.1	9.53	
			1288	1325	1340			6.5	10.5	8.26	
OR2576H	HT-33 [a]	19	1416	1454	1455	2759	ORNL	6	21.7	11.4	ORNL-5539
			1410	1448	1449			5	18.1	9.52	Private communication T. N. Tiegs, ORNL
			1418	1456	1457			10	36.2	19.0	
			1425	1463	1464			18	65.2	34.3	
			1372	1408	1409			6	21.7	11.4	
			1372	1408	1409			6	21.7	11.4	
			1399	1437	1437			10	36.2	19.0	
		6	1157	1189	1190			1	3.62	1.90	
			1188	1222	1223			5	18.1	9.52	
			1183	1217	1218			2	7.25	3.80	
			1182	1215	1217			2	7.25	3.80	
			1152	1184	1185			1	3.62	1.90	
			1144	1175	1176			2	7.25	3.80	
	HT-34	28	1335	1341	1342	2686		3	11.2	5.79	
		37	1311	1316	1318			5	18.6	9.65	
		41	997	1004	1006			0.5	1.86	0.96	
		44	1017	1023	1025			1.4	5.21	2.70	
		47	1022	1028	1030			1.8	6.70	3.47	
		50	1006	1011	1013			0.5	1.86	0.96	
6252-14-0161-001	HT-34 [b]	10	1242	1263	1268			18	67.0	34.7	GA-A15612
6252-15-0161-001		11	1252	1274	1279			9	33.5	17.4	
		11	1252	1274	1279			9	33.5	17.4	
6252-16-0161-001		13	1181	1204	1209			10	37.2	19.3	
		13	1181	1204	1209			10	37.2	19.3	

(b) Time weighted particle surface temperature
(c) Time weighted

Table 4.2 (continued)

SiC PENETRATION OBSERVED DURING ACCELERATED IRRADIATION TESTING OF TRISO HTGR FUEL

Data Retrieval Number	Irradiation Test	Position	Irradiation Temperature[c] °C	Activation Energy Weighted		Irradiation Time hr	PIE	Decrease in SiC Thickness µm	Rate		Reference
				Linear Model °C	Square Root Model °C				µm/hr x 10^4	µm/$\sqrt{hr}$ x 10^2	
6252-17-010	HRB-14	1	1130	1145	1151	5124	GA	5	9.76	6.98	GA-A15969
								7	13.7	9.78	
								7	13.7	9.78	
								7	13.7	9.78	
								11	21.5	15.4	
								14	27.3	19.6	
6155-05-020		4	1090	1126	1132			1	1.95	1.40	
								2	3.90	2.79	
								2	3.90	2.79	
								2	3.90	2.79	
								2	3.90	2.79	
								2	3.90	2.79	
								3	5.85	4.19	
6152-01-010		6	1070	1048	1119			1	1.95	1.40	
								1	1.95	1.40	
								2	3.90	2.79	
								2	3.90	2.79	
								2	3.90	2.79	
								2	3.90	2.79	
								2	3.90	2.79	
								2	3.90	2.79	
6157-08-010		8	1055	1100	1107			2	3.90	2.79	
								3	5.85	4.19	
								3	5.85	4.19	
								3	5.85	4.19	
6157-08-020		10	1042	1081	1087			3	5.85	4.19	
								3	5.85	4.19	
								3	5.85	4.19	
								3	5.85	4.19	
								3	5.85	4.19	
								3	5.85	4.19	
								3	5.85	4.19	
								4	7.81	5.59	
								4	7.81	5.59	
								4	7.81	5.59	
								4	7.81	5.59	
								4	7.81	5.59	
								5	9.76	6.98	
								6	11.7	8.38	
								6	11.7	8.38	
								6	11.7	8.38	
								7	13.7	9.78	
								7	13.7	9.78	
								9	17.6	12.5	

[c] Time weighted

Table 4.2 (continued)

SiC PENETRATION OBSERVED DURING ACCELERATED IRRADIATION TESTING OF TRISO HTGR FUEL

Rate Retrieval Number	Irradiation Test	Position	Irradiation Temperature °C[c]	Activation Energy Weighted		Irradiation Time hr	PIE	Decrease in SiC Thickness µm	Rate		Reference
				Linear Model °C	Square Root Model °C				µm/hr x 10^4	µm/$\sqrt{hr}$ x 10^2	
6157-08-010	HRB-14	12	1025	1073	1082	5124	GA	2	3.90	2.79	GA-A15969
								3	5.85	4.19	
								3			
								3			
								3			
								3			
								3			
								3			
								4	7.81	5.59	
								4	7.81	5.59	
								5	9.76	6.98	
		14	1010	1060	1069			2	3.90	2.79	
								3	5.85	4.19	
								3	5.85	4.19	
								4	7.81	5.59	
OR2486-H	HRB-12	4	1155	1155	1165	6602	ORNL	16.3	24.7	20.1	Private communication T. N. Tiegs (ORNL) ORNL-5584
OR2494-H		5	1260	1165	1175			16.9	25.6	20.8	
OR2460-H	HRB-11	2	1000	1091	1099	6559		17	25.9	21.0	
OR2458-H		16	1250	1230	1241			11	16.8	13.5	
OR2471-H		21	1220	(d)	(d)			11	16.8	13.5	
OR52-A	HRB-4	3A	1300	1153	1161	5855		20	34.2	26.1	ORNL-5115
OR52-A		3B	1300	1118	1126			13	22.2	17.0	
A615	OF-2	C2-1	1200	(d)	(d)	8440		1.8	2.13	1.96	Private communication T. N. Tiegs (ORNL) ORNL-5428

(d) Not determined

Table 4.3

SiC PENETRATION OBSERVED DURING REAL TIME IRRADIATION TESTING OF HTGR FUEL IN PEACH BOTTOM TEST ELEMENTS

Data Retrieval Number	Irradiation Test	Position	Time Weighted Irradiation Temperature °C	Activation Energy Weighted: Linear Model °C	Activation Energy Weighted: Square Root Model,°C	Irradiation Time	PIE	Decrease in SiC Thickness μm	Rate: μm/hr x 10^4	Rate: μm/$\sqrt{hr}$ x 10^2	Reference
4161-01-030	FTE-14	TS8-3	1534[b]	(c)	(c)	8712	GA	10	11.5	10.7	GA-A13944
		TS5-6	1418[b]	(c)	(c)			10	11.5	10.7	
		TS4-6	1364[b]	(c)	(c)			4.5	5.17	4.82	
4161-01-031		2-1-7	1275	1305	1313			5.0	5.74	5.36	
4161-01-030	FTE-15	TS8-3	1468[b]	(c)	(c)	14901		2	1.34	1.64	
		TS5-6	1389[b]	(c)	(c)			15	10.1	12.3	
		TS4-6	1355[b]	(c)	(c)			3	3.36	4.10	
4161-01-031		2-2-5	1299	1333	1343			12	8.05	9.83	
		2-1-5	1319	1354	1365			9	6.04	7.37	
		2-1-9	1185	1227	1238			4	2.68	3.27	
4000-325	RTE-1	3-6-6	1267	1302	1310	18358	ORNL	5	2.72	3.69	
4000-307	RTE-2	6-1-1	1036	1068	1079	18641		1.0	0.536	0.732	
		6-1-3	1041	1074	1084		GA	2.5	1.34	1.83	
		Body 3	1044	(c)	(c)		ORNL	5	2.68	3.66	
	RTE-4	4-7-3	1237	1240	1241	9931	GA	5	5.03	5.02	
		4-1-3	1237	1240	1241		ORNL	5	5.03	5.02	
	RTE-5	3-5-6	1034	1061	1066	24832	ORNL	5	2.01	3.17	
	RTE-6	4-1-1	1095	1119	1124	24832		5	2.01	3.17	
	RTE-7	5-5-5	1056	1076	1077	6474		1.5	2.32	1.86	
	RTE-8	5-7-1	1072	1097	1101	24832		5	2.01	3.17	
	FTE-5	2-5-7	1110	1155	1164	24832	GA	1.7	0.685	1.08	
	FTE-5	3-5-2	1085	1115	1124	24832	GA	1.8	0.725	1.14	
ORNL-13-6	FTE-13	2-2-2	1186	1226	1237	12288	ORNL	1.9	15.5	17.1	ORNL/TM-7203
		2-2-6	1306	1348	1358			23	18.3	20.3	GA-904053A
		2-2-6	1306	1348	1358			22			ORNL/TM-7203
		2-2-9	1162	1200	1210			18	14.6	16.2	ORNL/TM-7203
		2-2-12	1091	1127	1138			2	1.63	1.80	ORNL/TM-7203
ORNL-13-1		2-5-9	1135	1173	1183			4	2.03	2.26	GA-904053A
		2-5-9	1135	1173	1183			1			ORNL/TM-7203
		2-5-12	1068	1106	1115			1	0.814	0.902	ORNL/TM-7203
ORNL-13-4		2-6-2	1186	1226	1237			4	2.85	3.16	GA-904053A
			1186	1226	1237			3			ORNL/TM-7203
			1186	1226	1237			12	9.77	10.8	ORNL/TM-7203
		2-6-6	1306	1348	1358			14	8.75	9.70	GA-904053A
		2-6-6	1306	1348	1358			7.5			ORNL/TM-7203
		2-6-9	1162	1200	1210			6	4.88	5.41	GA-904053A
		2-6-12	1091	1127	1138			2	1.63	1.80	ORNL/TM-7203
ORNL-13-2		2-7-6	1279	1325	1336			4.5	3.46	3.83	GA-904053A
		2-7-6	1279	1325	1336			4			ORNL/TM-7203
		2-7-12	1069	1103	1112			4	3.26	3.61	ORNL/TM-7203
ORNL-13-5		2-8-9	1137	1175	1185			3	2.44	2.71	GA-904053A

[a] Volume averaged

[b] Maximum loose particle temperature

[c] Not determined

[d] Maximum fuel rod temperature

Table 4.4

ORNL OUT-OF-PILE FISSION PRODUCT-SiC REACTION RESULTS FOR SYNTHETICALLY DOPED KERNELS FROM ORNL/TM-6991 (Ref. 21)

ORNL Sample	Temperature °C	Out-of-Pile Heating Time hr	SiC Penetration μm	Rate	
				μm/hr	μm/$\sqrt{hr}$
1-2[a]	1772	50	34	0.68	4.81
1-2	1760	50	43	0.86	6.08
1-2	1739	50	21	0.42	2.97
1-2	1703	50	37	0.74	5.23
1-2	1650	50	18	0.36	2.55
1-2	1632	50	19	0.38	2.69
1-2	1614	50	23	0.46	3.25
1-2	1614	50	21	0.42	2.97
1-2	1519	352.8	51	0.014	0.859
2-4[b]	1661	215	20	0.093	1.36
2-4	1646	215	28	0.13	1.90
2-6[c]	1688	215	30	0.14	2.05
2-6	1650	215	26	0.12	1.77
2-7[d]	1715	215	33	0.15	2.25
2-7	1621	215	24.5	0.11	1.67

[a] UC_2 plus Mo-Ru-Rh-Pd (batch OR-2773)

[b] UO_2 plus Mo-Ru-Pd (batch OR-2822)

[c] 90% UO_2/10% UC_2 plus Mo-Ru-Pd (batch OR-2823)

[d] 65% UO_2/35% UC_2 plus Mo-Ru-Pd (batch OR-2807)

Table 4.5

ORNL RAW DATA FOR NdC_2-SiC INTERACTION IN SiC-COATED PARTICLES AT 278°C/cm[a]

Run Number/ Time (hr)	Particle Number	Penetration of SiC (μm)	Temperature °C	Rate	
				μm/hr x 10^4	μm/$\sqrt{hr}$ x 10^2
1/144	1	11	1906	764	91.7
	2	10	1882	694	83.3
	3	15	1789	1040	125
	4	13	1828	903	108
	6	10	1760	694	83.3
	8	5	1676	347	41.7
	9	9	1711	625	75.0
	10	5	1723	347	41.7
	11	6	1654	417	50.0
	12	6	1635	417	50.0
	5	12	1819	833	100
	7	9	1743	625	75.0
4/187	6	35	1855	1872	256
	9	16	1868	656	117
	18	8	1607	428	58.5
	19	8	1596	428	58.5
	21	9	1600	481	65.8
4/90	2	14	1920	1556	148
	3	12	1901	1333	126
	4	14	1901	1556	148
	6	16	1855	1778	169
	7	14	1846	1556	148
	8	14	1832	1556	148
	9	15	1868	1667	158
	10	13	1841	1444	137
	11	14	1873	1556	148
	12	10	1819	1111	105
	13	9	1789	1000	94.9
	14	10	1747	1111	105
	15	7	1727	778	73.8

[a] Lindemer, T. B., et. al., Ref. 21

Table 4.5 (continued)

ORNL RAW DATA FOR NdC_2-SiC INTERACTION IN SiC-COATED PARTICLES AT 278°C/cm[a]

Run Number/ Time (hr)	Particle Number	Penetration of SiC (μm)	Temperature °C	Rate	
				μm/hr x 10^4	μm/$\sqrt{hr}$ x 10^2
4/90	16	10	1692	1111	105
	17	8	1639	889	84.3
	18	7	1607	778	73.8
	19	3	1596	333	31.6
	20	4	1614	444	42.2
	22	8	1614	888	84.3
6/500[b]	1	9.7	1741	194	43.4
	5	18.4	1720	368	82.2
	6	14.1	1670	282	63.1
	8	12.9	1700	258	57.7
	10	20.3	1682	406	90.8
	11	18.3	1686	366	81.8
	12	12.9	1668	258	57.7
	14	13.2	1650	264	59.0
	15	13.9	1636	278	62.2
	16	13.7	1641	274	61.3
	18	13.3	1550	266	59.5
	22	10.0	1552	200	44.7
	23	13.1	1614	262	58.6
	24	14.2	1618	284	63.5
	26	6.7	1586	134	30.0
	30	19.0	1470	380	85.0

[b] Linear fit of data obtained over 274h.

Table 4.5 (continued)

ORNL RAW DATA FOR NdC_2-SiC INTERACTION IN SiC-COATED PARTICLES AT 278°C/cm[a]

Run Number/ Time (hr)	Particle Number	Penetration of SiC (μm)	Temperature °C	Rate	
				μm/hr x 10^4	μm/$\sqrt{hr}$ x 10^2
3/4265	1	5	1409	11.7	7.65
	2	5	1368	11.7	7.65
	3	3	1294	7.03	4.59
	4	4	1303	9.38	6.12
	5	2	1317	4.69	3.06
	6	5	1298	11.7	7.65
	7	4	1201	9.38	6.12
	8	2	1215	4.69	3.06
	9	2	1191	4.69	3.06
	10	2	1178	4.69	3.06
	11	2	1215	4.69	3.06
	12	2	1259	4.69	3.06
	13	1	1238	2.34	1.53
	15	2	1196	4.69	3.06
	16	2	1150	4.69	3.06
	17	2	1131	4.69	3.06
	18	1	1099	2.34	1.53
	19	1	1108	2.34	1.53

Table 4.6

ORNL RAW DATA FOR LaC_2-SiC INTERACTION IN SiC-COATED PARTICLES AT 278°C/cm[a]

Run Number/ Time (hr)	Particle Number	Penetration of SiC (μm)	Temperature °C	Rate	
				μm/hr x 10^4	μm/$\sqrt{hr}$ x 10^2
1/144	4	18	1828	1250	150
	5	16	1751	1110	133
	6	18	1772	1250	150
	8	15	1680	1040	125
	9	10	1646	694	83.3
	10	11	1614	764	91.7
	7	14	1747	972	117
2/386	4	6	1635	155	30.5
	9	5	1548	130	25.5
	10	5.5	1497	143	28.0
	13	3	1532	77.7	15.3
	14	4	1500	104	20.4
	15	3	1463	77.7	15.3
	17	2	1445	51.8	10.2
	19	2	1451	51.8	10.2
	20	3	1500	77.7	15.3
	21	6	1451	155	30.5
	1	10	1688	259	50.9
	2	7	1673	181	35.6
	3	7	1661	181	35.6
	5	10	1646	259	50.9
	7	7	1593	181	35.6
	8	7	1562	181	35.6
	2	4	1552	104	20.4
	16	6	1431	155	30.5
	18	7	1481	181	35.6

[a]Lindemer, T. B. *et. al.*, Ref. 21

Table 4.6 (continued)

ORNL RAW DATA FOR LaC_2-SiC INTERACTION IN SiC-COATED PARTICLES AT 278°C/cm[a]

Run Number/ Time (hr)	Particle Number	Penetration of SiC (μm)	Temperature °C	Rate	
				μm/hr x 10^4	μm/$\sqrt{hr}$ x 10^2
3/3428	3	5	1396	14.6	8.54
	4	5	1411	14.6	8.54
	5	5	1399	14.6	8.54
	6	4	1388	11.7	6.83
	7	3	1372	8.75	5.12
	8	3	1364	8.75	5.12
	9	4	1343	11.7	6.83
	12	4	1335	11.7	6.83
	13	4	1377	11.7	6.83
	14	2	1302	5.83	3.42
	15	3	1307	8.75	5.12
4/90	1	23	1901	2560	242
	3	25	1901	2780	264
	4	25	1850	2780	264
	5	24	1841	2670	250
	7	18	1772	2000	190
	9	19	1751	2110	200
	11	18	1731	2000	190
	13	17	1747	1890	179
	15	19	1785	2110	200
	16	18	1785	2000	190
	17	15	1747	1670	158
	19	15	1723	1670	158
	20	14	1703	1560	148
	21	12	1676	1330	127
	23	11	1635	1220	116

Table 4.7

ORNL RAW DATA FOR Pd-SiC INTERACTION IN SiC COATED PARTICLES AT 275°C/cm[a]

Batch	Particle Number	Penetration of SiC (μm)	Temperature °C	Rate	
				μm/hr x 10^4	μm/$\sqrt{hr}$ x 10^2
Pd-1	2	2.5	1335	12.5	5.59
↓	3	3.0	1305	15.0	6.71
	1	3.0	1460	15.0	6.71
	4	2.0	1300	10.0	4.47
Pd-2	6	4.5	1425	22.5	10.1
↓	21	1.5	1275	7.5	3.35
Pd-3	3	2.0	1305	10.0	4.47
↓	1	3.0	1470	15.0	6.71
	2	2.0	1310	10.0	4.47
Pd-4	4	4.0	1350	20.0	8.94
Pd-5	1	3.0	1490	15.0	6.71
↓	11	4.0	1375	20.0	8.94
Pd-6	5	4.0	1420	20.0	8.94
↓	11		1360	22.5	10.1
	18	2.0	1320	10.0	4.47
Pd-7	2	6.0	1430	30.0	13.4
↓	6	5.5	1365	27.5	12.3
	14	3.5	1290	17.5	7.83

[a] Lauf, R. J., Ref. 19

[b] After 2000 hr anneal time

Table 4.7 (continued)

ORNL RAW DATA FOR Pd-SiC INTERACTION IN SiC COATED PARTICLES AT 275°C/cm[a]

Batch	Particle Number	Penetration of SiC (μm)	Temperature °C	Rate	
				μm/hr x 10^4	μm/$\sqrt{hr}$ x 10^2
Pd-8	1	7	1480	35.0	1.57
	2	8	1490	40.0	17.9
	3	6	1490	30.0	13.4
	5	8	1465	40.0	17.9
	9	6.5	1425	32.5	14.5
	17	5	1330	25.0	11.2
Pd-9	3	6.5	1425	32.5	14.5
	4	3.0	1400	15.0	6.71
	10	2.5	1340	12.5	5.59
Pd-10	2	7	1450	35.0	15.7
	10	7	1375	35.0	15.7
	13	4	1325	20.0	8.94
Pd-11	4	5	1390	25.0	11.2
	7	4.5	1370	22.5	10.1
	8	8	1345	40.0	17.9
Pd-12	1	6.5	1395	32.5	14.5
	2	6	1390	30.0	13.4
	3	11.5	1395	57.5	25.7
	8	7	1345	35.0	15.7

Table 4.8

COMPARISON OF MEASURED AND PREDICTED SiC PENETRATION IN PEACH BOTTOM TEST ELEMENT

Test Element	Rod	Measured µm	Linear Model			Square Root Model		
			$T_{eff.}$ °C	Predicted µm	90% Confidence Range	$T_{eff.}$ °C	Predicted µm	90% Confidence Range
FTE-14	2-1-7	5	1305	21	11-87	1313	11	6-28
FTE-15	2-2-5	12	1333	46	31-147	1343	16	11-36
	2-1-5	9	1354	54	12-59	1365	18	13-41
	2-1-9	4	1227	18	29-138	1238	8.8	6-21
FTE-5	3-5-2	1.8	1115	9.3	6-30	1124	5.3	4-12
	2-5-7	1.7	1155	14	10-47	1164	7.0	5-16
FTE-13	2-2-2	1.9	1226	18	11-64	1237	8.7	6-22
	2-2-6	22.5	1348	52	32-182	1358	18	12-42
	2-2-9	18	1200	14	9-49	1210	7.4	5-18
	2-2-12	2	1127	6.3	4-24	1138	4.5	3-12
	2-5-9	2.5	1173	10	6-39	1185	6.2	4-16
	2-5-12	1	1106	--	--	1115	--	--
	2-6-2	3.5	1226	18	11-64	1237	8.7	6-22
	2-6-2	12	1226	18	11-64	1237	8.7	6-22
	2-6-6	10.8	1348	52	32-182	1358	18	12-42
	2-6-9	6	1200	14	9-49	1210	7.4	5-18
	2-6-12	2	1127	6.3	4-24	1138	4.5	3-12
	2-7-6	4.5	1325	43	26-158	1336	16	10-39
	2-7-12	4	1103	4.8	3-19	1112	3.7	2-10
	2-8-9	3	1175	11	7-40	1185	6.2	4-16
RTE-1	3-6-6	5	1302	43	29-138	1310	15	10-33
RTE-2	6-1-1	1	1068	4	2-16	1079	3.2	1.9-9.0
	6-1-3	2.5	1074	4	3-17	1084	3.4	2-9.4
RTE-4	4-7-3	5	1240	13	8-52	1241	7.3	5-19
	4-1-3	5	1240	13	8-52	1241	7.3	5-19
RTE-5	3-5-6	5	1061	5	3-16	1066	3.4	2.4-7.7
RTE-6	4-1-1	5	1119	10	7-30	1124	5.2	3.9-11
RTE-7	5-5-5	15	1076	15	1-7	1077	1.9	1-6
RTE-8	5-7-1	5	1097	7.5	5-23	1101	4.4	3.3-9.4

4.6 Additional SiC Corrosion Mechanisms

Besides the fission products described in section 4.1, a number of materials have been shown to react with SiC. Particular care needs to be taken during fuel manufacturing to avoid contaminating fuel particles with these materials. Included in this section is a list of these materials which can react with SiC and a literature reference to the reaction. This list does not include all possible reactants; but those that may be present due to the coating process or as contaminates in the graphite fuel block or fuel rod resin.

1. Fe and Cu; KORTEL, A. A., et. al., 1ZV, Akad, Nauk SSR, Neorg. Mater. 1970, 6(10), 1740-3, from Chemical Abstracts, 74, 1971, Abstract No. 68923

2. CaO; PANKON, V. A., et. al., Viniti 4170-76 from Chemical Abstracts, 89, 1978 Abstract No. 94990m.

3. Fe and Ni; Yurchenko, O. S., Porosh. Met. 1971, 11(1) 45-9, from Chemical Abstracts 74, 1971 Abstract No. 114971a.

4. Al; KORTEL, A. A., et. al., Tr., Vs. Es. Gos. Inst. Nauchi-Issled. Pro Rab. Ogn Eupor. Prom., 1971 No. 42, 115-24, from Chemical Abstracts 76, 1972 Abstract No. 1441869

5. Ti, V, Al; RATLIFF, J. L., PhD Thesis, Ohio State Univ., Columbus Ohio, 1969, from Diss. Abstr. Int. B 1970, 30(10), 4638-9

6. Cl; GRÜBMEIER, et. al., Nuclear Technology, Vol. 35, Sept. 1977, p. 413

Of particular concern are chlorine and iron. Chlorine can contaminate the particles during SiC deposition if the inner pyrocarbon layer is porous. Grübmeier has shown that Cℓ, in combination with uranium or certain fission

products is extremely corrosive to SiC (Refs. 39, 40). In addition, unirradiated particles have shown SiC corrosion during out-of-pile thermal gradient testing and the cause has been attributed to the presence of Cℓ (Ref. 41).

Iron can be an impurity in the pitch which bonds the fuel particles into fuel rods. Deterioration of SiC, beginning at the outer PyC-SiC interface, has been observed in TRISO particles and was attributed to iron migrating through the outer pyrocarbon and reacting with the SiC to form iron silicides (Ref. 42).

SiC coating failure has also been attributed to the presence of free Si metal in the SiC coating. In a study on coated UC_2 particles containing free Si in the SiC layer, Fukuda, et. al., found that the SiC layer deteriorated after heating above 1460°C (Ref. 42). This phenomenon may explain the deterioration of the SiC in the LEU UO_2 particles shown in Fig. 3.15. Microprobe X-ray analysis shows that these out-of-pile heat treated samples of TRISO UO_2 have islands of pure Si in the SiC. Since the samples were heated at 1500°C, it is probable that the void areas were caused by melting of the excess silicon.

4.7 SiC Failure Criterion

The extent that the SiC layer can be penetrated before it losses it capability to retain fission products is of concern when working with HTGR fuel that will remain in a reactor for ∿6 years. The current model used to predict the impact of fission product-SiC reactions assumes that when the SiC thickness is reduced by 50%, metallic fission product release will begin at a rate controlled by diffusion through the intact outer pyrocarbon layer. Although the data are limited in this are, Tiegs has observed that no volatile Cs-137 loss occurred after Pd penetration 63% of the way through a 41.8 μm SiC layer in a dense LEU UO_2 particle which was irradiated in capsule HT-31 (Ref. 26). In addition, results of GA out-of-pile tests show that Cs-137 is not released from irradiated

TRISO UC_2 particles heated at ∿1500°C even though the SiC thickness is decreased by 73-80% (Ref. 44).

5. CONCLUSIONS

The following are conclusions concerning the reaction of fission products with the SiC layer in TRISO coated HTGR fuel. These conclusions and recommendations are based on experiments discussed in this report which included data from out-of-pile thermal gradient heating tests and from irradiation tests of HTGR fuel.

1. Fission products which react with SiC are the rare earth metals (cerium, neodymium, lanthanum, samarium, praseodymium, and europium); palladium, ruthenium, rhodium of the platinum family; strontium and silver. For low enriched fuels, oxide fuels and fuel operating at $\leq$1250°C, palladium is the major concern.

2. Chlorine, combined with uranium and fission products is extremely corrosive to SiC. Chlorine contamination of the particles tested during in-pile irradiation could have caused an accelerated SiC corrosion. This possibility needs to be studied further, and should include electron microprobe analysis of chlorine in historical samples of the particles used in capsule tests.

3. The data base on fission product-SiC reactions in LEU fuel candidates is not sufficiently large to warrant treating it separately from HEU data. In addition, the scatter in the rate data during in-pile fuel tests masks any differences in rate of fission product-SiC reactions in oxide, carbide or oxycarbide fuel. This data scatter may be caused by batch-to-batch differences in particle characteristics.

4. The time dependence of SiC thinning caused by fission product-SiC reactions during irradiation is not known. Both square-root time and a linear-time models fit the experimental data. During out-of-pile experiments, tests at $\gtrsim$1500°C generally show linear time

dependence; while at $\lesssim$1500°C both square root time dependence and linear time dependence has been observed.

5. The temperature dependence of the rate coefficient of SiC thinning for both models follow an Arrhenius expression. For the linear time dependence model,

$$k_{\ell}(\mu m/hr) = 2.114 \times 10^{3} \exp. - \frac{1.795 \times 10^{5}}{8.314\ T(K)}$$

and for the square root model,

$$k_{p}(\mu m^{2}/hr) = 7.957 \times 10^{5} \exp. - \frac{2.369 \times 10^{5}}{8.314\ T(K)}$$

6. Because of the temperature gradient across a fuel rod, further post-irradiation examinations should include measurement of the radial locations of the particles which exhibit SiC corrosion. This observation would allow a better estimate of particle temperatures.

7. The rate of SiC corrosion caused by fission product attack during real time irradiation testing in Peach Bottom test element fuel was slower than the rate observed during accelerated irradiation testing. The reason for this needs to be determined. Included in studies of this phenomenon should be a determination of the effect of thermal and fast neutron flux in the SiC-fission product reaction rate.

8. The amount of SiC thinning necessary before fission products are released from the particle needs to be determined. Design studies use a 50% reduction in the SiC thickness as the criteria for fission

product release. Two experiments suggest that this is a conservative factor and that the SiC layer may effectively retain fission products after $\sim$70% reduction in thickness has occurred. The effect of a reduced thickness on additional modes of failure also needs to be studied.

6. REFERENCES

1. REAGAN, P. E., F. L. CARLSEN, and R. M. CARROLL, "Fission Gas Release from Pyrolytic-Carbon-Coated Fuel Particles During Irradiation", Nucl. Sci. Eng., 18, 301(1964)

2. BENTZ, G., R. DOBROZEMSKY, F. P. VIEHBOCK and H. WOTKE, "Determination of the Distribution of Fission Products in Fuel Particles Coatings by the Spattering Technique", J. Nucl. Mater., 38, 77 (1971)

3. YOUNG, C. A. and C. B. SCOTT, "Postirradiation Examination of Capsule P13Q", General Atomic Report GA-A14174, General Atomic Co., 1977

4. KANIA, M. J., et. al., "Irradiation Performance of HTGR Fertile Fuel in HFIR Target Capsules HT-12 through HT-15: Part 1, ORNL/TM-5305 (February 1977)

5. LONG, Jr., E. L., et. al., "Performance of HTGR Fertile Particles Irradiated in HFIR Capsule HT-32, ORNL/TM-7035 (April 1980)

6. FOERTHMANN, R., GRUBMEIER, H. J. KLEYKAMP, H., and A. NAOUMIDIS, Thermodyn, Nucl. Mater. 1974, Proc. of an IAEA Symposium in Vienna, Sept. 21-25, 1974, Vol. 1 (1975)

7. MORLEVAT, J. P., J. Nucl. Mater., 1974, 50(2) 119-26

8. Analytical Chemistry Department Procedure, ACO; CL-025

9. Memo from Pam Koch, "Revised Stand-Alone Burnup Code", FMD:116:PK:78 (1978)

10. STANSFIELD, O. M., C. B. SCOTT, and J. CHIN, "Kernel Migration in Coated Carbide Fuel Particles", Nucl. Tech., 25, 517 (1975)

11. SMITH, C. L., "Migration of ThO_2 Kernels under the Influence of a Temperature Gradient", GA-A14058, General Atomic Company, 1976

12. KETTERER, J. W. and R. E. BULLOCK, "Capsule HRB-15B Postirradiation Examination Report GA-A15940", General Atomic Company (October 1980)

13. HOMAN, F. J., T. B. LINDEMER, E. L. LONG, JR., T. N. TIEGS, and R. L. BEATTY, "Stoichiometric Effects on Performance of High-Temperature Gas Cooled Reactor Fuels from the U-C-O System", Nucl. Technol. 35(2): 428-41 (Sept. 1977)

14. BROWN, P. E., BROWNSWORD, M., FAIRCLOTH, R. L., INSS, A. J. and E. W. HOOPER, "Metal Fission Product Behavior in HTR UO_2-Coated Particle Fuel", AERE-R-8065, AERE Harwell, 1975

15. SCOTT, C. B., D. P. HARMON, and J. F. HOLZGRAF, "Postirradiation Examination of Capsules P13R and P13S", ERDA Report GA-A13827, General Atomic Co., October 8, 1976

16. HARMON, D. P., and C. B. SCOTT, "Development and Irradiation Performance of LHTGR Fuel", ERDA Report GA-A13173, General Atomic Company, October 31, 1975

17. SMITH, S. L., "SiC-Fission Product Reactions in TRISO UC_2 and WAR UC_xO_y Fissile Fuel, Part 1: Kinetics of Reactions in a Thermal Gradient", General Atomic Report GA-A14313, September 1977

18. BROWN, P. E. and R. E. FAIRCLOTH, "Metal Fission Product Behavior in High-Temperature Reactors - UO_2 Coated Particle Fuel", J. Nucl. Mater. 59, 29 (1976)

19. LAUF, R. J., "The Interaction of Silver and Palladium with Silicon Carbide in HTGR Fuel Particles - Preliminary Report", ORNL/TM-7393, July 1980

20. Memo from C. L. SMITH to T. D. GULDEN, "Pd-SiC Reactions in HEU and MEU Fuels", September 4, 1979, FCB:090:CLS:79

21. PEARSON, R. L., LINDEMER, T. B. and E. C. BEAHM, "Simulated Fission Product-SiC Interaction in TRISO-Coated LEU or MEU HTGR Fuel Particles", Oak Ridge National Laboratory Report ORNL/TM-6991, November 1980

22. KLEYKAMP, H., "Mikrosondenumtersuchungen zum Verhalten der Spaltproducte in Hoch Abgebrannten HTR-Brennstoffen", Kernforschungszentrum Karlsruhe Report KFK 2213, October 1975

23. HTGR Base Program Quarterly Progress Report for the Period Ending May 31, 1973", Gulf-GA-A12599, p. 87, Gulf General Atomic Company (1973)

24. HOMAN, F. J. and E. L. LONG, JR., "Irradiation Performance of HTGR Recycle Fissile Fuel", ORNL/TM 5502, Oak Ridge National Laboratory (1976)

25. TIEGS, T. N., "Irradiation Performance of Pu-Containing Coated Particle Fuels", Trans. Am. Nucl. Soc. (TANSO 28): 175-77 (June 1978)

26. TIEGS, T. N., "Fission Product Pd-SiC Interaction in Irradiated Coated Particle Fuels", ORNL/TM-7203, April 1980

27. TIEGS, T. N., et. al., "Irradiation Performance of HTGR Fuel on HFIR Capsule HT-31", ORNL-5510 (May 1979)

28. WEBER, G. W., R. L. BEATTY, and V. J. TENNERY, "Processing and Composition Control of Weak-Acid-Resin DerivedFuel Microspheres", Nucl. Technol. 35(2): 217-26 (September 1977)

29. SHARP, J. H., G. W. BRINLEY, and B. N. NARAHARI ACHAR, "Numerical Data for Some Commonly Used Solid State Reaction Equations", Journal of the American Ceramic Society, 49(7), p. 379

30. HTGR Fuel Development Department Technical Status Report for the Quarter Ending March 31, 1980, General Atomic Report 904457, Issue A, April 1980

31. MONTGOMERY, F. C., "Kinetics of Fission Product-SiC Reactions", General Atomic Report 905239, September 1980

32. PEARSON, R. E. and T. B. LINDEMER, "The Interaction of LaC_2 and NdC_2 with SiC in HTGR Particles", CONF-770208-5, Oak Ridge National Laboratory, 1977

33. KAAE, J. L., "Chemical Attack of SiC and ZrC TRISO Coatings in Pd-Doped UO_2 Particles", General Atomic Document No. 905255/1. November 1980

34. Introduction ot Statistical Analysis, 3rd Edition, DIXON, W. J. and F. J. MASSEY, JR., McGraw Hill Book Co., New York, 1969, p. 199

35. TIEGS, T. N. and E. L. LONG, Jr., "Postirradiation Examination of Recycle Test Elements from the Peach Bottom Reactor", ORNL-5422

36. SAURWEIN, J. J., et. al., "Final Summary Report on the Peach Bottom Test Element Program", GA-15000, to be published

37. Introductory Mathematical Statistics, Erwin Kreyszig, John Wiley and Sons, Inc., New York, 1970, p. 352

38. Memo from J. J. SAURWEIN to F. C. MONTGOMERY, "Comparison of Measured and Calculated SiC Coating Penetration in Peach Bottom Test Element Fuel", JJS:004:CM:81, April 8, 1981

39. BENZ, R., H. GRÜBMEIER and A. NAOUMIDIS, "Experimental Observations on In-Pile and Out-Of-Pile Fission Products SiC-Interactions", IRW-TN-119/80, October 1980

40. GRÜBMEIER, H., A. NAOUMIDIS and B. A. THIELE, "Silicon Carbide Corrosion in High Temperature Gas-Cooled Reactor Fuel Particles", Nuclear Technology, 35, September 1977 (413)

41. BULLOCK, R. E. and S. A. STERLING, Private Communication, December 1976

42. BULLOCK, R. E., "Annealing Tests of Coated Fuel Particles", General Atomic, Document No. 905779, January 23, 1981

43. FUKUDA, K., KASHIMINA, S., TOBITA, T., and KAZUMI UOAMOTO, "Observations of Coating Failure at High Temperature in the Coated UC_2 Particles Containing UC and Free Si", J. Nucl. Sci. Technol., 10(10), 1973 (54)

44. HTGR Fuel Development Department Technical Status Report for the Quarter Ending June 30, 1980, General Atomic Report 904907, Issue A, August 1980